THE UNIVERSITY OF HULL

"A Structural and Thermodynamic Study of Non-aqueous Solvent / Wax Systems."

being a thesis submitted for the Degree of

Doctor of Philosophy

in the University of Hull.

by

Ian Theaker, B.Sc.(Hull).

December, 1996.

ACKNOWLEDGEMENTS

The author is grateful to Professors G.W. Gray and P.B. Wells for providing facilities for this project and to Reckitt and Colman, Household Products, Hull for their provision of funding and technical assistance.

I would also like to thank my academic supervisors Dr. P.G. Francis and Professor P.D.I. Fletcher for their constant help and encouragement, Professors G.W. Gray and A. Townshend for their interest and guidance, and Dr. R.A. Cowan and his colleagues at Reckitt and Colman Household Products for their useful advice.

I am also grateful to Mr. A.R. Rendall (University of Hull) for the production of the optical micrographs.

This thesis was prepared using Microsoft® Word for Windows version 6.0c and Hewlett Packard 4L and DeskJet 1200C printers.

DECLARATION

No part of this work has previously been submitted by the candidate for a degree in this or any other university.

To mum, dad and numerous friends for their unfailing support and encouragement.

ABSTRACT

Non-aqueous wax / solvent systems of industrial relevance for the manufacture of paste polishes have been investigated. These mixtures have been modelled using a paraffin wax of Japanese origin (Nippon Seiro 140/145°F) in a solution of pure heptane to which dopant components are added.

The stability of any resulting gel has been assessed via solubility studies and measurement of the solvent vapour pressure. A new technique for the measurement of vapour pressure in these systems has been developed. The operation of the apparatus has been made almost completely automatic by the use of modern control units.

Complementary analytical techniques such as Differential Scanning Calorimetry and Nuclear Magnetic Resonance have been used to augment the data where appropriate and the structure of these pastes has been investigated with the use of Optical Microscopy.

CONTENTS

LIST OF TABLES

LIST OF FIGURES

Chapter One

Introduction

§ 1.1 Preface

The work described in this thesis arose from a joint project initiated by Reckitt and Colman Ltd. They suggested that the University of Hull might be able to provide a more fundamental understanding of the principles behind some industrial processes. These have evolved from traditional formulations to which have been added modern analytical techniques.

The particular interest was in the formulation of non-aqueous mixtures of wax and solvent for the production of polish. This leads to questions about the stability and structure of polymer mixtures. As the project developed the emphasis was placed on the thermodynamic properties of wax / solvent systems.

§ 1.2 Classification of polish components①

In order to give some sort of structure to an already complex field, one has to answer initially the question "what is a wax ?". A typical dictionary definition of a wax[1] is "any of numerous plant or animal substances that are harder, more brittle, and less greasy than fats". An etymological definition of the word 'wax' reveals that its origins lie with the Anglo-Saxon word *'weax'*, which was used for the internal building material of bees' nests[2]. Rather confusingly, the term 'wax' is applied quite liberally to a wide range of

① See also appendices A and B

burnishing products as well as their individual components. In more scientific terminology, many conventions appear in the literature, depending on the slant of the author. Classically, a chemical definition of a wax would be the solid esters formed by the combination of fatty acids and long chain monohydric alcohols; although alone this has obvious limitations.

Waxes have been used for polishing applications for centuries, albeit as part of a rudimentary formulation. Beeswax dissolved in turpentine along with harder tallow wax was a common mixture used for polishing wooden floors and furniture although vigorous buffing was required to vaporise the solvent and remove excess wax in order to give a high resultant gloss finish. The gloss, or shine, of a polished surface is achieved by forming a thin, smooth and hard, highly reflective film on top of a substrate which has developed imperfections such as scratches.

In 1797 Kosler discovered carnauba wax which drastically transformed the formulation of polishes which included it. It is a hard, high melting point wax which can impart high gloss finishes without smearing and is obtained by scraping from the leaves of the Brazilian cerara palm. Although it is still used nowadays in pure wax / solvent pastes, it is commonly substituted in part by cheaper vegetable derived waxes such as candelilla, esparto and ouricuri.

More recently, the advances made in the petroleum industry at the turn of the century have contributed a wide range of paraffin waxes and led

to the development of many synthetic substitutes for inclusion in present day formulations.

The following section is intended to summarise some of the properties of those waxes which are of direct relevance to the polish industry and so does not attempt to reproduce more detailed accounts in the literature[3].

§ 1.2.1 Vegetable waxes

§ 1.2.1.1 Carnauba wax

This wax is obtained from the leaves of the Brazilian cerara palm (*Copernicia cerifera*) in the form of a fine powder which is then melted down in boiling water to yield a solid which varies in colour from yellow to grey. It is an extremely hard (0.2 mm at 25°C) [4], high melting (m.p. 82 - 86°C) material with an acid number of 8 (mg of KOH / g for neutralisation) and a saponification number of 80 (mg of KOH / g for saponification).

The ability of carnauba to gel with large concentrations of organic solvent make it ideal for its incorporation in solid and cream pastes which give rise to polished films of high depth of gloss and strength.

In its purer form carnauba wax consists of the following main constituents[5].

Component	Example of main compounds	wt.%
free acids	lignoceric ($^{n}C_{23}H_{47}COOH$), cerotic ($^{n}C_{25}H_{51}COOH$) and montanic ($^{n}C_{27}H_{55}COOH$)	4
free alcohols	melissyl ($^{n}C_{30}H_{61}OH$) and lacceryl ($^{n}C_{32}H_{65}OH$)	3
hydrocarbons	heptacosane ($^{n}C_{27}H_{56}$), nonacosane ($^{n}C_{29}H_{60}$) and hentriacontane ($^{n}C_{31}H_{64}$)	3
esters		82
aliphatic	45.3% C_{24}-C_{28} acids with 54.7% C_{30}-C_{34} alcohols (C_{32} being predominant)	(40)
ω-hydroxy	47% saturated n-acids [90% ω-hydroxy C_{22}-C_{28} and 10% n-C_{24}- C_{28}] with 53% saturated n-alcohols [90% n-C_{24}- C_{34} and 10% α-, ω-glycols C_{24}-C_{34}]	(13)
miscellaneous	cinnamic aliphatic diesters, resins, pigments etc.	8

Table 1.1 *Typical composition for a sample of refined Carnauba wax.*

§ 1.2.1.2 Candelilla wax

Candelilla wax is obtained from the stem of Mexican shrubs such as *Euphorbia antisyphlitica* and *Pedilantus pavonis* by treating the whole of the weed with water acidified with sulphuric acid. The wax skimmed from the surface is hard and pale brown in colour but it differs from carnauba in that it has a lower melting point (m.p. 70°C), an acid number of 15 and a saponification number of 55. Candelilla is mainly composed of wax esters (29%), hydrocarbons (49%), alcohols (11%) and acids (7%)[4]. The high hydrocarbon content is responsible for it producing much softer films, with less gloss than carnauba and so it is more often used for liquid polishes.

§ 1.2.1.3 Ouricuri wax

Ouricuri wax is obtained by manually scraping the undersides of the leaves of the Brazilian palm *Cocos coronata*. It is a hard high melting wax (m.p. 81 - 85°C) with similar properties to carnauba. It is sometimes used as a substitute for the latter when cost becomes an influential factor.

Chemically it has a higher hydrocarbon content (17% - mainly as $^{n}C_{31}H_{64}$) with an acid number of 15 and a saponification number of 90.

Other vegetable waxes such as esparto, Japan and sugar cane wax are also common but will not be discussed any further here.

§ 1.2.2 Animal waxes

§ 1.2.2.1 Beeswax

Like the natural vegetable waxes already discussed, beeswax contains no esters of glycerol. It consists mainly (70%) of the long chain esters myricyl palmitate ($C_{15}H_{31}COOC_{30}H_{61}$), myricyl palmitoleate ($C_{15}H_{29}COOC_{30}H_{61}$), myricyl cerotate ($C_{25}H_{51}COOC_{30}H_{61}$), cerotyl 2-hydroxypalmitate ($C_{14}H_{29}CH(OH)COOC_{26}H_{53}$) and lacceryl palmitate ($C_{15}H_{31}COOC_{32}H_{65}$) along with free acids (13% - cerotic, montanic and melissic) and hydrocarbons (12% - $C_{29}H_{60}$ and $C_{31}H_{64}$)[6,7]. It has a low melting point (63°C) with a saponification value of 95 and acid value of 20 and it is mainly used for the manufacture of candles and floor polishes. Beeswax is obtained by the treatment of honey combs with hot water and

then bleaching of the strained fraction (impure from pollen and honey) with hydrogen peroxide or chromic acid.

§ 1.2.2.2 Shellac wax

Shellac wax is obtained from the discharge of the lac insect (*Ficus religiosa*). It is essentially an ester wax (~60% $C_{26}H_{53}OOCC_{23}H_{47}$, $C_{26}H_{53}OOCC_{25}H_{51}$ etc.) which contains a large amount of free alcohols (~35% $C_{32}H_{65}OH$, $C_{30}H_{61}OH$ etc.) and has its main use in polish formulations due to the ability to impart a high depth of gloss.

§ 1.2.2.3 Spermacetti

Spermacetti, or Cetin, is the solid remaining after squeezing the oils taken from the sperm and bottlenose whales. It consists mainly of equal amounts of the lower chain fatty alcohols ($C_{16}H_{33}OH$) and fatty acid esters ($C_{16}H_{33}OOCC_{15}H_{31}$) and so finds more use in the formulation of cream polishes.

§ 1.2.3 Mineral waxes

§ 1.2.3.1 Ozokerite

Ozokerite, or Earth wax, occurs mainly in the U.S.A. and Russia. Although the crude form is green or brown in colour, the refined product (from treatment with H_2SO_4) often resembles beeswax. It has excellent

solvent retention properties due to its amorphous structure and hence shows little tendency to crystallise out of solution in a hydrocarbon solvent.

§ 1.2.3.2 Paraffin waxes

Paraffin waxes are obtained from the distillation of crude petroleum which occurs mainly in the North Sea, Russia, America or the Middle East. They are usually refined into fractions of a few degrees Celsius (within the melting range 40°-65°C) and are white in colour. Chemically they consist almost entirely of the straight chain alkanes in the region $C_{24}H_{50}$ - $C_{35}H_{72}$ along with a small proportion of the 2-methyl branched derivatives. Paraffin waxes are highly crystalline in nature and are actually obtained from the above distillates by chilling (de-waxing). Paraffin waxes are responsible for 60% of the total wax content of a polish and give rise to easy spreading pastes. They are cheap but their inclusion in such high quantities can impair the transparent, glossy film.

§ 1.2.3.3 Microcrystalline and oxidised microcrystalline waxes

Microcrystalline waxes are separated from the residues of the distillation process and so have a much higher melting range (typically 80°-95°C). They consist mainly of saturated branched and ring hydrocarbons in the range $C_{40}H_{82}$ - $C_{60}H_{122}$ and, as the name suggests, they adopt a structure containing small irregular crystallites when viewed under the microscope. Microcrystalline waxes are used to blend the other

waxes together. They are cheap and introduce heat resistance to the paste and transparency to the film. They show strong crystal modifying properties since they form firm, crisp pastes when included in polyethylene - paraffin blends which normally give soft, moist pastes.

When heated in the presence of a catalyst, microcrystalline wax is easily oxidised by oxygen to give a wide range of acidic compounds. These are extremely useful in the formulation of water-in-oil pastes since they are easily emulsified and impart high gloss and strength to the polished film.

§ 1.2.3.4 Fischer - Tropsch waxes

The process of synthesising hydrocarbons from the combination of hydrogen and carbon monoxide began in the early 1900's[8] but the industrial production of long chain alkanes was pioneered with work in Germany by Franz Fischer and Hans Tropsch[9]. Their original work showed that a mixture of hydrocarbons, along with a proportion of oxygenates, is produced when the reactants are passed over alkali treated iron turnings at pressures and temperatures around 80,000 Torr and 700 K respectively. Although various reaction mechanisms have been proposed for the process[10] they are irrelevant to the theme of this thesis. Typical chemical reaction schemes involve overall stoichiometries such as

$$(2n+1)\,H_2 + n\,CO \rightarrow C_nH_{2n+2} + n\,H_2O \qquad (1.1)$$

$$2n\,H_2 + n\,CO \rightarrow C_nH_{2n} + n\,H_2O \qquad (1.2)$$

Development of newer catalysts in the post war years typically reduced conditions to about 8000 Torr and 500 K using Co:ThO_2:MgO:kieselguhr for the selective production of oxygenates and ruthenium based catalysts for very long chain hydrocarbons.

§ 1.2.3.5 Montan (Hoechst / B.A.S.F.) waxes

Montan wax can be regarded as the fossilised equivalent of present day vegetable waxes and is generally obtained by solvent extraction from crude coal samples (Lignite). Hence, unrefined montan wax contains long chain esters, acids, alcohols and ketones, in addition to varying amounts of resinous material. When modified (e.g. by oxidation with chromic acid, de-resinification by dissolution in ethanol, esterification with various glycols etc.) this raw product leads to a series of waxes known as Hoechst or B.A.S.F. waxes.

Crude montan wax is dark and contains a high percentage of resins which tend to be removed by extraction into organic solvents. The resulting montan wax is still coloured due to the presence of carbonised plant material and has to undergo a bleaching process with chromic acid. This results in cleavage of the ester molecules and oxidation of the alcohols and ketones to their corresponding acids, giving rise to a series of so called 'acid waxes'. Esterification of the acid waxes with monohydric or polyhidric alcohols of different carbon chain length yields the 'ester waxes' which can be further modified by the addition of non-ionic surfactants for their incorporation into

emulsion polishes. A whole range of wax products[11] can be made via various modification techniques and are summarised in figure 1.1.

Table 1.2 lists some properties of some of the more common Hoechst waxes (formerly known as IG or Gersthofen waxes since they were originally produced by I.G. Farbenindustrie in Germany).

Hoechst Wax	m.p.* °C	Acid No.*	Sapon. No.*	Modification of Montan Wax†
S	80	140	160	**mw** oxidised with chromic acid. (**omw**)
L	80	125	150	**dmw** oxidised with chromic acid. (**odmw**)
O	102	10	105	Ethylene glycol ester of **omw** partly neutralised with lime.
OP	100	10	105	OP = butylene glycol ester of **omw**.
OM	93	20	115	Ca containing, partly esterified (various glycols) **odmw**.
Special	98	15	90	A mixture of butylene glycol esters partly neutralised with caustic potash and lime.
F	79	6	95	Esterified **omw**.
E	81	15	145	Ethylene glycol esterified **omw**.
CR	82	30	110	A mixture of **mw** and **omw** esterified with butylene glycol.
KPS	80	20	135	1 part **mw** and 3,5 parts **dmw**, esterified with ethylene and butylene glycols.
KPE	78	18	120	**omw** esterified with ethylene and butylene glycols (modified).
KP	80	20	135	**omw** esterified with ethylene and butylene glycols.
BJ Unbleached	70	17	135	Not a true derivative of **mw** but similar to beeswax.
BJ Bleached	70	65	155	Not a true derivative of **mw** but similar to beeswax.
N New	73	40	120	An emulsifying agent for the O/W type.

* Minimum Values. † **mw** = Montan Wax ; **o** = Oxidised ; **d** = De-resinified.

Table 1.2 *Chemical and physical properties of Hoechst waxes.*

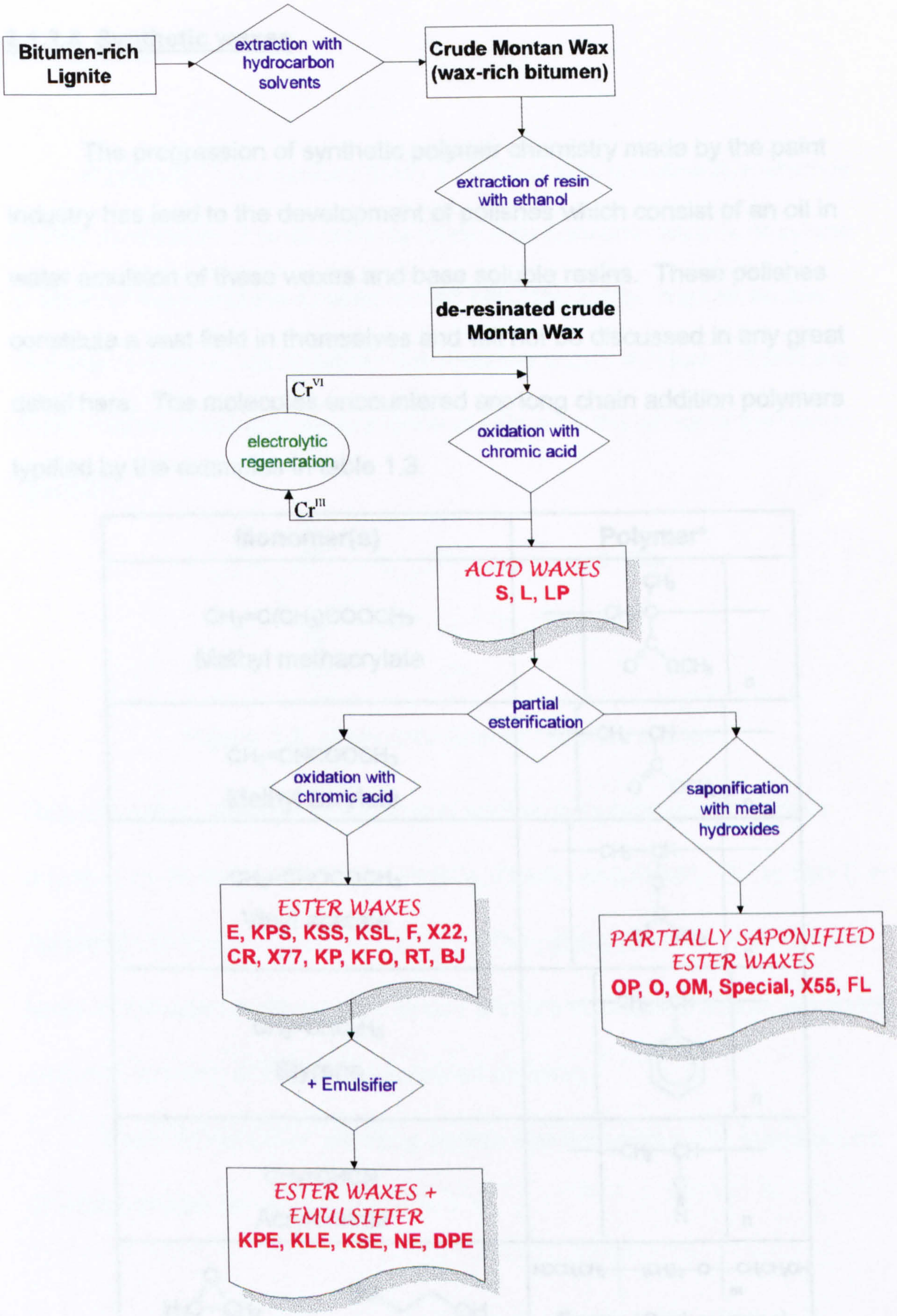

Figure 1.1 *Schematic Production of Montan Based Waxes.*

§ 1.2.4 Synthetic waxes

The progression of synthetic polymer chemistry made by the paint industry has lead to the development of polishes which consist of an oil in water emulsion of these waxes and base soluble resins. These polishes constitute a vast field in themselves and will not be discussed in any great detail here. The molecules encountered are long chain addition polymers typified by the examples in table 1.3.

Monomer(s)	Polymer*
$CH_2=C(CH_3)COOCH_3$ Methyl methacrylate	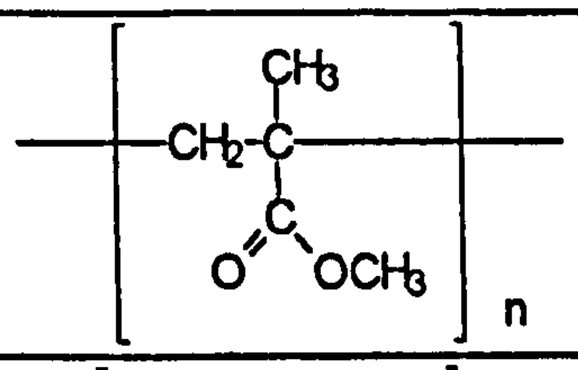
$CH_2=CHCOOCH_3$ Methyl acrylate	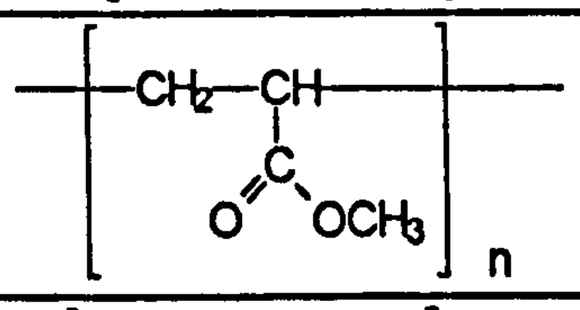
$CH_2=CHOCOCH_3$ Vinyl acetate	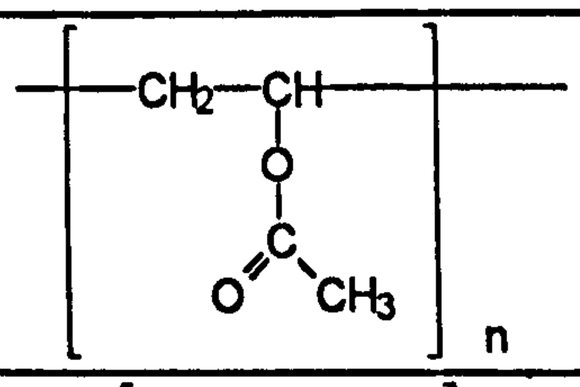
$CH_2=CHC_6H_6$ Styrene	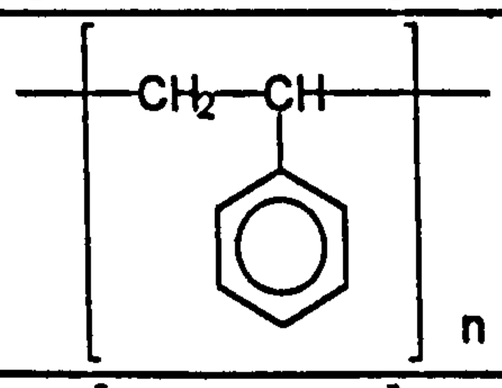
$CH_2=CHCN$ Acrylonitrile	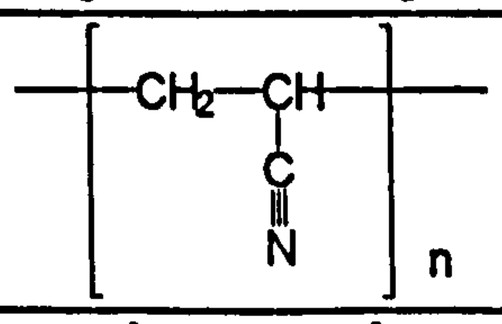
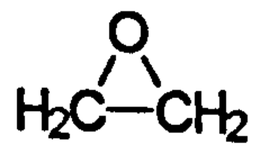 Ethylene oxide 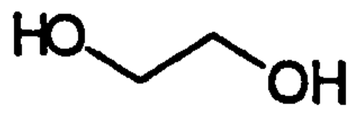 Ethylene glycol	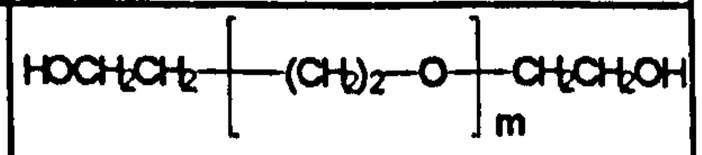 Forms 'Carbowaxes' when esterified

* $n \gtrsim 1000$; $6 \leq m \leq 12$.

Table 1.3 *Common forms of synthetic polymers.*

§ 1.2.5 Dyes

Nigrosine[12] (CI Solvent Black 5, CI 50415) is an azine dye which is soluble in mixtures of small chain alcohols with benzene, toluene or xylene or either of the components when mixed with fatty acids. Nigrosines are mixtures of compounds based on the structure shown in figure 1.2 and are black in appearance due to absorbtion of light over the whole of the visible spectrum.

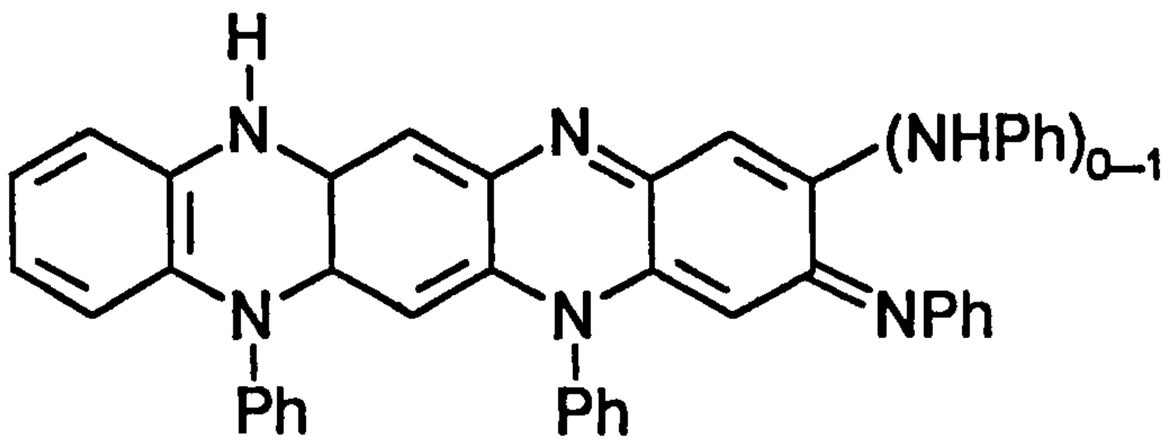

Figure 1.2 *Major constituent of Nigrosine base.*

They are often made by the reaction of sodium bicarbonate with excess aniline or by heating a mixture of $PhNO_2$, $PhNH_2$ and $PhNH_3^+Cl^-$ to 190°C in the presence of an iron-copper catalyst. They are one of the more common types of dye used in the polish industry and are sometimes added, in varying amounts, to many of the darker coloured polishes.

Examples of other colouring agents that are used in the manufacture of shoe polishes are shown in figure 1.3

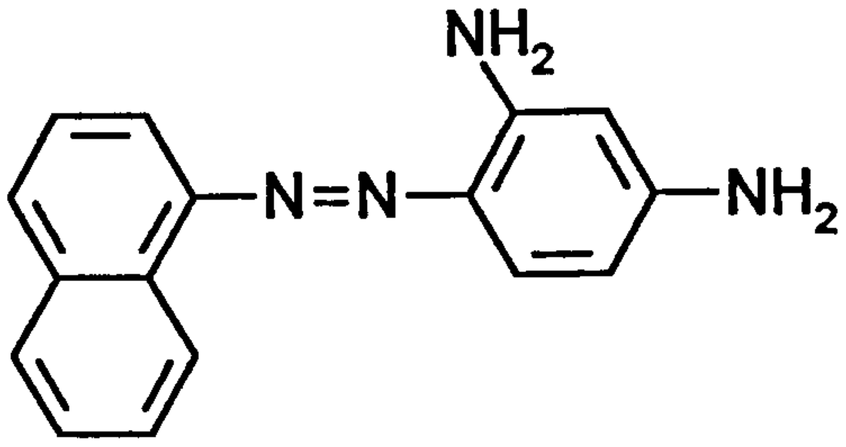

Fat Brown RR
(CI Solvent Brown, CI 11285)

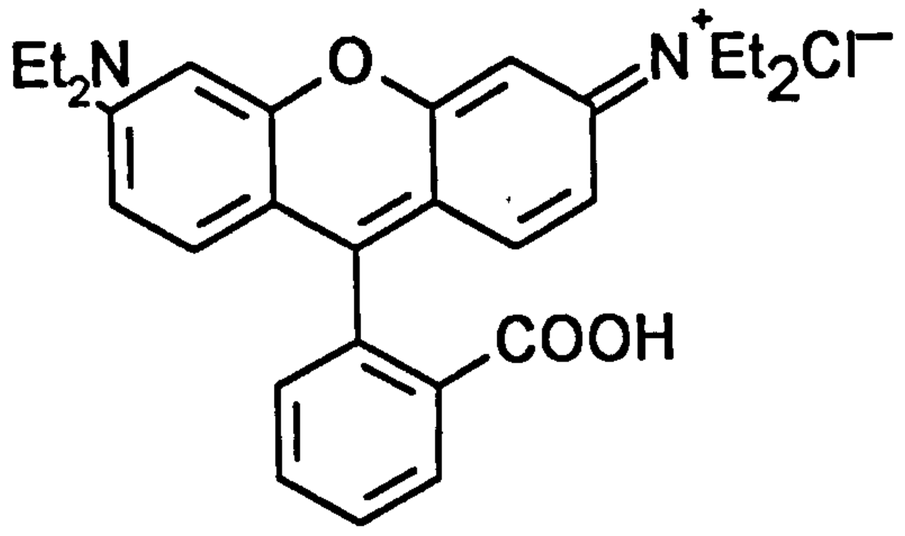

Rhodamine B Base
(CI Solvent Red 49, CI 45170:1)

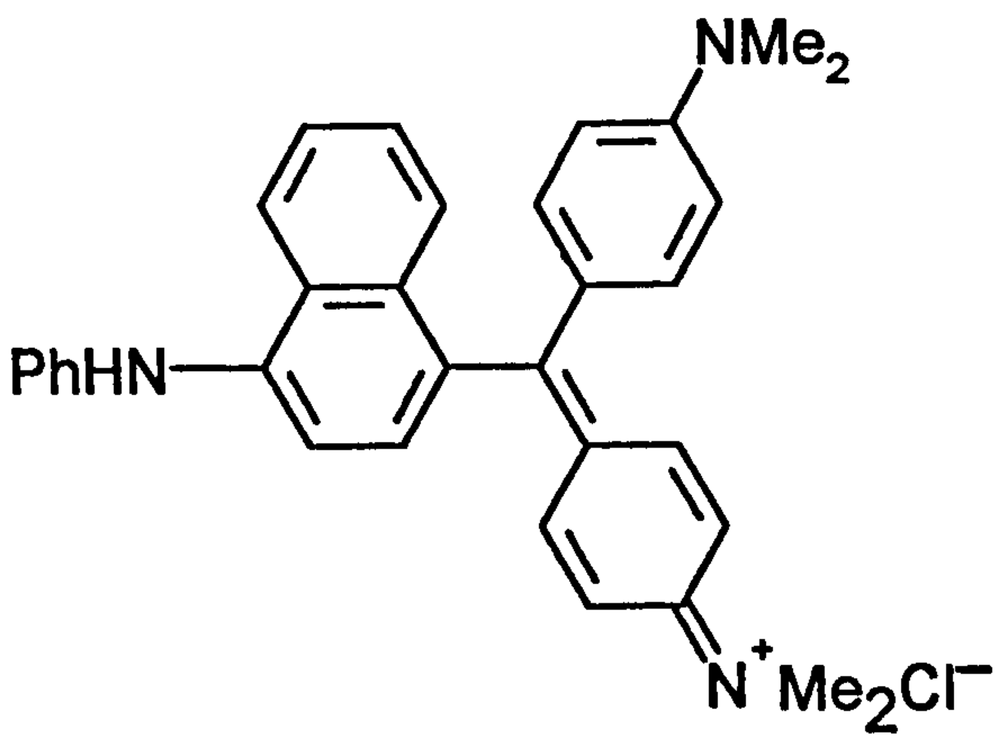

Victoria Blue B Base
(CI Solvent Blue 4, CI 44045:1)

Mixtures of ZnO, $Al(OH)_3$
and basic "$Al_2(SO_4)_3$"

DOP White TRN
(CI Pigment White 4 or 24)

Figure 1.3 *Dyes and pigments used in polish manufacture.*

§ 1.2.6 Solvents

The choice of solvent in the manufacture of paste polishes is also of prime importance. A large proportion of high molecular weight constituents will lead to a high boiling range solvent which results in a polish film that is too viscous to burnish via buffing resulting in a smeared film. Whereas a high percentage of volatile components leads to a wax film which dries before it can be evenly coated and the solvent readily evaporates when the tin is opened, leaving a hard and cracked polish. Also, one must consider

the temperature dependence of a solvent's ability to dissolve the wax components of a paste polish. Preferred solvents are ones which have a high 'solvent power' at elevated temperatures (~85°C) in order to ease manufacture and a low solvent power at ~20°C to obtain the desired consistency. The rate of increase of solvent power with temperature should be as low as possible in order to ensure solid pastes over a range of possible room temperatures for varying climates.

§ 1.2.6.1 Turpentine

The solvent more commonly used in the United States is turpentine and obtained by steam distillation of the wood or resins from various pine trees. A typical sample has a boiling point range of 150–200°C, a flash point of 32°C, a specific gravity of 0.86–0.87 and contains no more than 5% aromatic compounds. Although it evaporates fairly rapidly during polishing, it is more expensive than White Spirit and degrades with age leading to corrosion of the tin.

§ 1.2.6.2 White Spirit[13]

This solvent is sometimes called mineral spirit or mineral turpentine and is the preferred solvent in the United Kingdom. It is obtained from the distillation of petroleum and obtained as a fraction which boils between 150 and 200 °C. Its flash point is usually ~37°C with a specific gravity of 0.77–0.8 and an aromatic content of ~15%. Gas chromatography coupled with

mass spectrometry (G.C.M.S.) reveals a large proportion of straight chain alkanes and their mono- and di-methylated derivatives (C_9 - C_{12}) along with a significant amount of di-methylated cyclohexanes and benzenes. Figure 1.4 shows the vapour pressure characteristics of such a solvent[14] together with the vapour pressure for n-heptane which was chosen as the solvent in this system to model paste polishes.

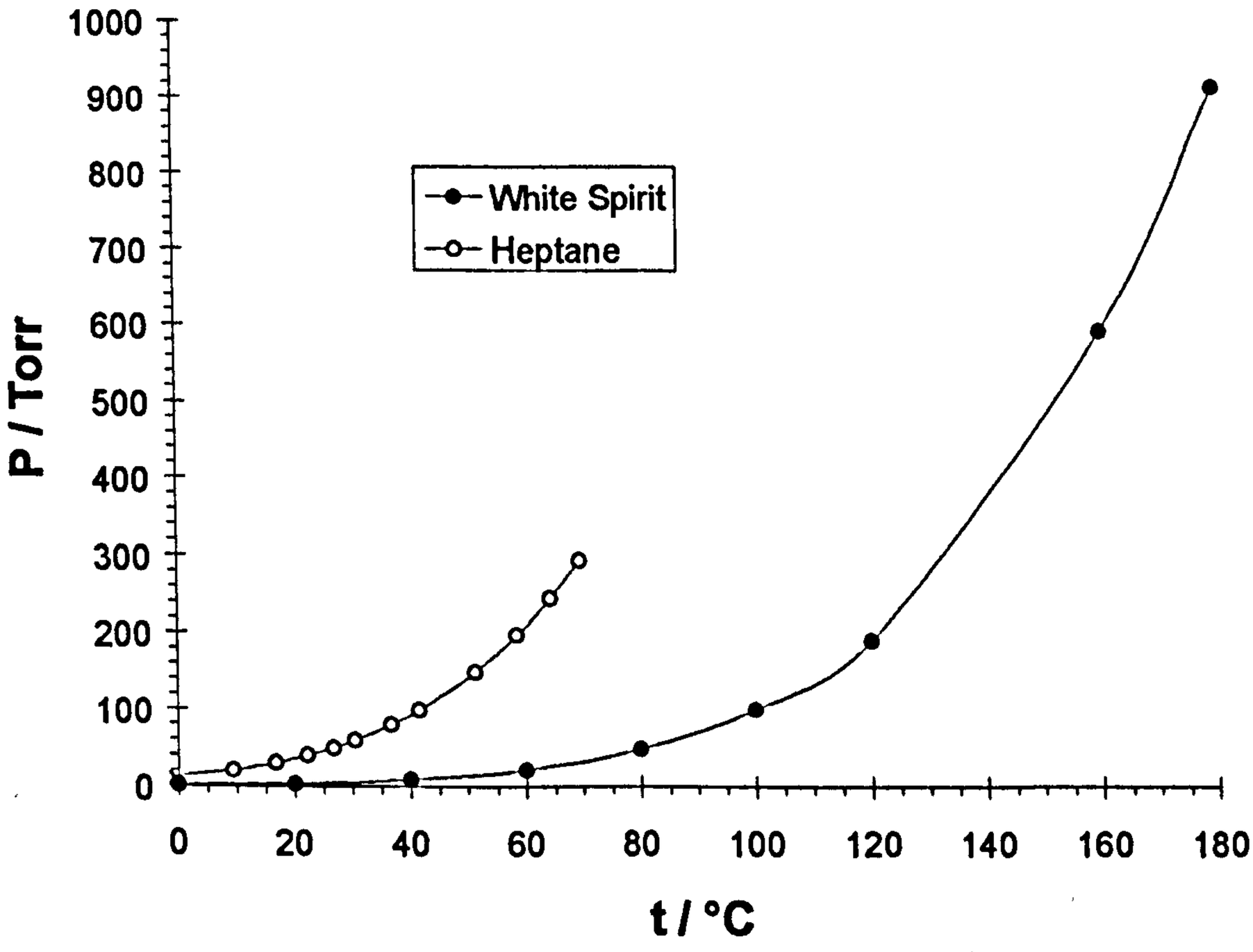

Figure 1.4 *Temperature dependence of vapour pressure for White Spirit and heptane.*

§ 1.3 Industrial interest in these systems – Polishes

§ 1.3.1 Wax blends in formulations

Figure 1.5 summarises the properties of various waxes (a key is given in table 1.4) when they are incorporated into wax paste formulations. The choice of solvent can also affect the paste structure. White Spirit gives a more crystalline and turpentine a more gelatinous paste structure.

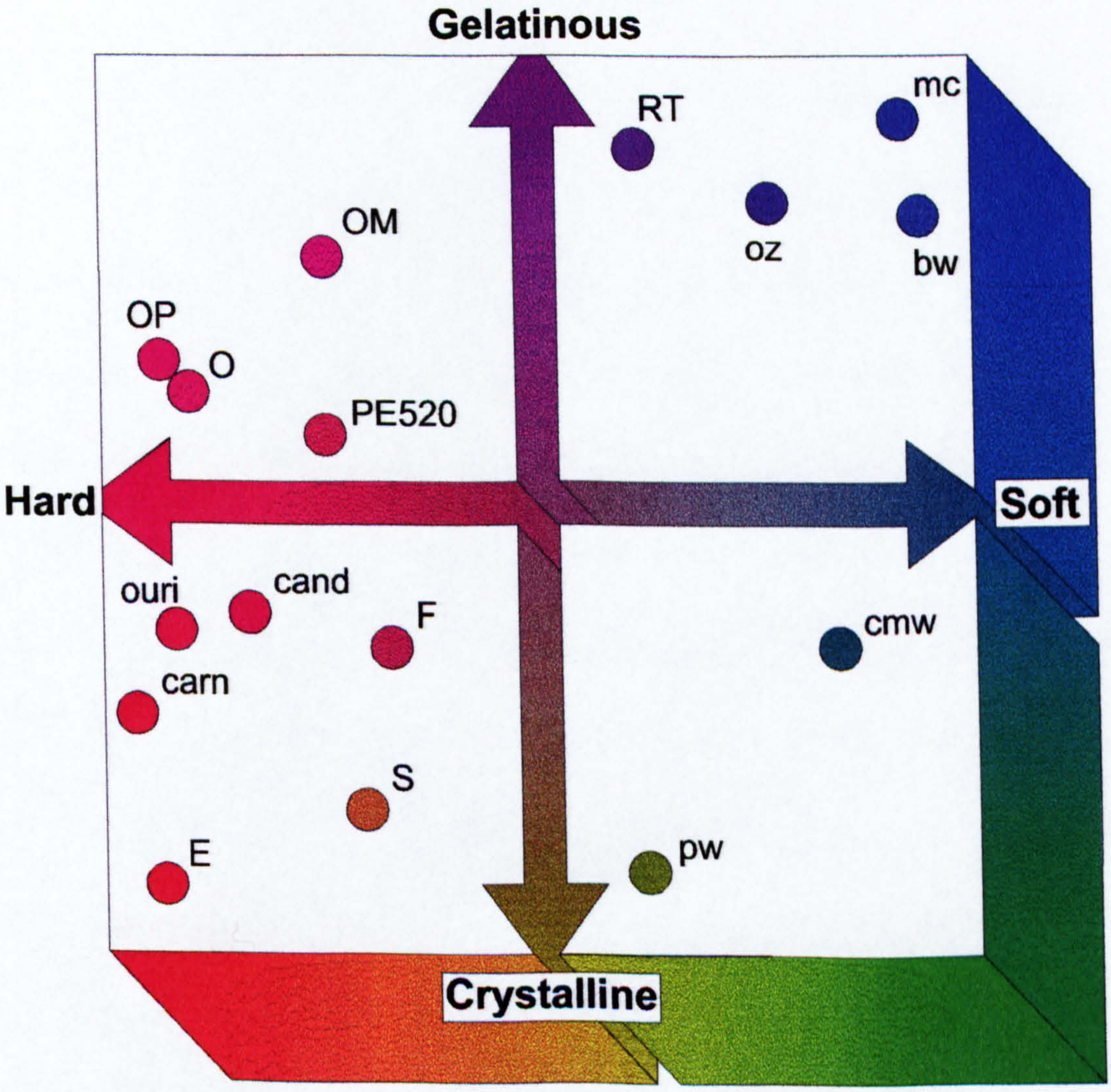

Figure 1.5 *The effect of raw materials on the hardness and structure of solvent pastes.*

E	Hoechst Wax E	PE520	Hoechst Wax PE520
F	Hoechst Wax F	mc	Typical Microcrystalline Wax
O	Hoechst Wax O	cmw	Crude Montan Wax
OM	Hoechst Wax OM	RT	Hoechst Wax RT
OP	Hoechst Wax OP	S	Hoechst Wax S
pw	Typical Paraffin Wax	bw	Beeswax
oz	Ozokerite	cand	Candelilla
ouri	Ouricouri	carn	Carnauba

Table 1.4 *Key for figure 1.5.*

§ 1.3.2 Manufacture

Manufacturing techniques and recipes may vary widely. A typical paste polish consists of ~70% solvent, such as turpentine or White Spirit, 26% waxes and the total made up with resins, pigments and thickeners[15]. The solvent is added to a hot stirred melt of the waxes and allowed to cool slowly whilst vigorously agitated by the action of a homogeniser. The homogeniser imparts a shearing action on the wax crystals as they are formed, thereby reducing their size and resulting in a more stable product of increased bulk. This process is only applied at temperatures above 48°C (the "pour point" of the product), and so has little effect on the more soluble components such as the paraffin waxes, resins and vegetable waxes. (Crystallisation range 25–45°C in White Spirit).

The crystallisation of the less soluble polyethylene waxes and high melting microcrystalline waxes is most affected and occurs over the range

50 - 70°C. The change in properties which occur due to this process are very pronounced and necessary in the manufacture of the paste polish.

Issues to consider from the point of view of the consumer are ease of application, consistency in the tin (i.e. cracking, contraction or phase separation are undesirable), high gloss finish and cost. As well as fulfilling these criteria (and more) the manufacturer also has to consider the availability and price of raw materials and the ease of manufacture of the product.

The relative quantities of the component waxes vary enormously depending on the required properties of the product. Below a typical industrial process and formulation is outlined[16].

Component	Example / Grade	Amount / kg	Wt %
Paraffin Wax	Nippon-Seiro 140/145	330	15
Hard Microcrystalline Wax	Crown700 or BD887	22	1
Vegetable Wax	Carnauba, Fatty Grey	125	5.7
Polyethylene Wax	AC629	40	1.8
Polyethylene Wax	AC8	33	1.5
Resin	Ennesin or Escorez	11	0.5
Oleine		33	1.5
Nigrosine Base		44	2
Carbon Black Mix	10%wt	132	6
White Spirit	sg 0.78 gml^{-1}	312 (=400 dm^3)	14.2
Stearine		44	2
Lime Mixture	25%wt	44	2
White Spirit	sg 0.78 gml^{-1}	1014 (=1300 dm^3)	46.1
Perfume	M.7948	15	0.7

Table 1.5 *A typical formulation for a black shoe polish.*

The paraffin wax, microcrystalline wax, Carnauba and AC629 are melted in a vessel which is heated with a steam jacket. At 120°C the AC8 is added with gentle stirring until completely dissolved followed by the Oleine and resin not more than thirty minutes before the waxes are run into the mixing vessel.

The Nigrosine base is incorporated into the blend, with gentle stirring, followed by the Carbon Black mixture. The White Spirit (400 dm^3) and Stearine are introduced to the vessel and the latter left to dissolve at 96°C for twenty minutes. The remainder of the solvent is added and the whole mixture is allowed to cool at a rate of $\not> 0.5°C min^{-1}$ under the action of a high shear homogeniser. When the temperature has dropped to 55°C the perfume is added and the homogeniser stopped at around 50°C. The polish will have now reached a consistency suitable for pouring into containers.

The final product will be a smooth, firm paste with a glossy convex surface which is free from imperfections such as bubbles or specks of undissolved dyestuff.

§ 1.4 Main Objectives

Since the art of polish formulation is very much a 'black art' and poorly understood by the experimental chemist, it is not surprising that industrially there is inadequate control over the required properties of the final product. This research project was initiated not only to give a greater understanding

of the factors affecting polish manufacture, but also to characterise the nature of these complex wax / solvent systems.

The use of waxes ranging from paraffins and synthetics to natural products leads to a corresponding range of composition covering saturated and aromatic hydrocarbons, and complex mixtures of long chain alcohols, acids and esters. Mixtures of these components will be expected to show variable behaviour in solution, depending on the system studied.

Apart from the wax composition affecting the behaviour of the system, it is expected that the crystallisation of waxes from solutions in solvents and other waxes will also be an important area of investigation.

Many of the problems faced by the polish industry concern the loss of solvent from, and phase separation of the product. Hence the main objective of the project is directed at obtaining an understanding of the thermodynamic properties of wax / solvent systems, in order to quantify the interactions between the wax and solvent components. One can then predict properties of the mixture such as solvent retention, and any modifications required to achieve desired properties in a blend.

§ 1.5 Experimental techniques

The research described in this thesis is directed towards an improved understanding of the properties of non-aqueous blends of waxes and solvents. This is achieved by the application and extension of the theoretical

and experimental techniques used in the general field of polymer mixtures. It arose from questions concerning the functions of the components, and the stability of the blends, which are commonly used in industrial formulations.

Model systems have been adopted to mimic the commercial blends and yet permit precise and reproducible measurements. The wax component is represented by two of the major ingredients which are used in blends; these are Nippon-Seiro paraffin wax as the lower molecular weight constituent and BD887 microcrystalline wax as the principal additive. Pure n-heptane is used to model the commercial solvent and some pure long chain saturated hydrocarbons were used to help bridge the gap between simple systems and commercial mixtures.

The properties which can be studied are those usually used for non-electrolyte mixtures, subject to restrictions arising from the peculiarities of the solutes. Thus solubility studies are complicated by the fact that the wax solutes include a range of molecular weight so that fractionation of the solute occurs in equilibrium with solvent. For this reason the emphasis tends to be put on the cloud point where a homogeneous solution is cooled to the point at which solid separation commences.

Equilibrium studies are further complicated by high viscosity of the paste systems produced at the high solute concentrations of most interest. In liquid mixture studies, vapour pressure measurements are conventionally made by bringing mixtures of known composition to equilibrium with vapour by stirring at fixed temperature. This does not lead to reproducible results in

polymer solutions at high solute concentration because adequate stirring is difficult and slow equilibration leads to pronounced hysteresis. A new technique for vapour pressure measurement in such systems has been developed and used (this is described in chapter 4).

Complimentary techniques have been used, where appropriate, to augment those already mentioned and will be discussed in subsequent chapters. These include Differential Scanning Calorimetry (D.S.C.), Optical Microscopy and Nuclear Magnetic Resonance (N.M.R.).

§ 1.6 References

1 F. Carney and M. Waite, "The Penguin English Dictionary", 1st Edition (1985-6), Penguin Books.

2 T. Davidson, "Chambers's Twentieth Century Dictionary of the English Language", (1902), W & R Chambers Ltd.

3 P. Tooley, "Chemistry in Industry Series; Fats, Oils and Waxes", John Murray, (1971).

4 (i) R.E. Kirk and D.F. Othmer, "Encyclopedia of Chemical Technology", vol. 24, pp 469 *et seq.*, 3rd Edition (1984), John Wiley & Sons.

(ii) Needle penetration test of American Society of Testing Materials - A.S.T.M. D-1321.

5 R.E. Kirk and D.F. Othmer, "Encyclopedia of Chemical Technology", vol. 22, pp 156 *et seq.*, 2nd Edition (1970), John Wiley & Sons.

6 A.H. Warth, "The Chemistry and Technology of Waxes", p.92 *et seq.*, 2nd Edition (1956), Reinhold Publishing Co., New York.

7 L. Chalmers and P. Bathe, "Domestic and Industrial Chemical Specialities", vol.2, p.8 *et seq.*, 2nd Edition (1979), George Godwin Limited, London.

8 P. Sabatier and J.B. Senderenas, **C.R.Hebd.Seances, Acad.Sci.,** 134,514,(1902).

9 (i) F. Fischer and H. Tropsch, **Brennst.Chem.,** 4,276,(1923).

(ii) F. Fischer and H. Tropsch, **Ber.Dtsch.Chem.Ges.,** 59,830,(1926).

10 (i) M. Ritschel and W. Vielstich, **Chem.Eng.Tech.,** 52,327,(1980).

(ii) G. Blyholder and P.H. Emmett, **J.Phys.Chem.,** 64,470,(1960).

(iii) H. Pichler and H. Schulz, **Chem.Eng.Tech.,**42,1162,(1970).

11 Product sales leaflet, Hoechst Aktiengesellschaft, Werk Gersthofen, Postfach 10 15 67, 8900 Augsburg 1, Germany, (1987).

12 R.E. Kirk and D.F. Othmer, "Encyclopedia of Chemical Technology", vol. 3, pp 813 *et seq.*, 4th Edition (1992), John Wiley & Sons.

13 Internal publication, "Shell Hydrocarbon Solvents", Library of Congress classification number TP247.5 S5

14 C. Marsden, "Solvents and Allied Substances Manual; with solubility chart", Cleaver-Hume Publishers, (1954).

15 L. Chalmers and P. Bathe, "Domestic and Industrial Chemical Specialities", vol.2, 2nd Edition (1979), George Godwin Limited, London.

16 Internal Report, reference SPWSBK (issue 2), Reckitt and Colman Household Products Division, Stoneferry Road, Hull, (6/4/89).

Chapter Two

Theoretical Behaviour

Many models are available to describe the conformation of polymer chains. The simplest 'rod-like' model is useful for linear polymer chains with a large length to diameter ratio. Other polymers may be better described by rigid segments connected by free moving joints (Kuhn chains), worm-like chains or mixtures of rod-like segments and random coils.

Flory's lattice theory[1,2], one of the simplest and most widely used, was first developed for rigid rod-like chains and later extended to Kuhn segments[3], mixed rod and random coils[4] and also the effects of polydispersity[5]. Although this theory is based on simple limiting assumptions, it leads to equations which are easily manipulated and can be used to predict theoretical phase behaviour for many systems. A more exact treatment of the lattice theory is available which leads to much more complex equations whilst not improving greatly on the accuracy of prediction[6,7].

The behaviour of non-electrolytes in solution is of paramount importance in this work and so an appraisal of the more pertinent theories in the literature will follow. The most logical progression seems to be to start with the case of ideal solutions of simple non-ionic molecules, along with the introduction of the Gibbs-Duhem equation and then to allow for extensions to analogous polymer systems. These polymer systems are often subject to long diffusion times and so it will be of interest to discuss gelation and phase separation phenomena.

§ 2.1 Ideal Solutions[①]

An ideal solution may be defined in terms of the vapour pressures $p_i°$ and p_i of component i, when pure and when in solution, at mole fraction x_i by $p_i = x_i p_i°$, or in terms of the chemical potentials $\mu_i°$ and μ_i by $\mu_i = \mu_i° + RT \ln x_i$. Consider the mixing of $(1-x_2)$ moles of pure solvent with x_2 moles of pure solute to give 1 mole of an ideal solution. For this process, the change in Gibbs function on mixing is given by

$$\Delta_m G = G_{mixt} - G_1 - G_2 \qquad (2.1)$$

where G_1 = Gibbs function of the solvent,

G_2 = Gibbs function of the solute, and

G_{mixt} = Gibbs function of the mixture.

Now, this latter quantity will be given by the sum of the chemical potentials of the components in the mixture and so

$$G_{mixt} = (1-x_2)\,\mu_1 + x_2\,\mu_2 \qquad (2.2)$$

so, rearranging we obtain the molar Gibbs function on mixing as

$$\Delta_m G = (1 - x_2)\mu_1 + x_2\mu_2 - (1 - x_2)\mu_1° - x_2\mu_2°$$

$$= (1 - x_2)[\mu_1 - \mu_1°] + x_2[\mu_2 - \mu_2°]$$

i.e. $$\boxed{\Delta_m G = RT\,[(1-x_2)\ln(1-x_2) + x_2\ln(x_2)]} \qquad (2.3)$$

The changes in enthalpy, volume, energy and entropy of mixing are given by

---

① The convention adopted throughout this thesis is to use the subscripts 1 and 2 for the solvent and the solute respectively, and x_i to denote the mole fraction of component i $\left(= n_i \Big/ \sum_j n_j \right)$.

$$\Delta_m H = \Delta_m G - T\left(\frac{\partial \Delta_m G}{\partial T}\right)_P \quad \text{i.e. } \Delta_m H = 0 \tag{2.4}$$

$$\Delta_m V = \left(\frac{\partial \Delta_m G}{\partial P}\right)_T \quad \text{i.e. } \Delta_m V = 0 \tag{2.5}$$

$$\Delta_m U = \Delta_m H - P\Delta_m V \quad \text{i.e. } \Delta_m U = 0 \tag{2.6}$$

$$\Delta_m S = -\left(\frac{\partial \Delta_m G}{\partial T}\right)_P \quad \text{i.e. } \boxed{\Delta_m S = -R\left[(1-x_2)\ln(1-x_2) + x_2\ln(x_2)\right]} \tag{2.7}$$

Real systems will deviate from ideality and can be accounted for by using the corresponding relative activities (a) and fugacities (P*) of the components (where the activity coefficient is given by $\gamma = a/x$).

[See also §2.6].

The equations for the ideal solution model emphasise the fact that these properties arise solely from the entropy change on mixing; such mixtures are called athermal.

The systems of interest here also show properties dominated by entropy change; enthalpies of mixing are either zero or not significantly large. The classical theory of such mixtures regards the configurational contributions as fundamental; energetic contributions are then superimposed.

§ 2.2 Gibbs-Duhem equation

The Gibbs-Duhem equation is the basic differential equation relating the various chemical potentials in solution. It can be expressed as

$SdT - VdP + \sum n_i \, d\mu_i = 0$ or in terms of activity coefficients (γ_i) and at constant temperature and pressure as $\sum x_i \, d \ln \gamma_i = 0$. It has an infinite number of solutions and only a few with any physical significance exist. These solutions are often expressed in terms of the partial excess Gibbs function (G_i^E) since they lead directly to activity coefficients via

$$G_i^E = \left[\frac{\partial\left(\Sigma n_i \, G_m^E\right)}{\partial n_i}\right]_{T,P,n_j} = RT \ln \gamma_i \qquad (2.8)$$

Excess functions are useful since they can be estimated directly from molecular models such as regular solution theory. Many semi-empirical models exist for the solution of the Gibbs-Duhem equation and are used for fitting to data.

§ 2.3 Lattice models of solution

Entropic models allow for differences in the arrangement of molecules in solution. The most notable developments have been made by Flory[8–10] and Huggins[11,12] for athermal solutions. The molar excess Gibbs function for the mixing of two components is given by

$$G^E = \Delta_m G^{real} - \Delta_m G^{ideal}$$

Enthalpic terms can be added for non-athermal mixtures and the most significant entropic idea incorporated in the Flory-Huggins approach is the effect of differences in size between the solute and solvent molecules. However, it should be noted that one can also get significant effects due to non-random mixing and association in solution.

Enthalpic models account for the energetic differences between the solutions and their pure components and show varying degrees of success. The strictly regular solution (liquid lattice) model of Guggenheim[13] considers the energy changes involved in exchanging solute and solvent molecules of similar size on a pseudocrystalline lattice. This model is too rigid and rarely applies to real mixtures, although it does provide a good background for the fitting of data with a computer[14] and also allows for extensions into the polymer solution field. Van Laar[15,16] provided a more useful expression for data fitting by the use of van der Waals' equation in relation to mixtures[17]. This gives a basis for the development of regular solution theory as given by Scatchard and Hildebrand[18–20] and provides a generally applicable method for the prediction of properties of a mixture from those of its pure components.

Conventional Flory-Huggins polymer solution theory[21,22] stems from the quasi-lattice model of ideal solutions discussed by Fowler and Rushbrooke[23] for liquid mixtures of elongated molecules which occupy

twice the volume of the solvent molecules and Meyer[24] for longer chain solutes in solvents of simple molecules. Inherent in these treatments are the assumptions of a regular quasi-crystalline lattice in the liquid and the interchangeability of solvent and solute molecules on lattice sites.

The lattice model was first developed[13] for mixtures of molecules sufficiently similar in size as to be interchangeable on lattice sites. This would be precise for an ideal solution for which the volume and energy changes on mixing are zero.

The Boltzmann relation from traditional statistical mechanics[25] leads to the configurational entropy of the mixture as given by

$$S_{mixt} = k \cdot \ln \Omega \qquad (2.9)$$

where k = the Boltzmann constant② (1.3807×10^{-23} J K^{-1} molec^{-1}), and

Ω = the number of ways of arranging n_1 solvent molecules and n_2 solute molecules on the lattice.

If all the particles were distinguishable Ω would be $(n_1 + n_2)!$, but since n_1 of them are identical and n_2 are identical, this leads to

$$\Omega = \frac{(n_1 + n_2)!}{n_1! n_2!} \qquad (2.10)$$

i.e. for $(n_1 + n_2)$ molecules of mixture,

$$S_{mixt} = k \cdot \ln \left[\frac{(n_1 + n_2)!}{n_1! n_2!} \right] \qquad (2.11)$$

Using Stirling's approximation, $N! \cong (N/e)^N$, leads to

② The recommended values of physical constants used throughout this thesis are derived from the CODATA consistent set of constants produced by E.R. Cohen and B.N. Taylor (**J.Res.Nat.Bur.Stds.**, 92,85,(1987)).

$$S_{mixt} \cong - k [n_1 \ln(1-x_2) + n_2 \ln(x_2)] \qquad (2.12)$$

Now, converting to molar quantities, $\Delta_{mix}S = S_{mixt} - S_1 - S_2$ (2.13)

i.e. $$\Delta_m S \cong \left[\frac{N_A}{(n_1 + n_2)}\right] \cdot k \cdot \ln \Omega \qquad (2.14)$$

where N_A is the Avagadro constant (6.0221×10^{23} molec mol^{-1}) and the configurational entropies of the pure substances are zero.

Hence, $$\boxed{\Delta_m S = -R [(1-x_2)\ln(1-x_2) + x_2 \ln(x_2)]} \qquad (2.15)$$

This being the molar entropy for random mixing when a solute forms a solution in a solvent.

This theory assumes that the energy of mixing, or the interchange energy[13], is zero. To look further we must consider the possible interactions of the solute and solvent molecules. Let the co-ordination number of the lattice be given by z and the interaction energy of a molecule **A** with a molecule **B** be represented by w_{AB}. If a solvent molecule is exchanged with a solute molecule, then the interchange energy will be given by the following relationship.

Interchange Energy = change in energy when 2z.(1,2) contacts are made − change in energy when z.(1,1) contacts are broken − change in energy when z.(2,2) contacts are broken

i.e. $$\Delta_{mix}U = 2zw_{12} - zw_{11} - zw_{22}$$

$$= 2z \left[w_{12} - \tfrac{1}{2}(w_{11} + w_{22})\right]$$

or $$\Delta_{mix}U = 2z\Delta w \qquad (2.16)$$

Now, (i) for ideal solutions, the energy of mixing is zero. i.e. $\Delta w = 0$.

(ii) The mixing of chemically similar substances (e.g. hexane and heptane) is found to be endothermic ($\Delta_m H > 0$), though may be very small[26]. Since volume changes in condensed systems do

not contribute significantly, this implies that $\Delta_m U$ is positive and unlike interactions are generally weaker than the arithmetic mean of the like interactions.

(iii) for substances giving rise to strong (1,2) interactions, w_{12} is large and negative so that the heat of mixing may be athermal or increasingly exothermic.

In order to extend the theory now to polymer solutions, the original assumptions are still applied such as the interchangeability of polymer chain segments with solvent molecules. It is also assumed that the polymer molecules are monodisperse, although a more complex treatment allows for variable chain length of the solute[21(ii)].

The expression for Ω is then the number of ways of arranging n_1 molecules of monomer solvent and n_2 r-mer solute molecules on a lattice of n_0 sites, where $n_0 = n_1 + rn_2$. For insertion of the ζ^{th} polymer molecule, the number of vacant sites for the first segment is $n_0 - (\zeta-1)r$. The theory then assumes that the number of sites, α, available for the next segment is (z-1) times the average fraction of sites still vacant. Hence,

$$\alpha = (z-1)\frac{[n_0 - r(\zeta-1)]}{n_0} \qquad (2.17)$$

However, the use of this assumption leads to too large a value for Ω, and the expected number of ways of arranging the ζ^{th} polymer chain, with fixed terminal segment, is more accurately $[z/(z-1)]\alpha^{r-1}$. Hence the total number of ways of arrangement for the polymer chain in the whole lattice is

$$v_\zeta = \frac{1}{2}[n_0 - r(\zeta-1)]\left[\frac{z}{(z-1)}\right]\alpha^{r-1} \approx \frac{1}{2}[n_0 - r(\zeta-1)]\alpha^{r-1} \qquad (2.18)$$

where the '$^1/_2$' is introduced as a symmetry number, since the ends of the polymer molecule are indistinguishable. The total number of arrangements for the system is given by

$$\Omega = \left(\frac{1}{n_2!}\right)\prod_{\zeta=1}^{n_2} v_\zeta \qquad (2.19)$$

where $(1/n_2!)$ eliminates the arrangements which differ only by exchanging one or more pairs of the polymer molecules.

Hence, $$\Omega = \left(\frac{z-1}{n_0}\right)^{n_2(r-1)} \frac{r^{r\,n_2}}{2^{n_2} n_2!}\left[\frac{(n_0/r)!}{(n_1/r)!}\right] \qquad (2.20)$$

Using Stirling's approximation and rearranging leads to

$$\Omega = \left[(z-1)^{n_2(r-1)}\left(\frac{r}{2e^{r-1}}\right)^{n_2}\right]\left[\left(\frac{n_0}{n_1}\right)^{n_1}\left(\frac{n_0}{r\,n_2}\right)^{n_2}\right] \qquad (2.21)$$

Hence for the configurational entropy of mixing, given by $S_{conf} = k\cdot\ln\Omega$, we obtain

$$S_{conf} = kn_2\left[(r-1)\ln\left(\frac{z-1}{e}\right)+\ln\left(\frac{r}{2}\right)\right]-k[n_1\ln\varphi_1+n_2\ln\varphi_2] \qquad (2.22)$$

where φ_1 and φ_2 are volume fractions, given by $\varphi_1 = \frac{n_1}{n_0}$ and $\varphi_2 = \frac{r\,n_2}{n_0}$

Looking at the two terms in equation (2.22) separately[27], the former term represents the entropy of disorientation of the pure liquid polymer, and the latter takes into account the effect of dilution. This latter term is called the combinatorial entropy of mixing and arises from the greater volume over which the molecules of both components are distributed in the mixture as opposed to the pure components. The geometry of the solute chain is of little importance, for large r, as far as the mixing entropy for formation of the

random solution is concerned. For this reason, the entropy of mixing n_1 molecules of solvent with n_2 molecules of solute to give $(n_1+ n_2)$ molecules of mixture is treated simply as

$$S_{comb} = - k (n_1 \ln \varphi_1 + n_2 \ln \varphi_2) \qquad (2.23)$$

Partial differentiation and conversion to molar quantities yields

$$\boxed{\Delta_{comb}S_1 = -R\left[\ln(1-\varphi_2)+\varphi_2\left(1-\frac{1}{r}\right)\right]} \qquad (2.24a)$$

$$\left(\text{and} \quad \Delta_{comb}S_2 = -R\left[\ln\varphi_2 +(1-\varphi_2)(1-r)\right]\right) \qquad (2.24b)$$

For polymer solutions, where the two components are far from similar, the interchange energy will have to be calculated as follows.

The number of contacts per polymer molecule is given by $[(z-2)r+2]$, which is approximately zr for large r, and the chance of a neighbour being a solvent molecule is $[n_1/n_0]$, so that the number of (1,2) contacts per r-mer is $[zr(n_1/n_0)]$. Hence the energy arising from the (1,2) contacts of n_2 r-mer molecules is $[n_2zr(n_1/n_0)w_{12}]$. Similarly for the (2,2) contacts we have $[(1/2)n_2zr(rn_2/n_0)w_{22}]$ and $[(1/2)n_1z(n_1/n_0)w_{11}]$ for the (1,1) contacts.

Hence, $$U_{mixt} = \frac{z}{n_0}\left(\frac{1}{2}n_1^2w_{11}+\frac{1}{2}r^2n_2^2w_{22}+n_1n_2rw_{12}\right) \qquad (2.25)$$

Now, the energies for the pure substances are given by

$$U_1 = \frac{1}{2}n_1zw_{11} \quad \text{and} \quad U_2 = \frac{1}{2}r\,n_2zw_{22} \qquad (2.26)$$

so for $\Delta_{mix}U = U_{mixt} - U_1 - U_2$ we obtain by substitution,

$$\Delta_{mix}U = \frac{zr\,n_1n_2\Delta w}{n_0} \qquad (2.27)$$

and since $\Delta_m U = \Delta_m H$ for $\Delta_m V = 0$ we have, on conversion to molar quantities,

$$\Delta_m H = z\Delta w\, x_1\, \varphi_2 N_A \qquad (2.28)$$

which is simply a van-Laar enthalpy of mixing[15,16]. Partial differentiation with respect to component 1 leads to

$$\Delta_m H_1 = z\Delta w \varphi_2^2 N_A \qquad (2.29)$$

Flory[27] defines the parameter χ as $z\Delta w/kT$. Hence, the change of partial molar Gibbs function for the solvent is given by

$$\Delta_m G_1 = \mu_1 - \mu_1^\circ = RT\left[\ln(1-\varphi_2)+\varphi_2\left(1-\frac{1}{r}\right)+\chi\varphi_2^2\right] \qquad (2.30)$$

But,
$$\mu_1 - \mu_1^\circ = RT\ln(a_1) = RT\ln\left(\frac{P_1^*}{P_1^{\circ *}}\right) \qquad (2.31)$$

where a is the activity and P* and P°* are the fugacities of the solvent in the presence of the solute and of the pure solvent respectively.

This treatment has considered the mixing of n_2 r-mer solute molecules and n_1 molecules of monomer solvent, but the systems we will be investigating would be better described by considering the mixing of n_2 molecules of r_2-mer solute with n_1 r_1-mer solvent molecules. Here the solvent is treated as a chain molecule itself and the strategy gives,

$$\ln\left(\frac{P_1^*}{P_1^{\circ *}}\right) = \left[\ln(1-\varphi_2)+\varphi_2\left(1-\frac{1}{\rho}\right)+\chi\varphi_2^2\right] \qquad (2.32)$$

where $\rho = r_2/r_1$. For the present study, this equation has been used in the form,

$$\ln\left(\frac{P_1^*}{P_1^{\circ *}}\right)=\left[\ln(1-\varphi_2)+\varphi_2\left(1-\frac{1}{\rho}\right)+\frac{w'}{kT}\varphi_2^2\right] \qquad (2.33)$$

where w' is an interaction energy per molecule and equal to [zΔw].

This theory has been shown[28] to be successful in fitting experimental data for equilibrium properties of liquid mixtures of the kind studied in this thesis. The dominant effect is the influence of chain length, given by the first two terms, from configurational entropy, in equation 2.33. The energetic contribution in the third term is small but may become significant at low temperature.

§ 2.4 Solubility

Assuming the solid phase to be pure crystalline solid wax, for equilibrium in the saturated solution at temperature T,

$$\mu_2^L(T)=\mu_2^S(T) \qquad (2.34)$$

where the superscripts S and L signify the solid and liquid phase respectively, and μ_2 is the chemical potential of the wax component. Hence, in terms of component 2, the equivalent form of equation (2.33) for the liquid mixture becomes

$$\frac{\mu_2^S-\mu_2^{\circ L}}{RT}=\left[\ln\varphi_2+(1-\varphi_2)(1-\rho)+\left(\frac{\rho w'}{kT}\right)(1-\varphi_2)^2\right] \qquad (2.35)$$

or by differentiating with respect to (1/T), assuming w' to be independent of temperature, gives

$$\frac{H_2^S - H_2^L}{R} = \frac{d}{d(1/T)}[\ln\varphi_2 + (1-\varphi_2)(1-\rho)] + \frac{\rho w'}{k}(1-\varphi_2)^2 + \frac{\rho w'}{kT}\frac{d}{d(1/T)}(1-\varphi_2)^2 \qquad (2.36)$$

Rearranging leads to

$$-\int_{1/T_m}^{1/T}\left(\Delta_f H_2^\circ + (1-\varphi_2)^2 N_A \rho w'\right)d(1/T) = R[\ln\varphi_2 + (1-\varphi_2)(1-\rho)] + \frac{N_A \rho w'}{T}(1-\varphi_2)^2 \qquad (2.37)$$

where $\Delta_f H_2^\circ = H_2^L - H_2^S$ = the partial molar enthalpy of fusion of pure wax.

Hence, for the particular case of an athermal mixture, w'=0 and

$$\frac{d}{d(1/T)}[\ln\varphi_2 + (1-\varphi_2)(1-\rho)] = -\frac{\Delta_f H_2^\circ}{R} \qquad (2.38)$$

or

$$\ln\varphi_2 + (1-\varphi_2)(1-\rho) = -\frac{\Delta_f H_2^\circ}{R}\left(\frac{1}{T} - \frac{1}{T_m}\right) \qquad (2.39)$$

§ 2.5 Application to the vapour pressure apparatus

The sample will be liquid above the cloud point (T_m), and for equation (2.33) we have

$$\ln P_1^* = \ln P_1^{\circ *} + \left[\ln(1-\varphi_2) + \varphi_2\left(1-\frac{1}{\rho}\right) + \frac{w'}{kT}\varphi_2^2\right] \qquad (2.40)$$

At, and below, the cloud point we expect the solubility equation (2.37) to apply in the form presented below

$$-\left(\frac{\Delta_f H_2^\circ}{R} + \frac{(1-\varphi_2)^2 \rho w'}{k}\right)(1/T - 1/T_m) = \ln\varphi_2 + (1-\varphi_2)(1-\rho) + \frac{\rho w'}{kT}(1-\varphi_2)^2 \qquad (2.41)$$

The results are often shown on a $\ln(P_1^*)$ vs $^1/_T$ plot as represented in figure 2.1. The vapour pressure of the pure solvent is given by the solid straight line and the red cloud point curve is calculated from equations 2.40

and 2.41. Values of φ_2 are incremented and the calculations performed using known values for $\Delta_f H_2°$, T_m and the assumption that w' = 0.

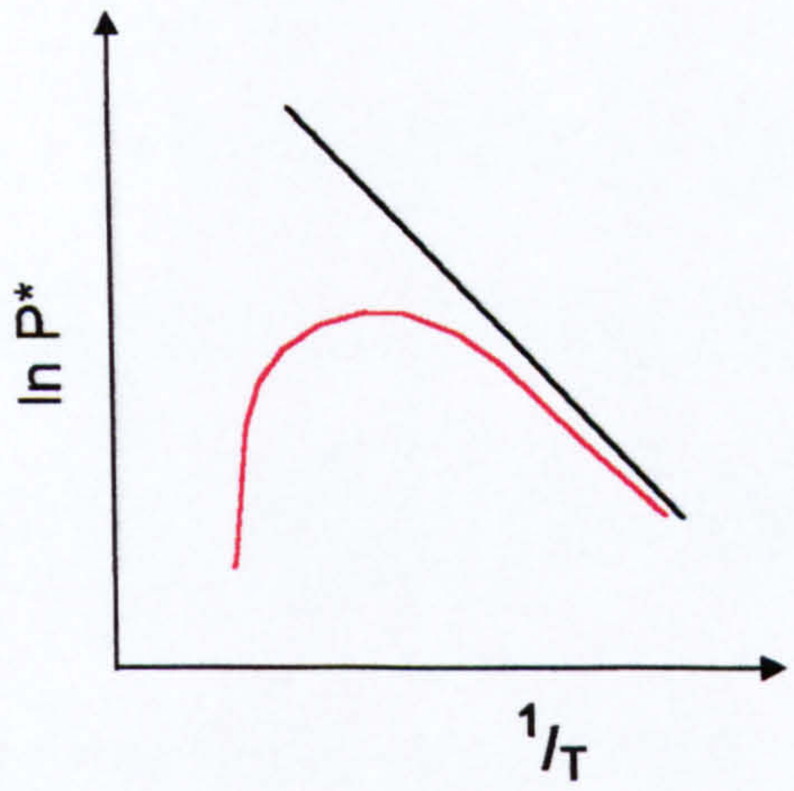

Figure 2.1 *Typical cloud point curve.*

§ 2.6 Correction of vapour pressure measurements for gas imperfections

An **extensive** property (such as G, S, **V** etc.) will, by definition[29], depend on the amounts of constituents of the system as well as its state (i.e. T and P). So, for example,

$$dG = \left(\frac{\partial G}{\partial T}\right)_{P,n_1,n_2\cdots} dT + \left(\frac{\partial G}{\partial P}\right)_{T,n_1,n_2\cdots} dP + \left(\frac{\partial G}{\partial n_1}\right)_{T,P,n_2\cdots} dn_1 + \cdots \qquad (2.42)$$

but, $dG = -SdT + VdP + \sum \mu_i dn_i$ and so

$$V = \left(\frac{\partial G}{\partial P}\right)_{T,n_1,n_2\cdots} \quad \text{or for one mole of pure substance} \quad V = \left(\frac{\partial \mu}{\partial P}\right)_T \qquad (2.43)$$

Now, for an ideal gas we have PV = RT, hence substitution for **V** into equation (2.43) and integrating leads to

$$\mu - \mu^{\ominus} = RT \ln P - RT \ln P^{\ominus} \qquad (2.44)$$

where the standard state chosen for $P^{\ominus}$ is 1 atm[③] . However, for a real gas, the corresponding equation of state would be given by a power series in terms of volume

$$\text{i.e. } PV = RT\left[1+\frac{B}{V}+\frac{C}{V^2}+\ldots\right].$$

Or, inverting to give a series in terms of pressure i.e.

$$PV = RT\left[1+B\left(\frac{P}{RT}\right)+\frac{1}{2}\left(C-B^2\right)\left(\frac{P}{RT}\right)^2+\cdots\right] \qquad (2.45)$$

where B, C, etc. are called the second, third, etc. virial coefficients and are functions of temperature. Clearly, at low pressures (< 1 atm), the terms in P^2 and above on the right hand side of equation (2.45) are negligible and the equation simplifies to

$$PV = RT + BP \qquad (2.46)$$

or, by rearrangement and differentiation with respect to pressure at constant temperature leads to

$$BdP = VdP - RT(dP/P) \qquad (2.47)$$

We may define the fugacity (P*) by

$$\mu - \mu^{\ominus} = RT \ln P^* - RT \ln P^{*\ominus} \qquad (2.48)$$

which on differentiating affords

$$VdP = RT\, d \ln P^* \qquad (2.49)$$

Substitution of this back into equation (2.47) and rearranging gives

$$RT\, d \ln P^* = RT\, d \ln P + BdP \qquad (2.50)$$

---

③ where 1 atm ≙ 760 Torr ≙ 101325 Pa.

Hence, the fugacity is obtained for measured pressure by the equation④

$$\ln P^* = \ln P + \frac{BP}{RT} \qquad (2.51)$$

where the data for the second virial coefficient for heptane is taken from McGlashan and Potter[30] and is then custom fitted to various functions using the Levenberg - Marquardt method[31] for a least squares minimisation of the sum of the squared residuals. The best fit, as given by $\left|\sqrt{\Sigma\Delta^2/n}\,/\bar{y}\right|$, was afforded by the function

$$\frac{B}{cm^3mol^{-1}} = a + \frac{b}{(T/K)^2} + \frac{c}{(T/K)^6} \qquad (2.52)$$

where $a = 4.0802\times10^{2}\ cm^3mol^{-1}$

$b = -2.4549\times10^{8}\ cm^3mol^{-1}K^2$

$c = -3.9514\times10^{17}\ cm^3mol^{-1}K^6$

and the standard error in each constant is calculated to be 2×10^{-4} %.

§ 2.7 Phase separation phenomena

A particular concern of the work described in the thesis is the behaviour when the systems are cooled to temperatures below the region of homogeneous liquid phase. The time scale of the process then becomes involved because, owing to the complexity of the substances involved, thermodynamic equilibrium may, or may not, be achieved.

---

④ For low pressures where the condition $\ln(P^*/P) \approx (P^*/P) - 1$ is valid then $(P^*/P) = 1 + (PB/RT) = (PV/RT) \Rightarrow P^* = (P^2V/RT)$

The equilibrium theory discussed above can apply in two cases; either the formation of regular crystals of solid, when the solubility equations apply, or to liquid - liquid phase separation. In the latter case the above theory can still apply. If the interaction term w' in equation 2.33 is negligible or zero, mixing will be athermal, the distribution of molecular segments on the assumed lattice will be random and liquid - liquid phase separation will not occur. Similarly a negative contribution from w', corresponding to enhanced solvent - solute interaction, will give a lower vapour pressure and the homogeneous bulk solution will still be stable. If, on the other hand, the interaction between solute and solvent is weak, (the solvent is a "poor" one), then w' will be positive, mixing will be endothermic and the vapour pressure will be increased. The mixing of very similar substances, such as hydrocarbons, is usually weakly endothermic. If w' is sufficiently large and positive however, the liquid will separate into two phases, each containing an increased concentration of one or other of the components. This will occur below a critical temperature, T_c, the value of which can be predicted by lattice theory depending on the assumptions made in the model. The number of contacts of various kinds, for a given value of w', are found by minimising the free energy in the normal way. The necessary algebra is well described in the literature[28] and leads to the conditions for critical mixing that $w'/kT_c = ½$ for infinite coordination number of the assumed lattice, or $w'/kT_c = 0.669$ for the simple cubic coordination number of 6.

Although thermodynamic equilibrium is sometimes shown to be achieved in the work described here, and in polymer mixtures in general, quite often it is not. Empirical interpretation of the observations then becomes necessary.

The phase diagram of a polymer solution often shows biphasic regions where the solution separates into a polymer-rich phase and a solvent-rich phase. At one extreme, complete separation into two layers can result from a classical nucleation and growth type of mechanism. More common for polymer solutions is the process of spinodal decomposition[32]. Here phase separation occurs as each component of the system spontaneously diffuses towards regions of higher concentration. Figure 2.2(b) shows a typical phase diagram for a simple binary system. Above the binodal curve the system exists as a thermodynamically stable homogeneous solution. Below the solid curve the system is stable when separated into two phases. Part of this region lies between the binodal and spinodal curves in which there is an energy barrier to phase separation. In this metastable region a small amount of the stable phase may form providing a nucleus for growth to occur and result in complete phase separation[33]. Inside the spinodal curve the system is thermodynamically unstable and the shape of the Gibbs function curve (Figure 2.2(a)) within this region favours spontaneous diffusion of each component toward increasing concentrations until the system completely separates[34].

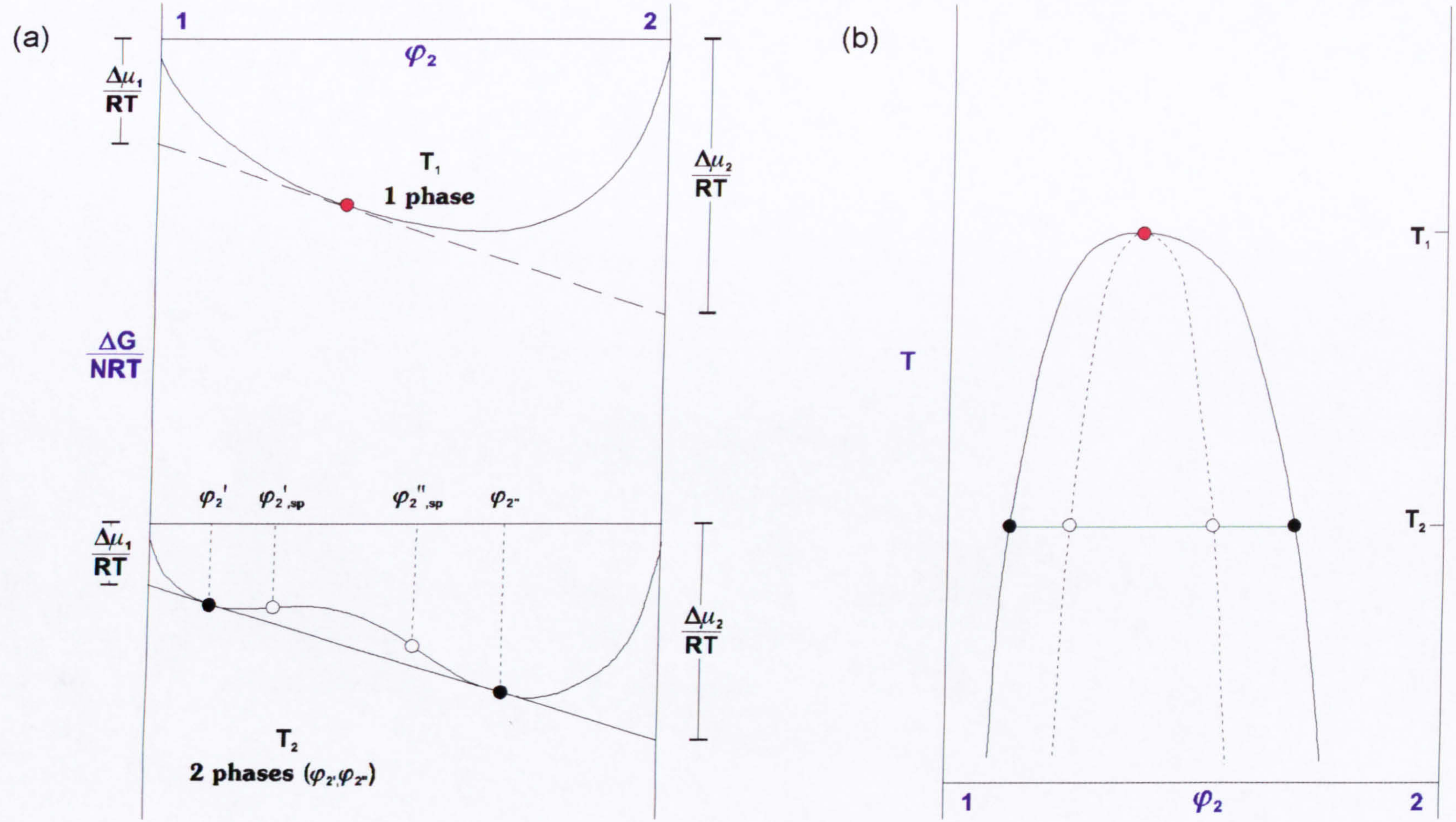

Figure 2.2 *(a) Change in Gibbs function of mixing two components as a function of volume fraction of polymer (b) Phase diagram with binodal (——), spinodal (- - - -), critical point (●) and tie line (●——●).*

The binodal curve is evaluated by equating the chemical potentials of each phase whereas the spinodal is often determined by letting $\frac{\delta\mu}{\delta\varphi}\left(=\frac{\delta^2 G}{\delta\varphi^2}\right)=0$. Only systems which have both a continuous Gibbs function vs composition curve and continuous first derivatives below a certain critical temperature will have a spinodal. Figure 2.3 shows a three dimensional representation of a mixture undergoing spinodal decomposition with each phase being continuous.

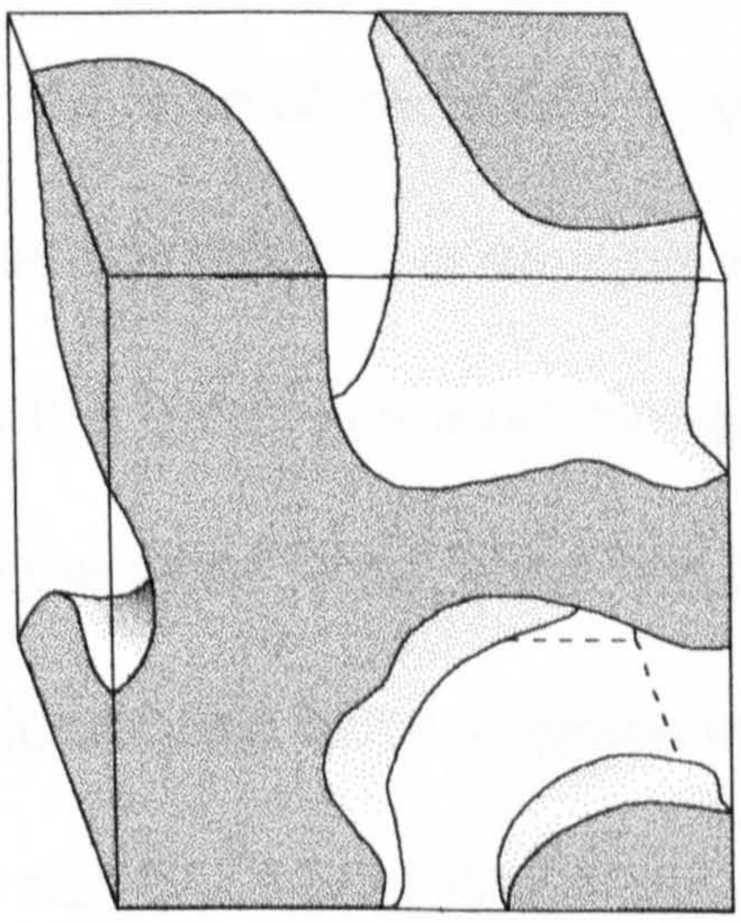

Figure 2.3 *Three dimensional representation of spinodal decomposition.*

Certain systems may exhibit phase separation by both the nucleation and growth mechanism and also the spinodal decomposition mechanism[35]. The rate of quenching into the unstable region of the phase diagram can often bypass one mechanism in favour of the other.

Phase separation by spinodal decomposition may not be a uniform process and regions of high concentration of polymer may lead to

entanglement of the chains which forms a physical barrier to further phase separation and hold the system in this non-equilibrium state for considerable periods of time.

§ 2.8 Gelation

When these wax / solvent systems are cooled they may crystallise, but quite often they form a gel. The definition of a gel is not a trivial matter and the author draws the attention of the reader to various attempts in the literature[36,37]. One of the main characteristics usually ascribed to a bulk gel is that it exhibits solid-like behaviour even though it may consist mostly of liquid. Structurally, on the other hand, a gel can be considered to consist of a three dimensional microscopic network which extends to a macroscopic scale. Many subclasses can be divised for this broad definition and table 2.1 summarises that of Flory[38].

Gelation can arise, for the examples in case two, via the irreversible formation of point junctions in the form of chemical bonds (see figure 2.4). Once created, the network can only be broken by extreme conditions such as thermal decomposition. These structures fit well within the realms of the more classical theories of gelation[39,40].

Subclass	Common Examples
Well-ordered lamellar structures	Clays, phospholipids, soaps and other mesophases
Completely disordered covalent polymeric networks (Often undergo swelling in suitable solvents)	Vulcanised rubbers, elastin, phenolic resins, polysilicic acids, cross-linked polystyrene gels, etc.
Polymer networks formed via physical aggregation (mainly disordered regions bound through the formation of crystallites)	Gelatin in ethylene glycol, vinylidene / methacrylate copolymers, poly-(vinyl acetate) gels, etc.
Disordered particulate structures	protein aggregates, flocculent precipitates (e.g. V_2O_5)

Table 2.1 *Structural subclassification of gels.*

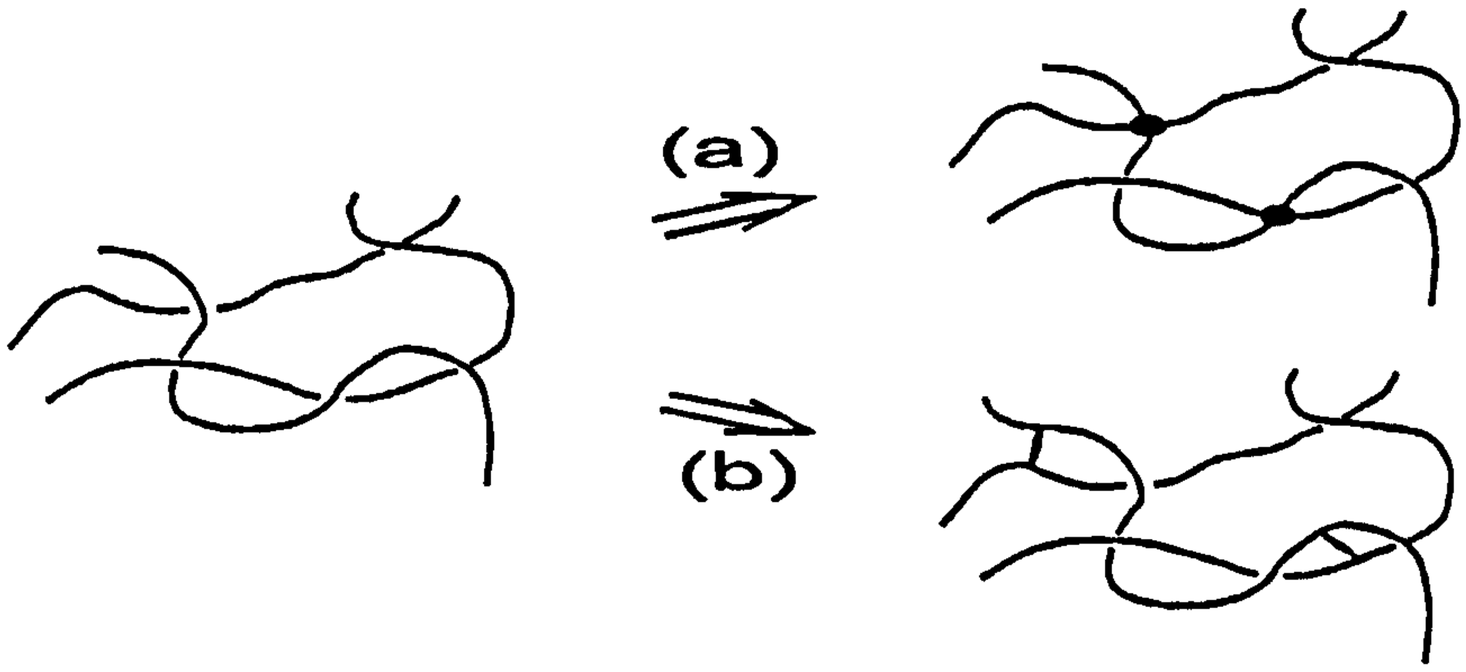

Figure 2.4 *(a) Cross-linking by chemical reaction of polymers alone. (b) Bridge formation of polymers with different species.*

Alternative views of the structures afforded by some types of gel include (i) continuous networks composed of distinct domains of different polymer concentration and (ii) networks formed by the geometric interlinking or "knotting" of polymer molecules (see figures 2.5 and 2.6).

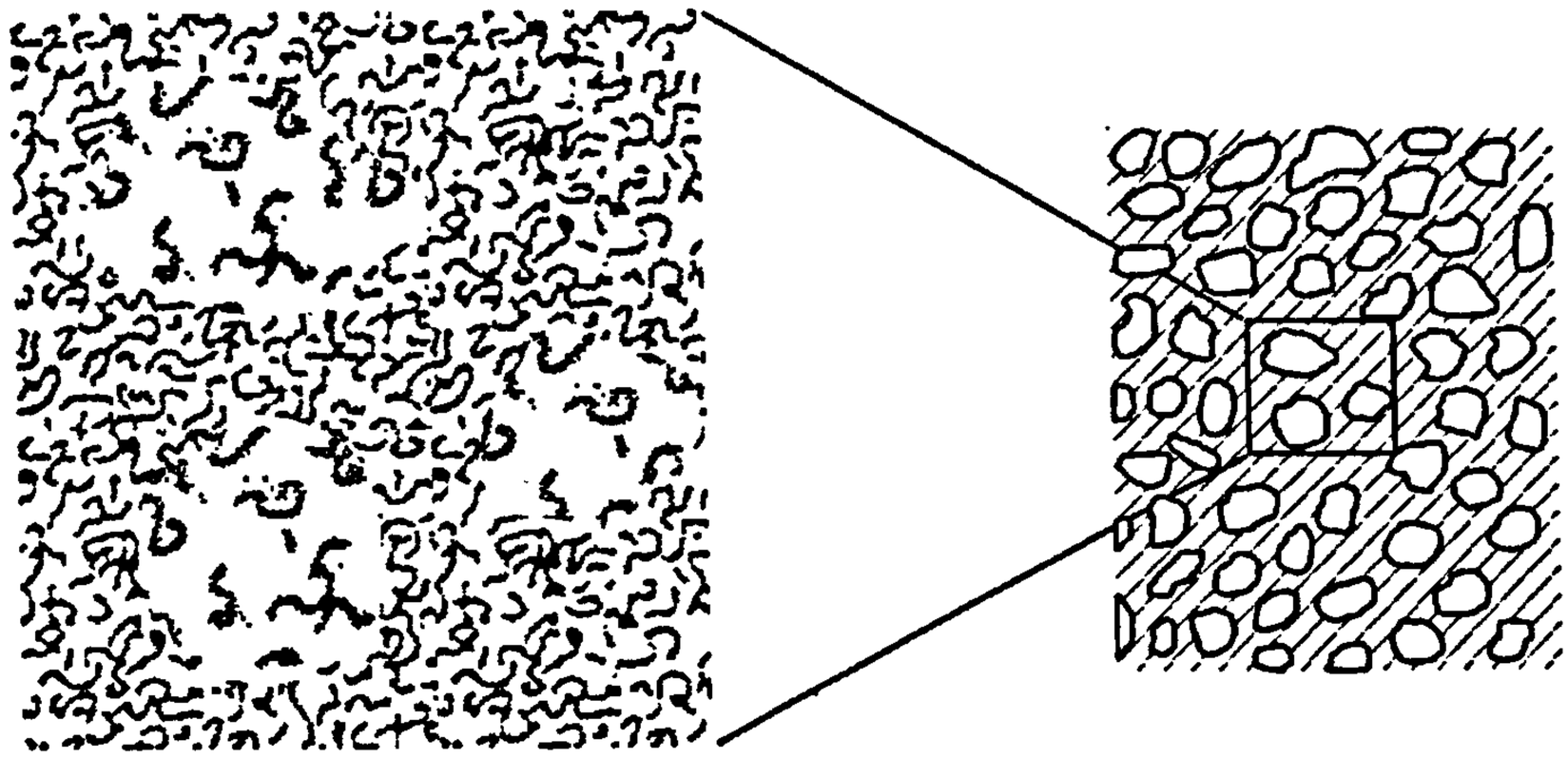

Figure 2.5 *Network formed by continuous polymer-rich phase.*

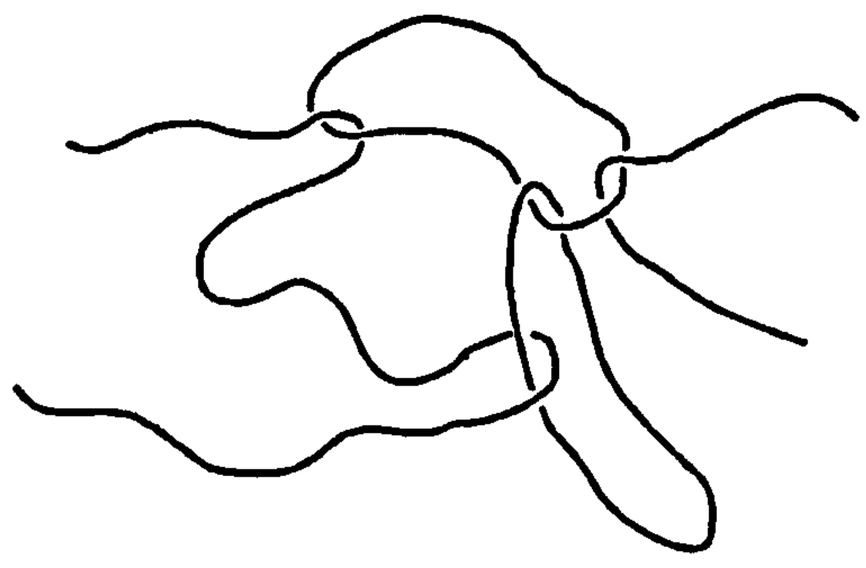

Figure 2.6 *Pictorial view of a topological knot.*

When a solution of linear, high molecular weight polymer is formed in a solvent, a paste with solid-like characteristics often results. This gel is easily broken by agitation but soon reforms when the external force is removed. The reversible change in consistency caused by mechanical strain is known as ***thixotropy*** (from the Greek '*change by touch*'). Frequently, such gels also undergo ***syneresis***; i.e. sweating or exudation of solvent accompanied by a contraction of the gel. These networks are obviously meta-stable states and may be schematically represented as in figure 2.7 showing the coexistence of both crystallites and amorphous regions.

Figure 2.7 *Representation of crystallites as junctions in a network.*

§ 2.9 References

1 P.J. Flory, **Proc.Roy.Soc.**, A234,73,(1956)

2 P.J. Flory, **Proc.Roy.Soc.**, A234,60,(1956)

3 P.J. Flory, **Macromolecules**, 11,1141,(1978)

4 P.J. Flory, **Macromolecules**, 11,1138,(1978)

5 P.J. Flory, **Macromolecules**, 11,1119,(1978)

6 P.J. Flory and G. Ronca, **Mol.Cryst.Liquid Cryst.**, 54,289,(1979)

7 P.J. Flory, **Adv.Polym.Sci.**, 59,1,(1983)

8 P.J. Flory, **J.Chem.Phys.**, 9,660,(1941).

9 P.J. Flory, **J.Chem.Phys.**, 10,51,(1942).

10 P.J. Flory, "Principles of Polymer Chemistry", Cornell U.P., New York, (1953).

11 M.L. Huggins, **J.Chem.Phys.**, 9,440,(1941).

12 M.L. Huggins, **Ann.N.Y.Acad.Sci.**, 43,1,(1942).

13 E.A. Guggenheim, "Mixtures", Chapter 3, Oxford U.P. (1952).

14 O. Redlich, A.T. Kister and C.E. Turnquist, **Chem.Eng.Progr. Symp.Ser.**, 48(2),49,(1952).

15 J.J. van Laar, **Z.Phys.Chem.**, 72,723,(1910).

16 J.J. van Laar, **Z.Phys.Chem.**, 185,35,(1929).

17 H.C. Carlson and A.P. Colburn, **Ind.Eng.Chem.**, 34,581,(1942).

18 J.H. Hildebrand, J.M. Prausnitz and R.L. Scott, "Regular and Related

Solutions", Van Nostrand Reinhold, New York, (1970).

19 J.H. Hildebrand and R.L. Scott, "Regular Solutions", Prentice–Hall, New Jersey, (1962).

20 J.H. Hildebrand and R.L. Scott, "The Solubility of Nonelectrolytes", 3rd Edition, Dover, New York, (1964).

21 (i) P.J. Flory, **J.Chem.Phys.,** 12,425,(1944).

(ii) P.J. Flory, **J.Chem.Phys.,** 13,453,(1945).

22 M.L. Huggins, **J.Phys.Chem.,** 23,1063,(1940).

23 (i) R.H. Fowler and G.S. Rushbrooke, **Trans.Farad.Soc.,** 33,1272,(1937).

24 (i) K.H. Meyer, **Helv.Chim.Acta.,** 23,1063,(1940).

25 E.A. Guggenheim, "Thermodynamics", 5th revised edition, p63, North–Holland Publishing Company, Amsterdam, (1967).

26 (i) J.S. Rowlinson and F.L. Swinton, "Liquids and Liquid Mixtures", 3rd Edition, p149, Butterworth Scientific, London, (1982).

(ii) M.L. McGlashan and K.W. Morcom, **Trans.Farad.Soc.,** 57,581,(1961).

27 P.J. Flory, **Disc.Farad.Soc.,** 49,7–29,(1970).

28 E.A. Guggenheim, "Mixtures", Chapter 12, Oxford U.P. (1952).

29 S. Glasstone, "Textbook of Physical Chemistry", p186, 2nd Edition, Macmillan and Co., London, (1962).

30 M.L. McGlashan and D.J.B. Potter, **Proc.Roy.Soc.,** A267,478,(1962).

31 D.M. Marquardt, **J.Soc.Indust.Appl.Math.,** 11,431,(1963).

32 J.W. Cahn, **Trans.Mettalurg.Soc.AIME**, 242,166,(1968).

33 J.W. Cahn, **J.Chem.Phys.**, 42,93,(1965).

34 (i) J.W. Cahn and J.H. Hilliard, **J.Chem.Phys.**, 28,258,(1958).

(ii) J.W. Cahn and J.H. Hilliard, **J.Chem.Phys.**, 31,688,(1959).

35 G.T. Feke and W. Prins, **Macromolecules**, 7(4),527–530,(1974).

36 H.G. Bungenberg de Jong, "Colloid Science II", Ed. H.R. Kruyt, Elsevier Publ. Co., Inc., Amsterdam, p 2, (1949), *et seq.*

37 P.H. Hermans, "Colloid Science II", Ed. H.R. Kruyt, Elsevier Publ. Co., Inc., Amsterdam, pp 483–494, (1949), *et seq.*

38 P.J. Flory, **Farad.Disc.Chem.Soc.,** 57,7–18,(1974).

39 P.J. Flory, **J.Amer.Chem.Soc.,** 63,3083,(1941).

40 W.H. Stockmayer, **J.Chem.Phys.,** 11,45,(1945).

Chapter Three

Solubility Studies

§ 3.1 Solubility of dotriacontane

Solubility measurements provide a quick and easy method to determine the ideality or otherwise of solutions of various solutes. The temperature dependence of the solubility allows the determination of the heat of solution. For ideal solutions this is equal to the heat of fusion of the pure solute. Usually, the difference between the two heats gives the heat of mixing of the two components which is non-zero for non-ideal solutions. The data for the cloud point temperature of dotriacontane in heptane is given in table 3.1, and figure 3.1 shows the temperature dependence of the solubility along with the behaviour predicted for ideal solutions (solid lines calculated from the heats of fusion and transition measured by Differential Scanning Calorimetry – D.S.C.[1]). Namely, equation 3.1, with the assumption that w' = 0.

$$-\left(\frac{\Delta_f H_2^o}{R}+(1-x_2)^2\frac{w'}{k}\right)\left(\frac{1}{T}-\frac{1}{T_m}\right)=\ln x_2+\frac{w'}{kT}(1-x_2)^2 \qquad (3.1)$$

x_{32}	T / °C	ln x_{32}	10^3K/T
0.0104	32.4	-4.5659	3.2724
0.0142	34.9	-4.2545	3.2461
0.0218	36.6	-3.8258	3.2283
0.0326	40.1	-3.4234	3.1917
0.0534	44.6	-2.9299	3.1465
0.0964	48.5	-2.3392	3.1083
0.1524	51.0	-1.8812	3.0841
0.3287	57.6	-1.1126	3.0233

Table 3.1 *Solubility of dotriacontane in heptane.*

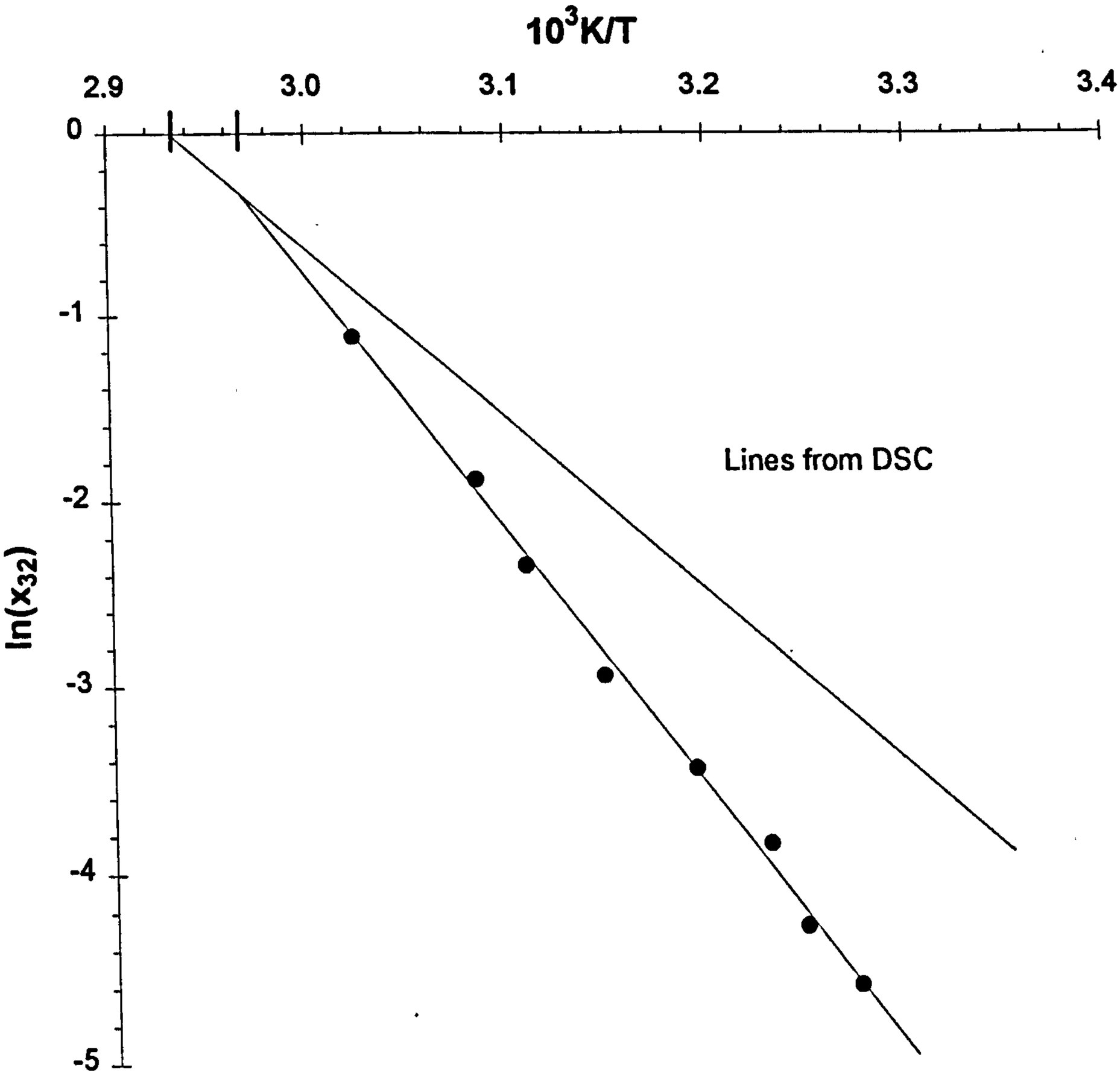

Figure 3.1 *Solubility of dotriacontane in heptane.*

The graph is linear so that terms in $(1-x_2)^2$ are insignificant and w' = 0 for this system. The blue line in figure 3.1 indicates the melting point as determined by D.S.C.[1] and the red line corresponds to the temperature of a pre-melting transition. From the graph it can be concluded that the heat of fusion, $\Delta_f H_2°$ = 115 ± 3 kJmol^{-1} and the melting point, T_m = 339.9 ± 0.6 K for the form of the solute which is stable in the experimental range of temperature (i.e. the β form - see chapter 6). These compare well with values in the literature ranging from 106 to 117 kJmol^{-1} and 339 to 343 K[1-4]. Treatment of the

data using the corresponding polymer solution equation (i.e. 2.41), gives a straight line of steeper slope ($\Delta_f H_2° = 160 \pm 7$ kJmol^{-1}, $T_m = 340 \pm 1$ K) which compares to literature values of 152 kJmol^{-1} and 340 K[3].

§ 3.2 Solubility of Nippon-Seiro wax

Nippon-Seiro (140/145) is a commercial paraffin wax of Japanese origin which melts in the temperature range 140–145°F. It consists mainly of straight chain alkanes (~95%) in the carbon number range 20–40, with the main impurity being the 2-methyl derivatives. Figure 3.2 shows the carbon number distribution of a typical wax sample by Gas Chromatography (G.C.) using the conditions given in table 3.2.

Column	1.85m x 2mm i.d. stainless steel, 5% OV-1 on Supelcoport (85/100).
Temperatures	Detector 400°C Injection port 375°C Oven 120°C (0 mins.) ramp @ 5°Cmin^{-1} 325°C (20 mins.)
Carrier gas	30 cm^{3}min^{-1} of Helium.
Sample	1 μl of solution made up from 0.5g wax in 10 cm^3 heptane.

Table 3.2 *Gas chromatography conditions for Nippon-Seiro (140/145) paraffin wax.*

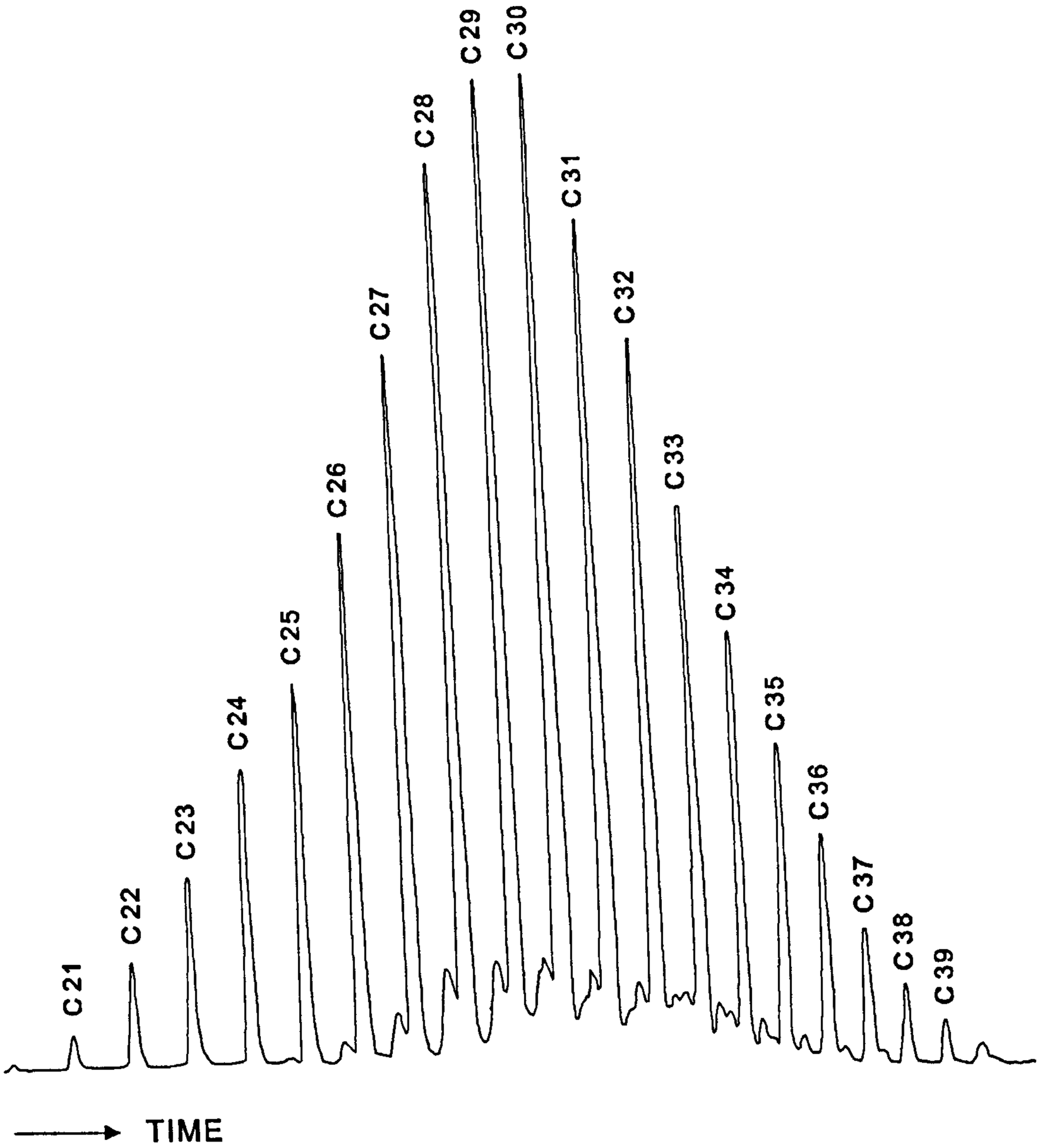

Figure 3.2 *Gas chromatograph of Nippon Seiro (140/145) paraffin wax.*

Integration of the peak areas and calculation of the carbon number distribution using the formula

$$\text{Carbon number } (n/\%) = \frac{\text{Area beneath peak n}}{\text{Total area}} \times 100 \qquad (3.2)$$

leads to an average carbon number ($\bar{n}$) of 29.79 and hence a mean molecular weight of 419.87 $gmol^{-1}$ (assuming an overall stoichiometry of $C_{\bar{n}}H_{2\bar{n}+2}$).

As noted in §1.5, solubility studies are complicated by the fact that the wax solutes include a range of molecular weight so that fractionation of the

solute occurs in equilibrium with solvent. Hence, homogeneous solutions of known weight fractions of wax in hot solvent were made and on cooling their cloud points recorded. Figure 3.3 shows the solubility of Nippon Seiro (140/145) paraffin wax in heptane (●), cyclohexane (x), acetone (Δ) and toluene (o) together with the behaviour predicted for ideal solutions (solid and dashed lines - calculated from the heats of fusion and transition as measured by D.S.C.[5]). The data are presented in table 3.3.

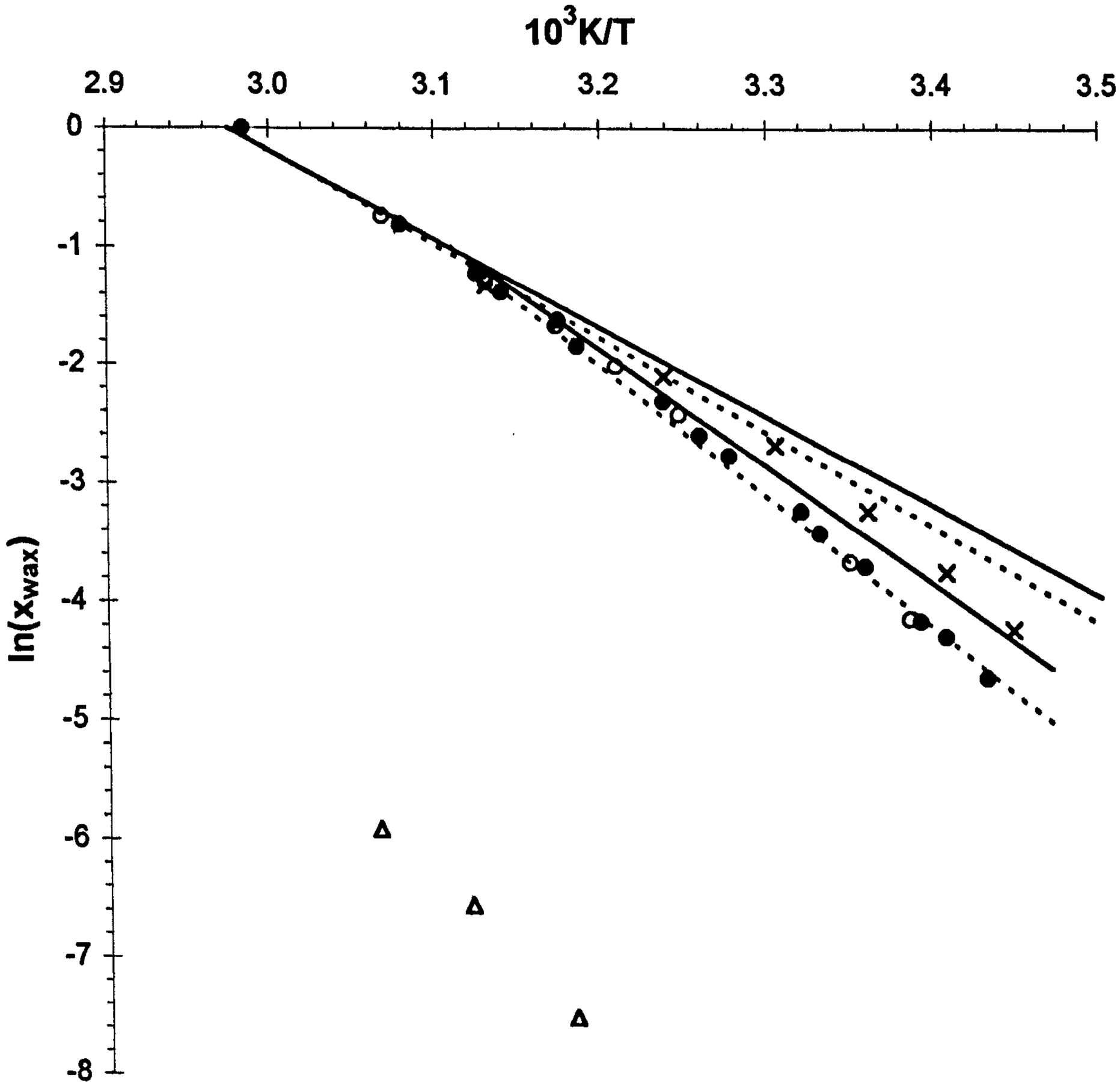

Figure 3.3 *Solubility of Nippon Seiro (140/145) paraffin wax in various solvents.*

$\ln(x_{wax})$	$\ln(\varphi_{wax})+(1-\varphi_{wax})(1-\rho)$	$10^3K/T$
-1.3815	-1.8719	3.1407
-1.8425	-2.6178	3.1857
-2.3023	-3.3462	3.2373
-2.7630	-4.0320	3.2765
-3.2240	-4.6652	3.3201
-3.6844	-5.2489	3.3580
-4.1445	-5.7935	3.3910
-4.6057	-6.3111	3.4305

Table 3.3a *Solubility of Nippon Seiro (140/145) paraffin wax in heptane.*

$10^3K/T$	$\ln(x_{wax})$	$\ln(\varphi_{wax})+(1-\varphi_{wax})(1-\rho)$
3.0689	-0.7411	-2.4452
3.1311	-1.2969	-3.6626
3.1733	-1.6674	-4.3087
3.2089	-2.0115	-4.8317
3.2467	-2.4085	-5.3714
3.3489	-3.6524	-6.8238
3.3844	-4.1288	-7.3322

Table 3.3b *Solubility of Nippon Seiro (140/145) paraffin wax in toluene.*

$10^3K/T$	$\ln(x_{wax})$	$\ln(\varphi_{wax})+(1-\varphi_{wax})(1-\rho)$
3.0644	-5.9020	-9.1490
3.1200	-6.5372	-9.7884
3.1822	-7.4900	-10.7441

Table 3.3c *Solubility of Nippon Seiro (140/145) paraffin wax in acetone.*

$10^3K/T$	$\ln(x_{wax})$	$\ln(\varphi_{wax})+(1-\varphi_{wax})(1-\rho)$
3.1311	-1.323	-3.7123
3.2378	-2.091	-4.9443
3.3044	-2.673	-5.7042
3.3600	-3.229	-6.3558
3.4067	-3.732	-6.9097
3.4467	-4.208	-7.4156

Table 3.3d *Solubility of Nippon Seiro (140/145) paraffin wax in cyclohexane.*

It can be seen that the solutions of Nippon Seiro in heptane and toluene show near ideal behaviour, although the slopes of the lines predicted from different D.S.C. values show appreciable variation. Cyclohexane shows a slight deviation, although it is possible that the solid actually crystallises in the α-form from this particular solvent, and acetone behaves extremely non-ideal due to its highly polar character[6].

In figure 3.4 the solubility of Nippon Seiro paraffin wax in heptane is plotted in the form $[\ln\varphi_2+(1-\varphi_2)(1-\rho)]$ against $({}^1/_T)$.

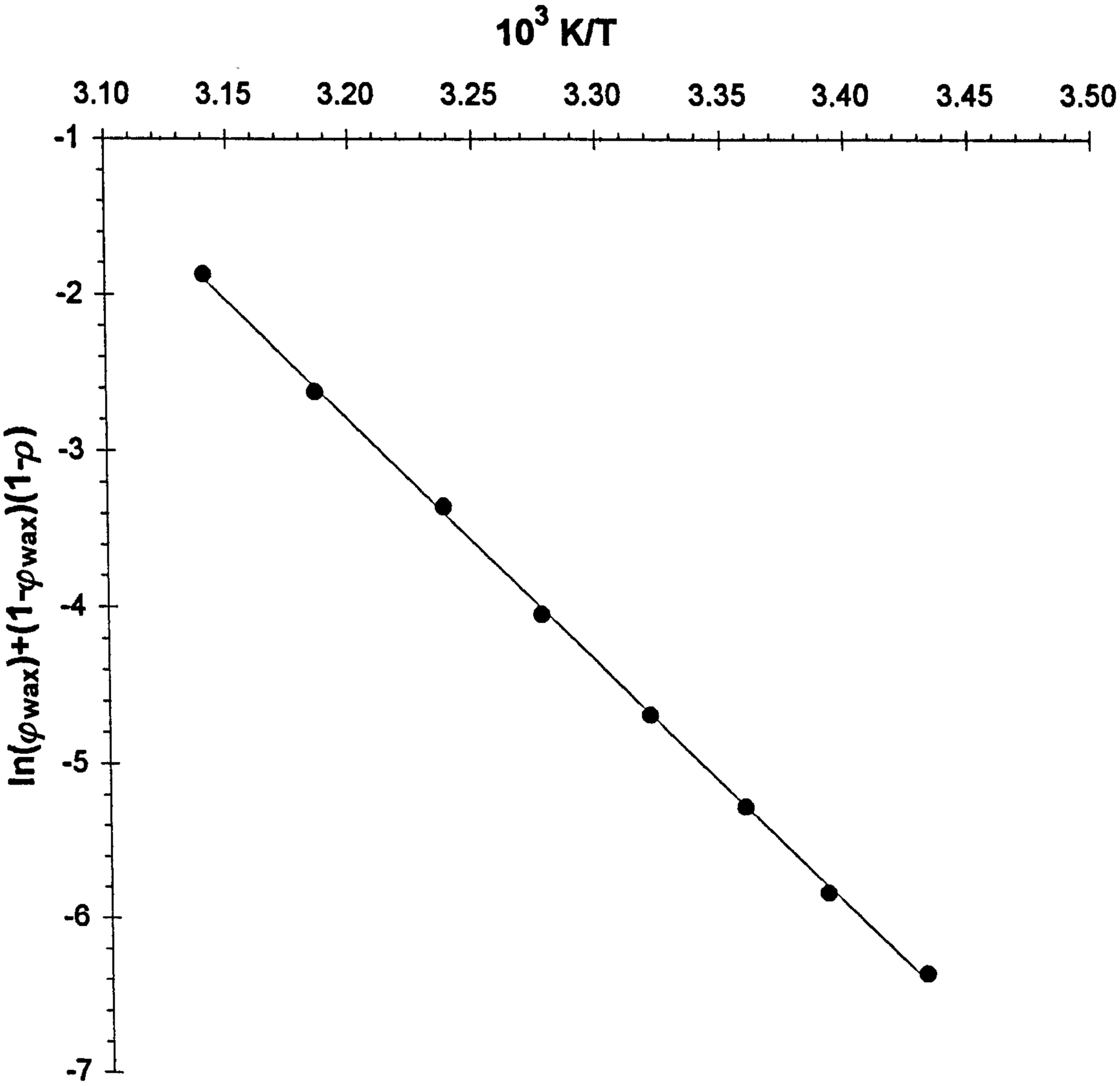

Figure 3.4 *Solubility of Nippon Seiro (140/145) paraffin wax in heptane.*

The graph is strictly linear so that the terms in $(1-\varphi_2)^2$ in equation (2.41) are insignificant. One may therefore assume that w'=0 for this system. From the graph it can be concluded that $\Delta_f H_2° = 128 \pm 1$ kJmol^{-1} and $T_m = 331 \pm 6$ K for the form of wax which is stable in the experimental range of temperature (i.e. the β form).

§ 3.3 Solubility of BD887 microcrystalline wax

In contrast to the behaviour of waxes consisting essentially of normal alkanes, the microcrystalline wax BD887 does not show simple solubility behaviour but can be separated into soluble and non-soluble fractions. An attempt to determine cloud point data in a manner similar to the above procedure did not lead to data open to meaningful interpretation. This is presumably due to the wax being a mixture of diverse chemical components whereas cloud point measurement is determined by the least soluble component. Hence, some differently averaged properties of the wax may be more appropriate for use in making theoretical predictions.

§ 3.4 Discussion

For pure n-alkanes in alkane solvents data points lie close to the line responsible for solute crystallising in the non-rotating β form and Hildebrand[7] showed that the entropy of mixing is ideal if a solution of two

n-alkanes can maintain the parallel orientation that they have in their solid forms. In more polar solvents on the other hand, points are much less than the Raoult's law solubilities..

For certain other hydrocarbon solvents, points lie between the α and β lines, and it seems feasible that the crystallising solid could have sufficient associated solvent to make it difficult for the formation of the non-rotating β form.

Measurements of the solubility of a solid in various solvents leads to information about the interactions between that solid and different molecules in solution.

Solubility measurements can be useful in the simpler wax systems but are of limited use in more complex waxes containing higher molecular weight components. Important considerations for paraffin systems include[6]

1 the nature of the solid phase formed,

2 non-ideal entropy of mixing for molecules of vastly differing size and chemical nature and

3 the accuracy of the actual solubility data and also the heats of fusion obtained from D.S.C.

§ 3.5 References

1 D.S.C. thermograms performed at Hull University give :

$$\beta_M \xrightarrow[34.6\,kJmol^{-1}]{337K} \alpha_H \xrightarrow[77.1\,kJmol^{-1}]{341\,K} L$$ in the notation of Broadhurst[2].

2 M.G. Broadhurst, **J.Res.Nat.Bur.Stand.**, 66A(3),241,(1962) – gives

$$\beta_M \xrightarrow[40.2kJmol^{-1}]{339K} \alpha_H \xrightarrow[76.6\,kJmol^{-1}]{343\,K} L.$$

3 J.H. Hildebrand and A.J. Wachter, **J.Phys.Coll.Chem.**, 53,886,(1949) – gives values of 106 ± 4 kJmol^{-1} and 339 ± 1 K (from ideal solution theory) and 152 ± 4 kJmol^{-1} and 340 ± 1 K (from polymer solution theory).

4 H.E. Lundager Madsen and R. Boistelle, **J.Chem.Soc.-Farad.Trans.I**, 72,1078,(1976) – gives values of ~109 kJmol^{-1} and 339 K.

5 Average of four D.S.C. thermograms performed at Hull University give : $\beta \xrightarrow[13.8\pm1.3\,kJmol^{-1}]{321\pm3\,K} \alpha \xrightarrow[62.3\pm0.9\,kJmol^{-1}]{336\pm4\,K} L$ (solid lines).

D.S.C. thermograms performed at Reckitt and Colman give :

$$\beta \xrightarrow[17.9\,kJmol^{-1}]{320\,K} \alpha \xrightarrow[66.4\,kJmol^{-1}]{336\,K} L$$ (dashed lines).

6 J.H. Hildebrand and R.L. Scott, "The solubility of nonelectrolytes", 3rd edition, Reinhold Publishing Corporation, (1950).

7 J.H. Hildebrand, **J.Am.Chem.Soc.**, 56,794,(1937).

Chapter Four

Vapour Pressure Apparatus

§ 4.1 The use of vapour pressure

The measurement of vapour pressure is particularly useful for wax / solvent systems because the solute can be regarded as completely involatile. The total vapour pressure is then, in effect, the partial pressure of the solvent. This leads directly to the chemical potential of the solvent in the vapour phase which, at equilibrium, is the same as in the mixture. As noted in the introduction, the difficulty is in establishing true equilibrium.

Measurements of vapour pressure for polymer solutions have been reported by Bonner *et al.*, and Gee[1]. These authors used the isopiestic method and found very long equilibration times as well as pronounced hysteresis. Clearly the difficulty is that any method requiring a change in composition of the condensed phase as a means of approach to equilibrium will be hindered by viscosity and slow diffusion times.

An alternative approach has been adopted in this work. We begin by establishing a known mixture composition at an initial temperature and pressure. We then step both temperature and pressure so as to maintain equilibrium at the same mixture composition, thereby eliminating any slow diffusion processes.

As the properties of the pure solvent are well known, we have a means of investigating the properties of the solvent within the wax paste and hence, by use of the Gibbs-Duhem equation, the properties of the solute.

For wax-solvent systems, at temperatures where the mixture is liquid, it is possible to apply conventional polymer solution theory[2,3]. At lower temperatures, where a gel or crystalline phase will be formed, the measurement of solvent activity can still be expected to give information of both theoretical and practical relevance.

§ 4.2 Design and construction

In the absence of stirring, the equilibration time will be dependent upon the surface to volume ratio of the sample. Short times therefore require a sample in the form of a thin film. The equilibration process involves the evaporation of solvent from, and condensation onto, the condensed phase. Hence, for a thin film, large changes in composition can occur and so this must be regarded as a variable to be determined during the course of the measurement, rather than initially being a fixed parameter. For these reasons the sample was supported on a sensitive electrobalance for continuous monitoring of the solvent content of a fixed mass of wax. Equilibration is achieved by suspending the sample in solvent vapour at known temperature and pressure.

Subsequent reviewing of the literature revealed that a similar technique had been used in the polymer field[1(i)], where a sample of molten polymer and a solution of the polymer were contained in a thermostatted

enclosure at a particular temperature. This enclosure was connected to another, at a lower temperature, containing degassed solvent. The experiment therefore consisted of successive vapour sorptions by the polymer and subsequent desorptions to obtain measurements at known solvent concentrations. The experimental parameters were therefore the weight of sample (and hence composition), the sample temperature and the lower temperature at which the solvent vapour was saturated relative to its pure liquid.

The availability of modern equipment enabled the use of a more straightforward experimental technique. The parameters involved are the composition of the wax / solvent sample, the temperature of the sample and the vapour pressure of the solvent. Each of these is connected into an automatic control loop. Vapour pressure is determined in a variation of the conventional dynamic method for liquid mixtures. The use of a static vapour system requires efficient degassing whereas this occurs naturally in a dynamic refluxing system. Pure solvent is refluxed into a condenser where the vapour is in contact with air. The vapour pressure is the equal to that of the air above the vapour–air interface. This pressure is measured using a gauge which can be set either to measure the pressure or provide a deviation signal from a set point.

The temperature of the sample is measured by coating it on a platinum thermometer element connected to a bridge which can be used

either to measure the temperature or to provide a deviation signal from a set point.

The composition of the sample is determined by weighing, first the wax and then the mixture, on an electrobalance. This provides the signal for deviations from fixed composition.

The apparatus is shown in figure 4.1 and broken-down schematically in figures 4.2 and 4.3. An accompanying key (table 4.1) is provided for the equipment specifications. It consists of a glazed ceramic platinum resistance thermometer element (B) coated with sample and suspended by four current and potential leads of 38 swg (0.152 mm) enamelled copper wire, which are contained by a 1.5 mm o.d. thin glass tube, from an electrobalance (A).

Four electrical leads have been added across the suspension of the electrobalance, as loops of phosphor bronze galvanometer suspension ribbon, and pass to a thermometer bridge (O). The sample hangs in refluxing solvent vapour (Fluka puriss n-heptane), which is controlled by a pressure transducer (C) so that constant conditions can be reproduced for each run. This control loop is shown in figure 4.4.

Figure 4.1 Photograph of vapour pressure apparatus.

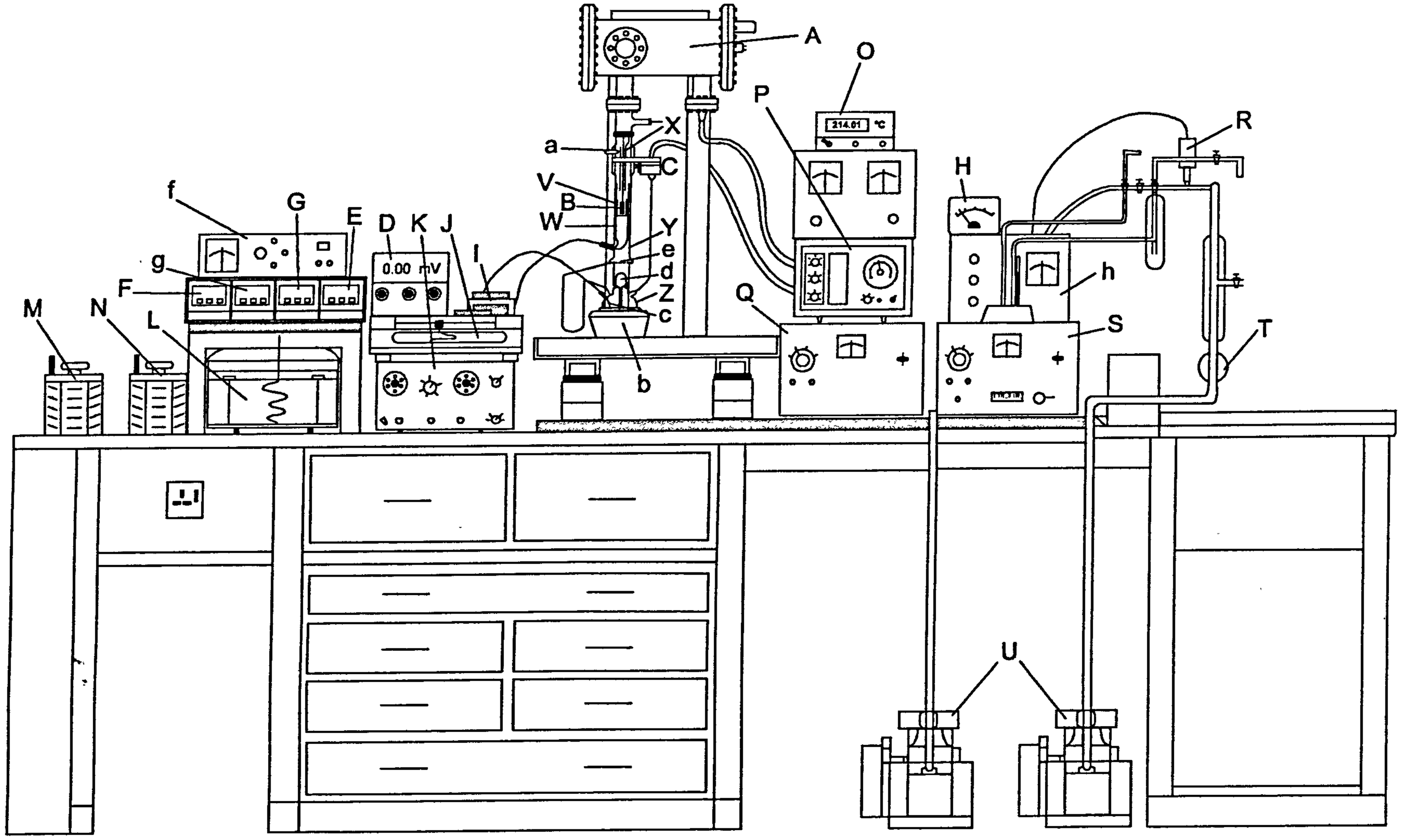

Figure 4.2 *Line drawing of vapour pressure apparatus.*

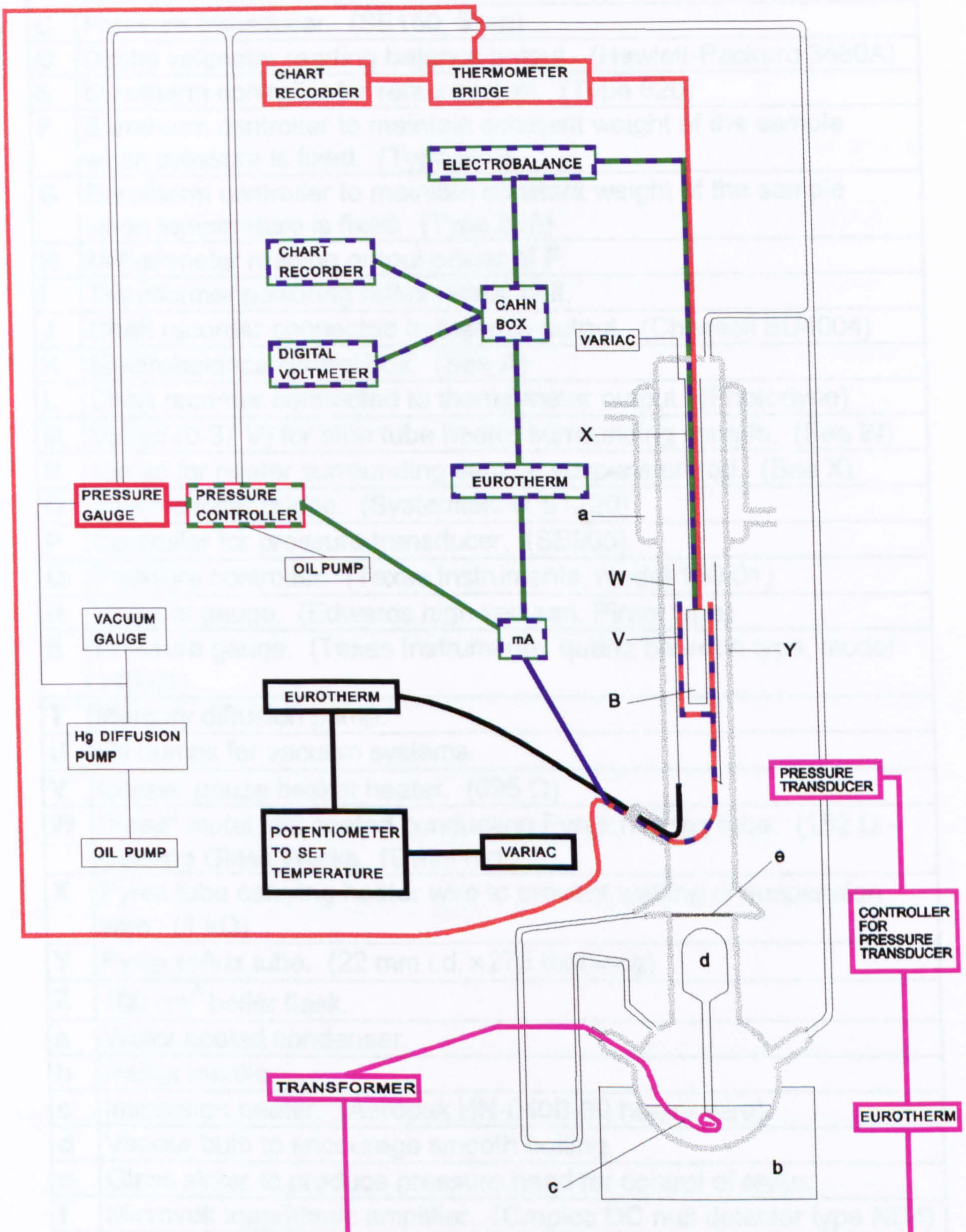

Figure 4.3 *Schematic of vapour pressure apparatus.*

A	Electrobalance mechanism inside stainless steel vacuum housing. (Cahn model RG, capacity 1g)
B	Sample coated on Pt resistance element. (25×3.2×0.8 mm - Matthey Thermafilm type 100W30, Class A)
C	Pressure transducer. (SE150, 5"wg)
D	Digital voltmeter reading balance output. (Hewlett-Packard 3480A)
E	Eurotherm controller for reflux system. (Type 820)
F	Eurotherm controller to maintain constant weight of the sample when pressure is fixed. (Type 820)
G	Eurotherm controller to maintain constant weight of the sample when temperature is fixed. (Type 818)
H	Milliammeter reading output power of **F**.
I	Transformer powering reflux heater coil.
J	Chart recorder connected to balance output. (Chessell BD4004)
K	Electrobalance control box. (See **A**)
L	Chart recorder connected to thermometer output. (Photodyne)
M	Variac (0-37 V) for blue tube heater surrounding sample. (See **W**)
N	Variac for heater surrounding sample suspension rod. (See **X**)
O	Thermometer bridge. (Systemteknik S1220)
P	Controller for pressure transducer. (SE905)
Q	Pressure controller. (Texas Instruments, model 150-01)
R	Vacuum gauge. (Edwards high vacuum, Pirani type)
S	Pressure gauge. (Texas Instruments, quartz bourdon type, model 145-01)
T	Mercury diffusion pump.
U	Oil pumps for vacuum systems.
V	Copper gauze basket heater. (695 Ω)
W	"Fired" metal film coated conducting Pyrex heating tube. (152 Ω - Corning Glass Works, 19 mm o.d.)
X	Pyrex tube carrying heater wire to prevent wetting of suspension wire. (1 kΩ)
Y	Pyrex reflux tube. (22 mm i.d.×275 mm long)
Z	100 cm^3 boiler flask.
a	Water cooled condenser.
b	Reflux mantle.
c	Immersion heater. (Aeropak HN-040B-30 heater wire)
d	Vapour bulb to encourage smooth boiling.
e	Glass sinter to produce pressure head for control of reflux.
f	Microvolt logarithmic amplifier. (Cropico DC null detector type ND4)
g	Eurotherm controller to fix temperature. (Type 820)
h	Nanovolt logarithmic amplifier. (Tinsley type 6050)

Table 4.1 *Key for vapour pressure apparatus.*

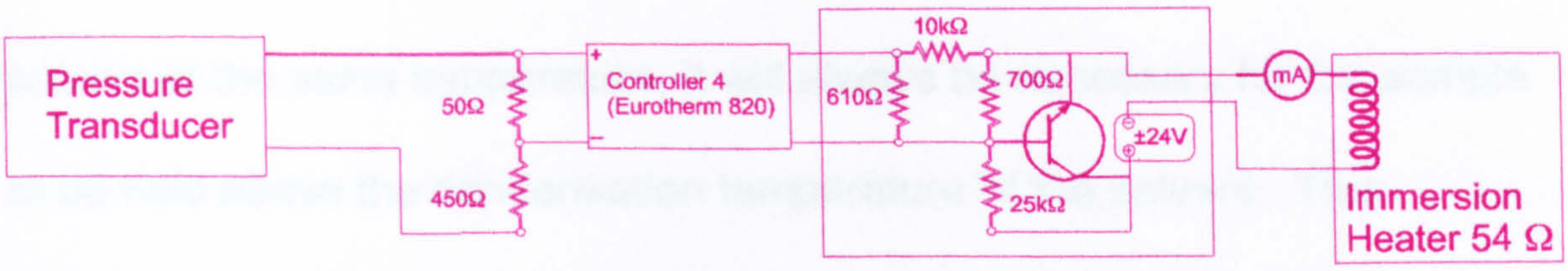

Figure 4.4 *Reflux control system.*

Stable reflux conditions are achieved by the use of two heaters on the boiler. An external heating mantle provides a permanent heat input along with an internal immersion heater. A glass sinter is inserted between the flask of boiling liquid and the condensing vapour column. This produces a pressure difference between the boiler and the air in the condenser and a pressure transducer is connected between these two. Here a constant pressure difference corresponds to a constant rate of reflux, so the output of the pressure transducer is used to power the immersion heater. This control is as used in high performance distillation columns. Smooth boiling is further encouraged by the presence of an open ended vapour bulb dipping into the boiling liquid. For this control loop, the required PID parameters for the Eurotherm controller were determined manually to be P = 70%, I = 19 s, D = 3.8 s (see § 4.3).

The tube forming the vapour bath for the sample contains also parts for controlling its temperature. These are a section of glass tube coated with resistive heater film, as a permanent heater component, within which is a copper gauze cylinder carrying an intermittent heater wire. Since the vapour pressure of solvent in the sample will always be lower than that of the pure

solvent at the same temperature, it will always be necessary for the sample to be held above the condensation temperature of the solvent. This intermittent heater acts in the temperature control loop of the sample.

The sample is coated on the thermometer element by soaking liquid wax onto a layer of paper tissue. This is surrounded by two heating elements (V and W) to maintain constant sample weight by means of a feedback system (F and G) linked to the balance output. The sample weight (and hence composition) is held constant for each experiment so that the need for long contact times, or the occurrence of hysteresis, is overcome. Hence, the solvent doesn't have to diffuse through the wax matrix.

Prior to initiating reflux, the sample temperature has to be raised above the condensation temperature of the solvent (at the chosen pressure), to prevent the hot solvent condensing directly onto the sample and dissolving the wax to give a solution which may be lost by dripping. Once reflux is established at a known pressure, the composition is set and the temperature settles to an equilibrium value. By lowering the pressure and allowing equilibrium to re-establish, vapour pressure and temperature data are obtained for a particular composition. Changes in the composition and repeating the experiment will lead to a complete vapour pressure, temperature and composition dependence for each sample.

The above section describes the procedure for controlling constant composition of the sample at a fixed pressure by varying it's temperature.

This control system will be known as system **A** and is shown in figures 4.3 and 4.5 with each loop coloured separately. If however, a situation arises where large changes in temperature are accompanied by only small changes in pressure, the alternative set-up of controlling constant composition of the sample at a fixed temperature by varying the pressure will tend to give better control. This control system will be known as system **B** and is shown in figures 4.3 and 4.6 with a different colour scheme.

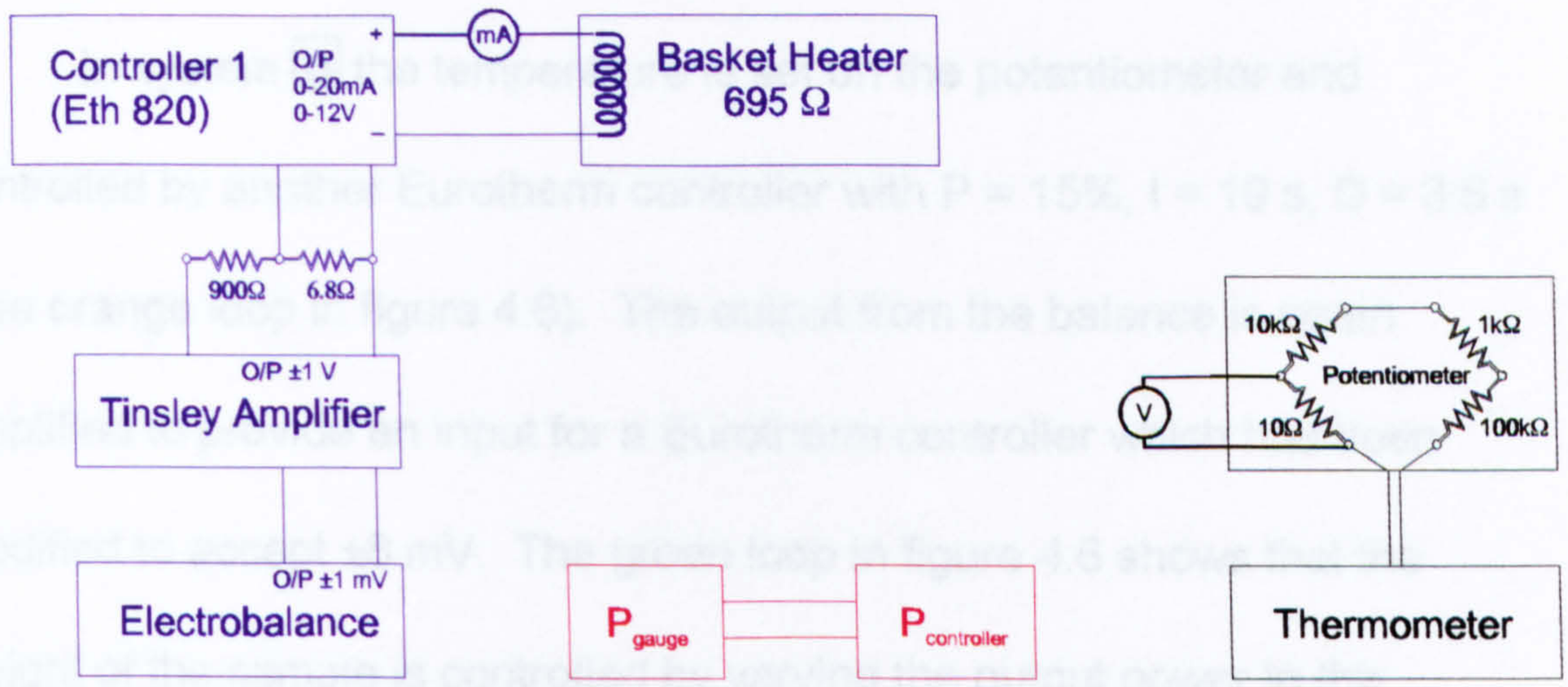

Figure 4.5 *Fixed pressure control system* **A**.

In system **A** the pressure is set on the pressure gauge and controlled by the pressure controller (see red loop in figure 4.5). The output from the balance is amplified to provide an input for a Eurotherm controller which has been modified to accept ±2.5 mV. The blue loop in figure 4.5 shows that constant weight of the sample is controlled by varying the output power to the heater surrounding the sample and hence its temperature. For this control loop, the required PID parameters for the Eurotherm controller were determined manually to be P = 2%, I = 0 s, D = 0 s. The sample temperature is that of the calibrated resistance thermometer substrate. This is obtained

by measurement of the potential across the element and that across a standard resistance in series with it. The thermometer current used is small enough as to produce negligible heating of the element. Potential measurements are made using a Cambridge Instrument vernier potentiometer and Weston standard cell (L–384109; 1.01836 V at 17.4°C). The potentiometer output signal is amplified and passes to a chart recorder and, when required, to the fixed temperature control system.

In system **B** the temperature is set on the potentiometer and controlled by another Eurotherm controller with P = 15%, I = 19 s, D = 3.6 s (see orange loop in figure 4.6). The output from the balance is again amplified to provide an input for a Eurotherm controller which has been modified to accept ±8 mV. The green loop in figure 4.6 shows that the weight of the sample is controlled by varying the output power to the pressure controller with the required PID parameters being P = 5%, I = 128 s, D = 21.3 s.

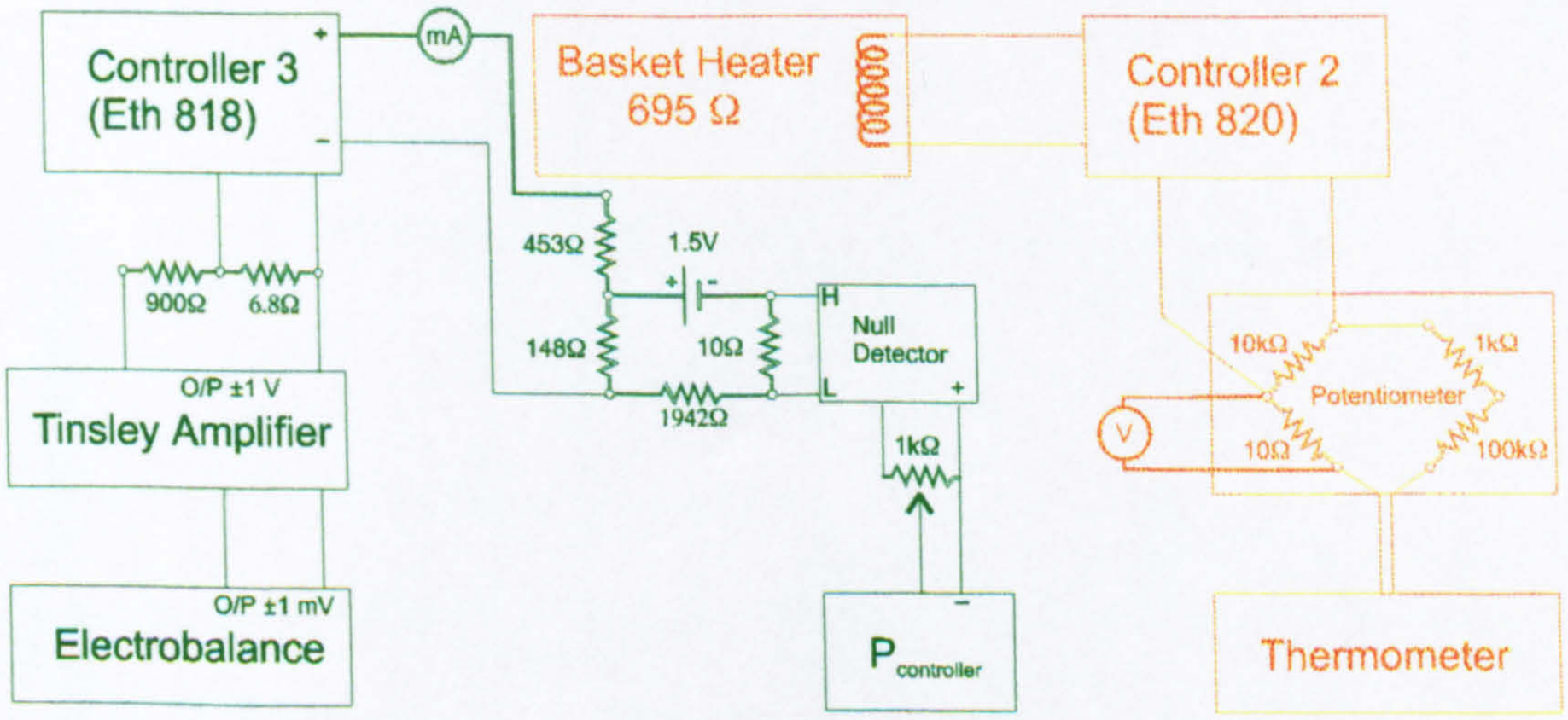

Figure 4.6 *Fixed temperature control system* **B**.

The apparatus was designed to take into account easy transition between the two control mechanisms and a switching device was constructed to perform this operation. The device consisted of a bank of four double-pole double-throw switches and its wiring diagram is represented in figure 4.7.

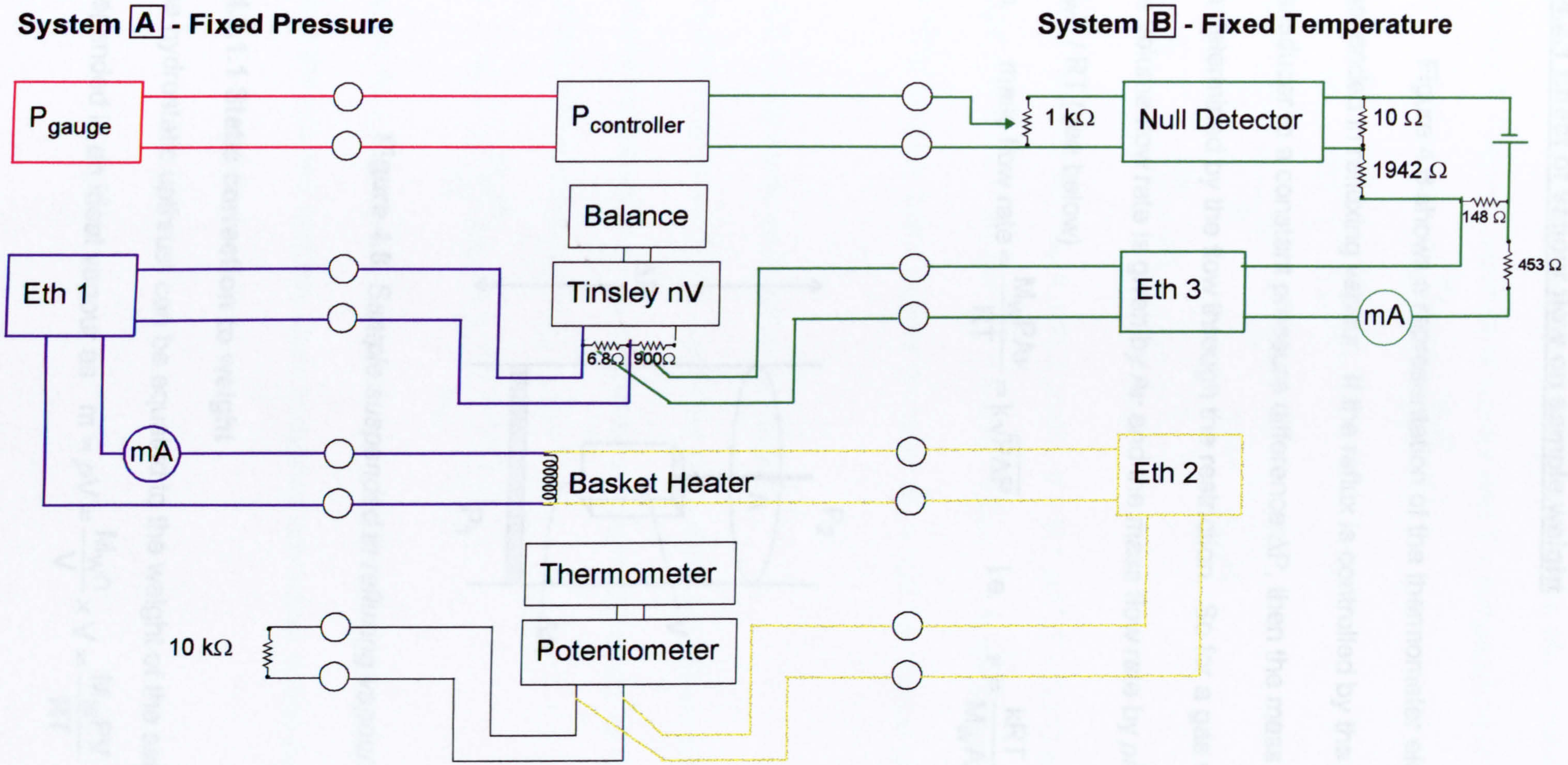

Figure 4.7 *Schematic of switching mechanism.*

§ 4.2.1 Effect of vapour flow on sample weight

Figure 4.8 shows a representation of the thermometer element suspended in refluxing vapour. If the reflux is controlled by the pressure transducer to a constant pressure difference ΔP, then the mass flow rate will be determined by the flow through the restriction. So for a gas velocity of v, the volume flow rate is given by Av and the mass flow rate by ρAv where ρ = $M_W P$ / RT (see below)

i.e. mass flow rate $= \frac{M_W P A v}{RT} = k\sqrt{P\Delta P}$ i.e. $v = \frac{kRT}{M_W A}\sqrt{\frac{\Delta P}{P}}$

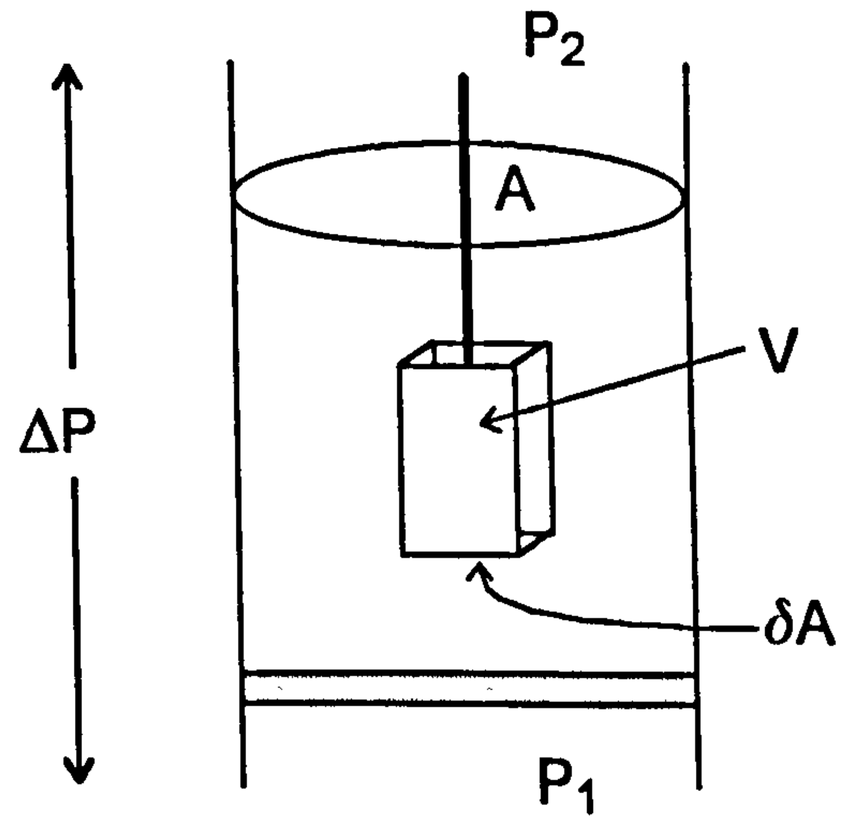

Figure 4.8 *Sample suspended in refluxing vapour.*

§ 4.2.1.1 Static correction to weight

The hydrostatic upthrust can be equated to the weight of the sample suspended in an ideal vapour as $m = \rho V = \frac{M_W n}{V} \times V = \frac{M_W PV}{RT}$ i.e. $\propto P$

where ρ = density of vapour, V = volume of sample, M_W = molar mass of sample, P = vapour pressure of vapour and T = temperature of vapour

i.e. $$\delta(m) = Vd\rho = V\left(\frac{M_W}{RT}dP - \frac{M_W P}{RT^2}dT\right)$$

or $$\frac{dm}{dP} = \frac{VM_W}{RT}\left(1 - \frac{d\,lnT}{d\,lnP}\right)$$

but $$\frac{d\,lnP}{d\,1/T} = \frac{-\Delta_{vap}H}{R} \quad \text{i.e.} \quad \frac{d\,lnT}{d\,lnP} = \frac{RT}{\Delta_{vap}H}$$

hence $$\frac{dm}{dP} = VM_W\left(\frac{1}{RT} - \frac{1}{\Delta_{vap}H}\right)$$

So for heptane with $M_W = 100.2\ gmol^{-1}$, $V \sim 0.1\ cm^3$, $T \sim 30°C$ and $\Delta_{vap}H \sim 36\ kJmol^{-1}$ we get $\frac{dm}{dP} \sim 5\times10^{-7}\ gTorr^{-1}$. At temperatures as high as 70°C heptane has a vapour pressure of ~ 300 Torr hence dm ~ 0.0001 g.

§ 4.2.1.2 Dynamic correction to weight

The kinetic upthrust (F_k) is due to the drag of flowing gas on the element and assumed to be equal to the stagnation pressure difference on the lower surface area of the sample. $F_k = \frac{1}{2}\rho v^2 \delta A$

ie $$F_k = \frac{1}{2}\frac{M_W P}{RT}\delta A v^2 = \frac{1}{2}\frac{\delta A.\Delta P.RT}{M_W}\left(\frac{k}{A}\right)^2$$

Hence, for a given pressure difference ΔP, the flowing of vapour will not affect the balance and any static buoyancy correction seems insignificant.

§ 4.2.2 Calibration of pressure gauge

The Texas Instrument pressure gauge had a direct analogue readout for pressure and so was calibrated against a primary standard.① The results are shown in table 4.2 and figure 4.9 and a cubic fit was determined to be

$$\left(\frac{P_{obs}}{Torr}\right) = 3.28\times10^{-8}\left(\frac{P_{corr}}{Tx}\right)^3 + 2.262\times10^{-4}\left(\frac{P_{corr}}{Tx}\right)^2 + 2.6095\left(\frac{P_{corr}}{Tx}\right) - 0.2403$$

P_{corr}/Tx	P_{obs}/Torr
29.770	77.626
39.641	103.501
49.472	129.376
59.297	155.252
69.104	181.127
69.099	181.127
78.660	207.002
88.660	232.878
98.377	258.753
98.406	258.753
108.159	284.628
117.871	310.504
127.564	336.379
127.570	336.379

P_{corr}/Tx	P_{obs}/Torr
137.255	362.254
146.958	388.129
156.591	414.005
166.213	439.880
166.200	439.880
175.818	465.755
185.429	491.631
195.011	517.506
195.026	517.506
204.569	543.381
214.119	569.257
223.675	595.132
223.686	595.132
233.199	621.007

P_{corr}/Tx	P_{obs}/Torr
242.697	646.882
252.176	672.758
261.657	698.633
261.659	698.633
271.124	724.508
280.567	750.384
127.594	336.379
280.566	750.384
214.128	569.257
146.906	388.129
69.089	181.127
261.598	698.633

Table 4.2 *Pressure gauge calibration.*

① Dead weight tester previously calibrated at National Physics Laboratory.

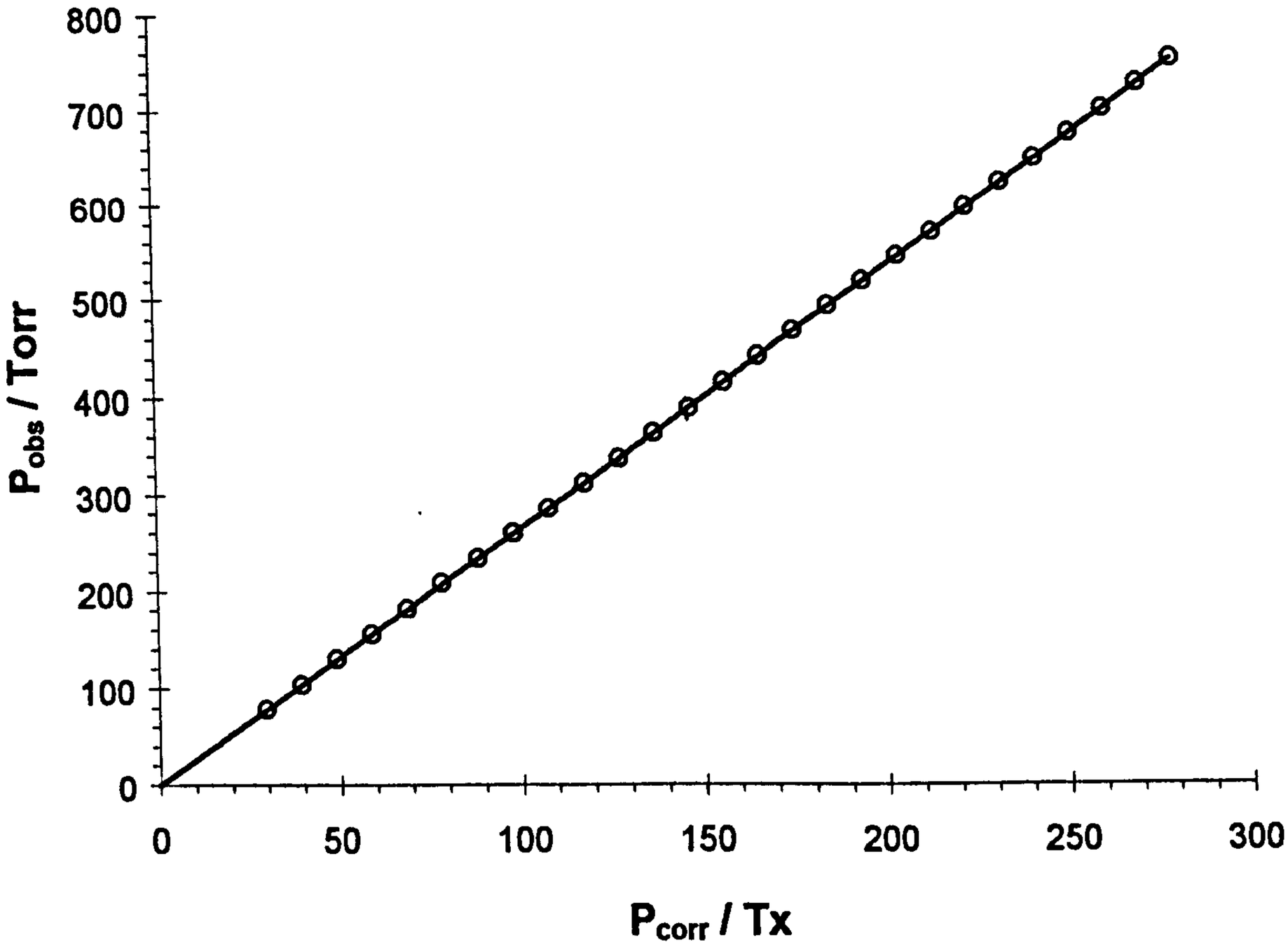

Figure 4.9 *Pressure gauge calibration.*

§ 4.3 Principles behind electronic automation

Due to the complex nature of the equilibria involved, automation of the system was necessary from the onset of the investigation. For example, during a run to determine the temperature dependence of solvent vapour pressure at fixed composition, three control loops are needed to work together in order to maintain equilibrium conditions.

If we take the control loop required to maintain constant composition of the sample by varying the temperature at a fixed pressure (system [A]), we can break this down as shown in figure 4.10.

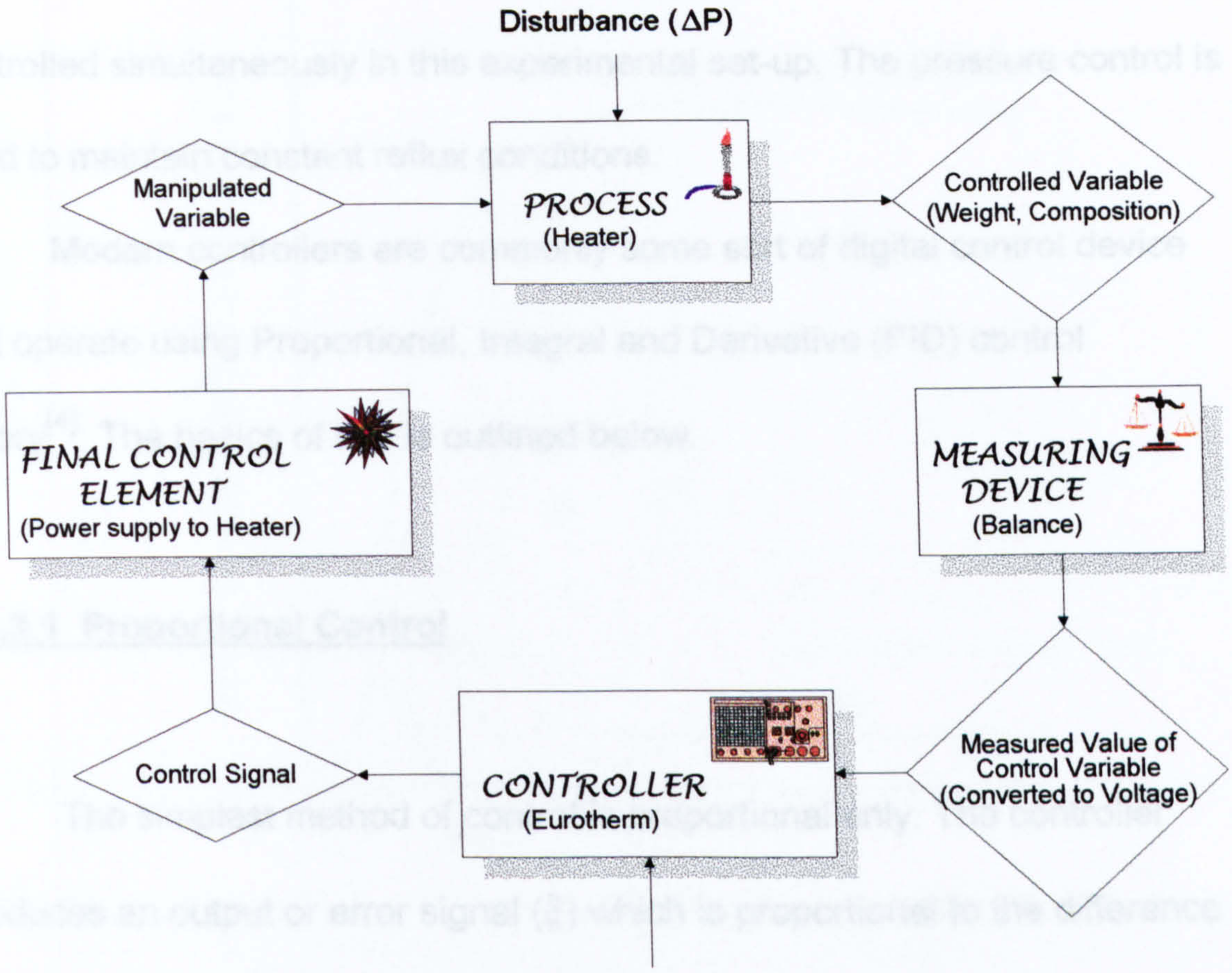

Figure 4.10 *Schematic representation of typical control loop.*

For this loop, a process (sample heater) is used to maintain constant sample weight (and hence composition) under the influence of a disturbance (change in vapour pressure). The controlled variable is measured using an electrobalance and the output is fed as an input signal to a control unit. Here it is compared to the setpoint and a control signal is generated which varies the power supplied to the heater. For obvious reasons, this type of loop is known as a ***feedback*** control loop and is one of the simplest and most widely used control systems.

The commonest variables to be controlled in a chemical process are flowrate, temperature, pressure and composition. The latter three are

controlled simultaneously in this experimental set-up. The pressure control is used to maintain constant reflux conditions.

Modern controllers are commonly some sort of digital control device and operate using Proportional, Integral and Derivative (PID) control theory[4]. The basics of this is outlined below.

§ 4.3.1 Proportional Control

The simplest method of control is proportional only. The controller produces an output or error signal (ξ) which is proportional to the difference between the setpoint (SP) and the measured or process value (PV).

i.e. $\xi = (SP - PV)$

Hence the output (OP) from the controller is given by

$$OP = K.\xi + C$$

where K is the ***gain*** or proportional sensitivity and C is the output constant.

i.e. the steady output required to give an error of zero.

A schematic representation of a system's response to perturbation is shown in figure 4.11. The black curve shows the response when no control is employed. Proportional control leads to a new steady state after a long period of oscillations resulting in an ***offset*** from the original setpoint. This is also known as a steady state error and is required to maintain the changed output of the controller (see magenta curve).

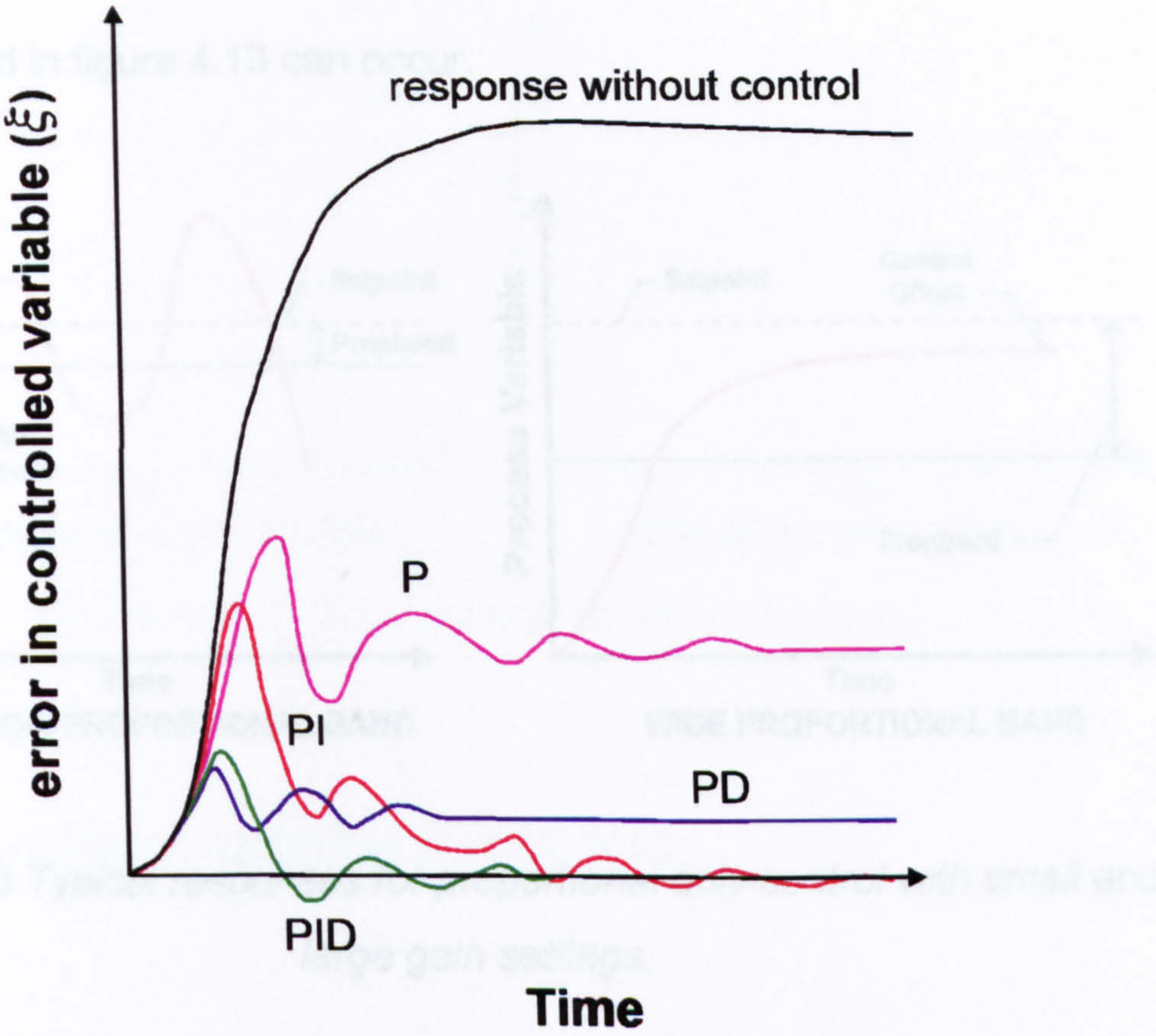

Figure 4.11 *The response of a system to different control modes.*

A special case of P only control is that of ***on/off*** control where the ***proportional band*** (= $^{1}/_{gain}$) is sufficiently small to induce permanent oscillations about the new setpoint. This is shown below in figure 4.12. where τ is the time of oscillation under on / off control.

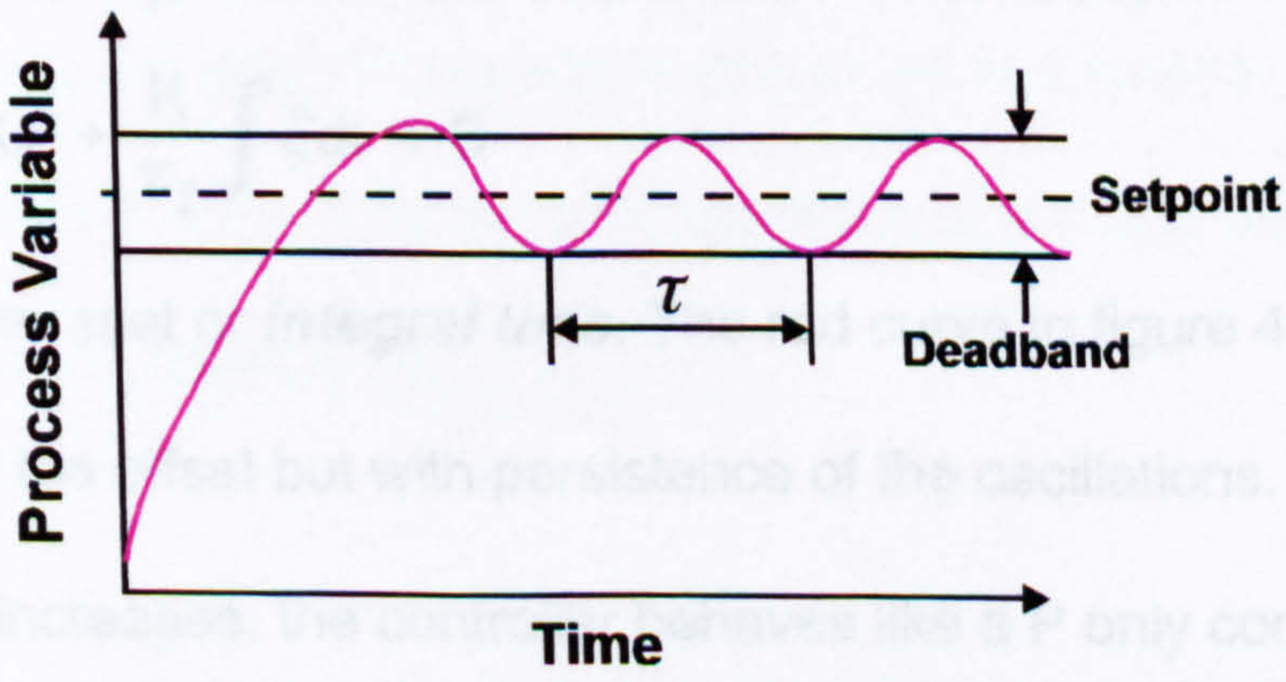

Figure 4.12 *The output of a system under on / off control.*

If the proportional band is set too large or too small, then situations similar to

those depicted in figure 4.13 can occur.

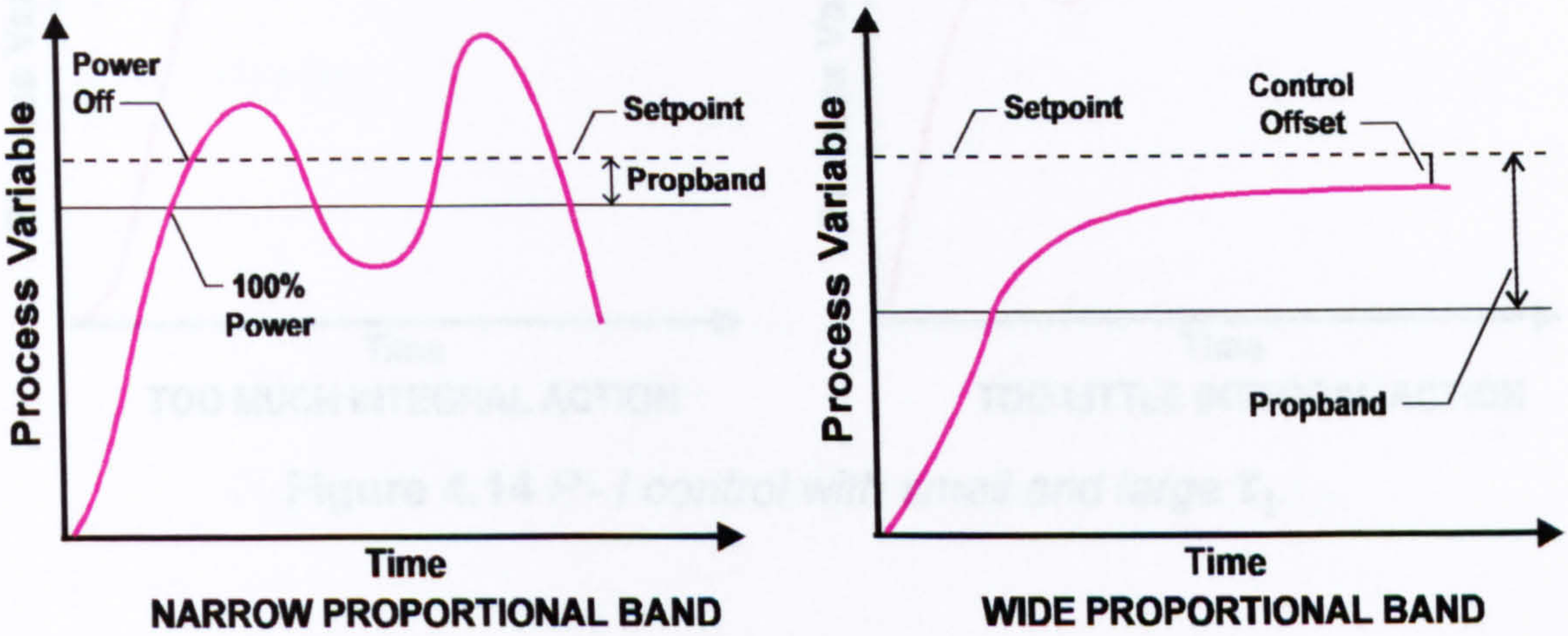

Figure 4.13 *Typical responses for proportional only control with small and large gain settings.*

§ 4.3.2 Proportional - Integral (P - I) Control

The P - I mode, or 'automatic reset' control mode compensates for the error between the setpoint and the measured value which is caused by P only control. The equation for the output of a P - I controller is

$$OP = K.\xi + \frac{K}{\tau_I}\int \xi dt + C$$

where τ_I is the reset or ***integral time***. The red curve in figure 4.11 shows the elimination of the offset but with persistence of the oscillations. As the integral time increases, the controller behaves like a P only controller. The influence of adding integral control to a system is shown in figure 4.14.

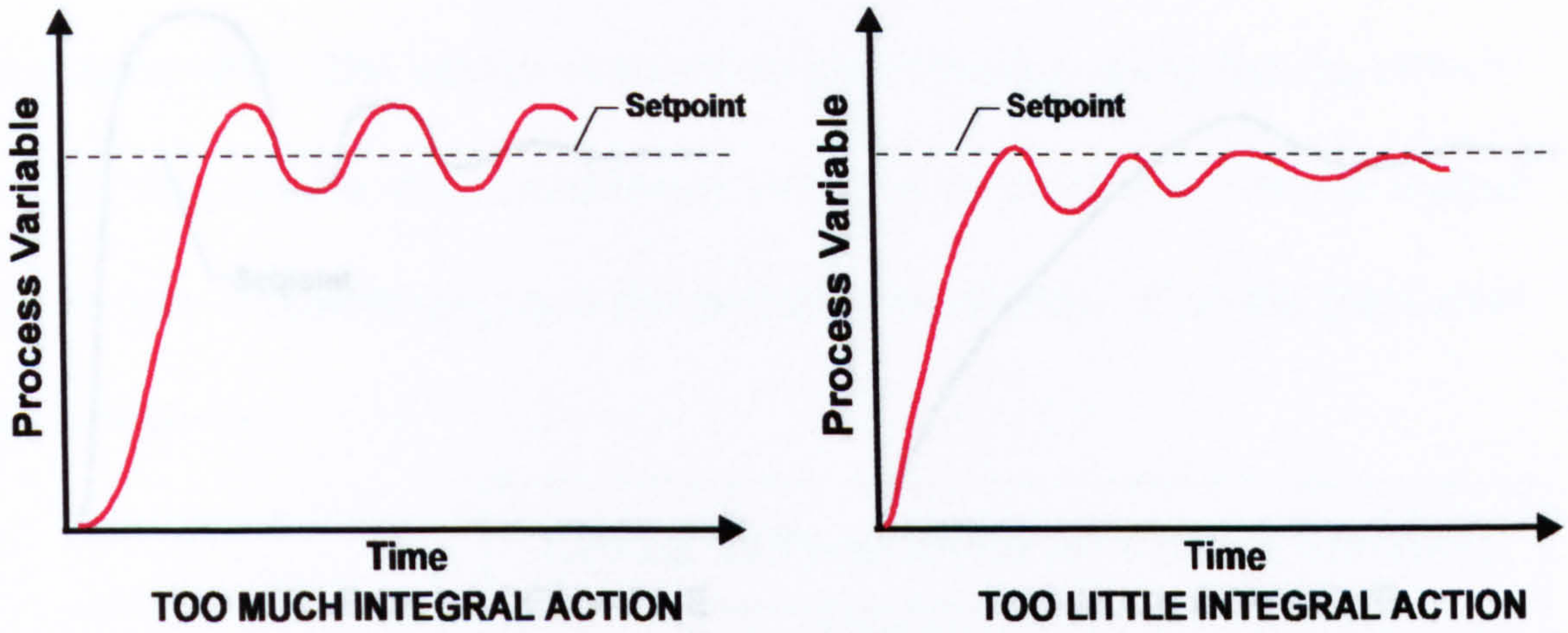

Figure 4.14 *P - I control with small and large* τ_I.

§ 4.3.3 Proportional - Derivative (P - D) Control

The effect of adding derivative mode to a P controller is to reduce the oscillations more rapidly by anticipating the initial overshoot in the response. The controller output is also then proportional to the rate of change of the error and is given by

$$OP = K.\xi + K\tau_D \frac{d\xi}{dt} + C$$

where τ_D is the rate or ***derivative time***. The reduction in oscillations enables a higher proportional gain setting and hence leads to a smaller offset (see blue curve in figure 4.11). The effect of too much or too little derivative control is shown in figure 4.15.

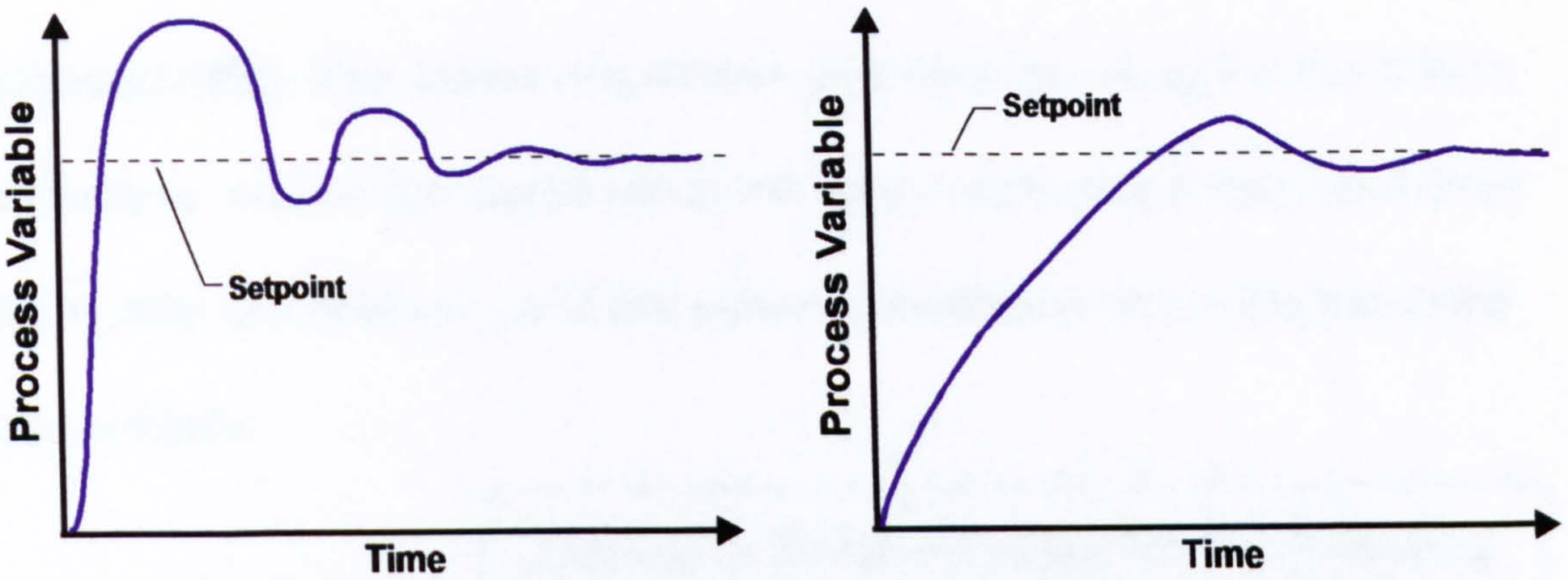

TOO LITTLE OR NO DERIVATIVE **TOO MUCH DERIVATIVE**

Figure 4.15 *P - D control with too small and large* τ_D.

§ 4.3.4 Proportional - Integral - Derivative (PID) Control

By governing the previous modes of control one can optimise the controller for minimising both oscillations and offset which leads to the output power being described by the equation

$$OP = K.\xi + \frac{K}{\tau_I}\int \xi dt + K\tau_D \frac{d\xi}{dt} + C$$

See green curve in figure 4.11. The normal PID equation assumes an *analogue* signal (i.e. continuous) but there are adaptations for a *digital* signal (i.e. discrete) to allow computerisation[5].

§ 4.3.5 Manual Loop Stabilisation

The controller parameters can be set manually using the Ziegler-Nichols method[6,7] of getting the response to become unstable at the normal running temperature in the proportional only mode by reducing the

propband (**PB**). The values required to give stability, using the Eurotherm controllers, can be calculated using the value of propband that just makes the system unstable ($\mathscr{P}_u$) and the period of oscillation (τ) in the tabulated values below.

	Setting of Parameters for Critical Damping		
Control Loop Type	Propband (**PB**)	Integral Time Constant (τ_I)	Derivative Time Constant (τ_D)
Prop Only (P)	$2\times\mathscr{P}_u$	—	—
Prop. + Int. (PI)	$(^{20}/_{9})\times\mathscr{P}_u$	$0.83\times(\tau)$	—
3 - Term (PID)	$(^{5}/_{3})\times\mathscr{P}_u$	$(^{1}/_{2})\times(\tau)$	$(^{1}/_{8})\times(\tau)$

Table 4.3 *Parameters for manual loop stabilisation.*

Some controllers can monitor automatically the behaviour of the measured variable to an applied perturbation. This *self-tuning* procedure provides a simple means of evaluating the PID terms.

§ 4.4 Performance achieved by the control system

The electrobalance signal was controlled by the green and blue loops in figure 4.7 to ± 0.5 mg or 2.5% of the weight of a typical sample. When under control, the sample temperature was constant to within ± 0.05 K. When this was allowed to change to reach equilibrium at a fixed pressure it was measured to ± 0.5 K. The pressure control system gave constancy to ± 0.2 Torr and could be read to ± 1 Torr.

§ 4.5 References

1 (i) D.C. Bonner and J.M. Prausnitz, **J.Polym.Sci.**, 12,51,(1974).

(ii) G. Gee, **J.Chem.Soc.**, 1947(i),280-288,(1947).

2 (i) P.J. Flory, **J.Chem.Phys.,** 10,51,(1942).

(ii) P.J. Flory, **J.Chem.Phys.,** 12,425,(1944).

(iii) P.J. Flory, **J.Chem.Phys.,** 13,453,(1945).

3 (i) M.L. Huggins, **J.Chem.Phys.,** 9,440,(1940).

(ii) M.L. Huggins, **J.Phys.Chem.,** 23,1063,(1940).

4 P.W. Murrill, "Fundamentals of Process Control Theory", Instrument Society of America, (1981).

5 D.W. Pessen, **J.Dynamic Systems Measurement and Control - Trans. of the A.S.M.E.**, 116(3),553-557,(1994).

6 C.C. Hang, K.J. Astrom and W.K. Ho, **I.E.E. Proceedings(D) - Control Theory and Applications,** 138(2),111-118,(1991).

7 (i) J.G. Ziegler and N.B. Nichols, **Trans. of the A.S.M.E.,** 64,759-768,(1942).

(ii) J.G. Ziegler and N.B. Nichols, **J.Dynamic Systems Measurement and Control - Trans. of the A.S.M.E.,** 115(2B),220-222,(1993).

Chapter Five

Vapour Pressure Results

The vapour pressure results are shown in the form of ln P_1^* versus $^1/_T$. In the systems being studied, the vapour phase is regarded as pure solvent because the volatility of the solutes used is negligible.

At high enough temperatures the condensed phase is liquid of known, fixed composition. As shown from the solubility studies in chapter 3, the solutions formed are effectively athermal and the logarithmic vapour pressure plots are linear, of slope determined by the enthalpy of vaporisation of pure liquid solvent.

As the temperature is reduced a third phase appears. The simplest case is when this is in the form of crystals which are impermeable to solvent; the liquid phase is then a saturated solution of solute in the solvent.

§ 5.1 Pure alkanes

Samples of dotriacontane ($C_{32}H_{66}$ - Koch-Light Ltd., 99%) and heptacosane ($C_{27}H_{56}$ - Lancaster Synthesis Ltd., 99%) were obtained and used after purification by recrystallisation from toluene. Typical sample weights of the solids were ~20 mg and solvent vapour pressures were measured at various compositions.

§ 5.1.1 Dotriacontane

The results for dotriacontane and heptane at various volume fractions (φ_2) are given in table 5.1, and figure 5.1 shows the natural logarithm of the solvent vapour pressure as a function of reciprocal temperature.

φ_2/%	10^3K/T	ln(P_1*/Torr)
95.4	2.7554	4.3556
	2.8028	4.1734
	2.8600	3.9504
	2.9343	3.6630
93.9	2.8853	3.9503
	2.9000	3.8990
	2.9146	3.8450
	2.9312	3.7879
	2.9504	3.7273
80.5	2.9499	4.4809
	2.9497	4.4907
	2.9348	4.5487
	2.9348	4.5514
	2.9652	4.4294
75.6	2.9586	4.6400
	2.9754	4.5756
	3.1606	4.5730
	3.1647	4.5597
	3.1686	4.5461
	3.1725	4.5324
	3.1798	4.5043
86.1	2.8911	4.5080
	2.8982	4.4790
	2.9063	4.4492
	2.9153	4.4185
	2.8943	4.5048
	2.9357	4.3407

φ_2/%	10^3K/T	ln(P_1*/Torr)
86.1	2.9354	4.3251
	2.9563	4.2387
	2.9636	4.2208
	3.0401	4.7617
	3.0081	4.6558
	2.9858	4.3913
	3.0542	4.7820
	3.0541	4.7734
	3.0542	4.7784
	3.0776	4.7607
80.5	3.0865	4.7550
	3.1002	4.7325
	3.0999	4.7325
	3.0897	4.7518
80.5	3.0897	4.7511
	3.0984	4.7346
	3.1118	4.6981
	3.0673	4.7791
	3.0457	4.7727
	3.0247	4.7449
	2.8905	4.7128
	2.9084	4.6481
	2.9217	4.5992
	2.9354	4.5410
	2.9533	4.4637
	2.9647	4.4144
	2.9713	4.3837

φ_2/%	10^3K/T	ln(P_1*/Torr)
80.5	2.9783	4.4025
	2.9759	4.3955
	2.9740	4.3984
	2.9853	4.4532
	2.9921	4.5334
	2.9988	4.5933
	3.0082	4.6593
	3.0150	4.6841
	3.0359	4.7613
85.1	2.8720	4.6411
	2.8845	4.5899
	2.9050	4.5078
	2.9173	4.4491
	2.9313	4.3867
85.1	2.9288	4.3984
	2.9376	4.3624
	2.9464	4.3277
	2.9553	4.2929
	2.9641	4.2492
	2.9687	4.2477
	2.9731	4.3283
90.7	2.7412	4.6426
	2.7720	4.5092
89.9	2.7823	4.5249
	2.8023	4.4578

Table 5.1 *Vapour pressures of heptane in dotriacontane at various compositions.*

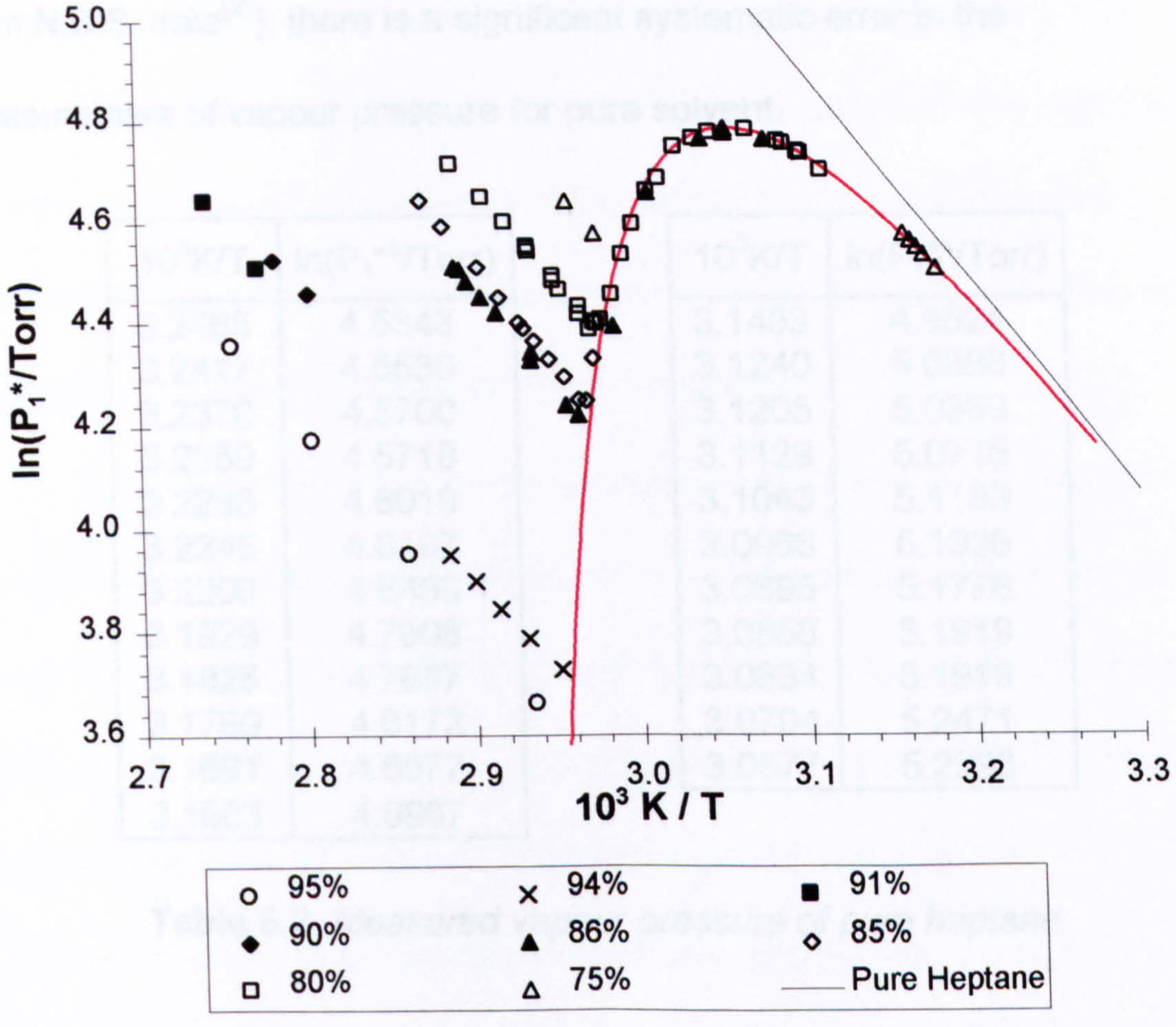

Figure 5.1 *Vapour pressures of heptane in dotriacontane at various compositions.*

The solid black line represents pure solvent data, obtained from National Bureau of Standards (N.B.S.) tables[1], and fitted to the equation $\ln(P_1^{*\circ}/\text{Torr}) = -4147.9x(K/T) + 17.758$. An attempt was made to measure the vapour pressure of the pure solvent directly, however, this was not too successful since the apparatus did not include any facility for inducing condensation of vapour onto a clean thermometer element. The results are given below in table 5.2, and figure 5.2 shows that although the gradient of the line of best fit is the same as that for literature values, leading to a calculated heat of vaporisation of 33.9 $kJmol^{-1}$ (c.f. 34.5 $kJmol^{-1}$ calculated

from N.B.S. data[2]), there is a significant systematic error in the measurement of vapour pressure for pure solvent.

10^3K/T	ln(P_1*°/Torr)
3.2465	4.5343
3.2417	4.5530
3.2370	4.5700
3.2359	4.5718
3.2293	4.6019
3.2248	4.6197
3.2200	4.6456
3.1929	4.7308
3.1825	4.7857
3.1769	4.8172
3.1691	4.8577
3.1603	4.8967

10^3K/T	ln(P_1*°/Torr)
3.1453	4.9524
3.1240	5.0388
3.1205	5.0389
3.1129	5.0715
3.1043	5.1183
3.0966	5.1336
3.0895	5.1776
3.0858	5.1919
3.0834	5.1919
3.0704	5.2471
3.0577	5.2993

Table 5.2 *Measured vapour pressure of pure heptane.*

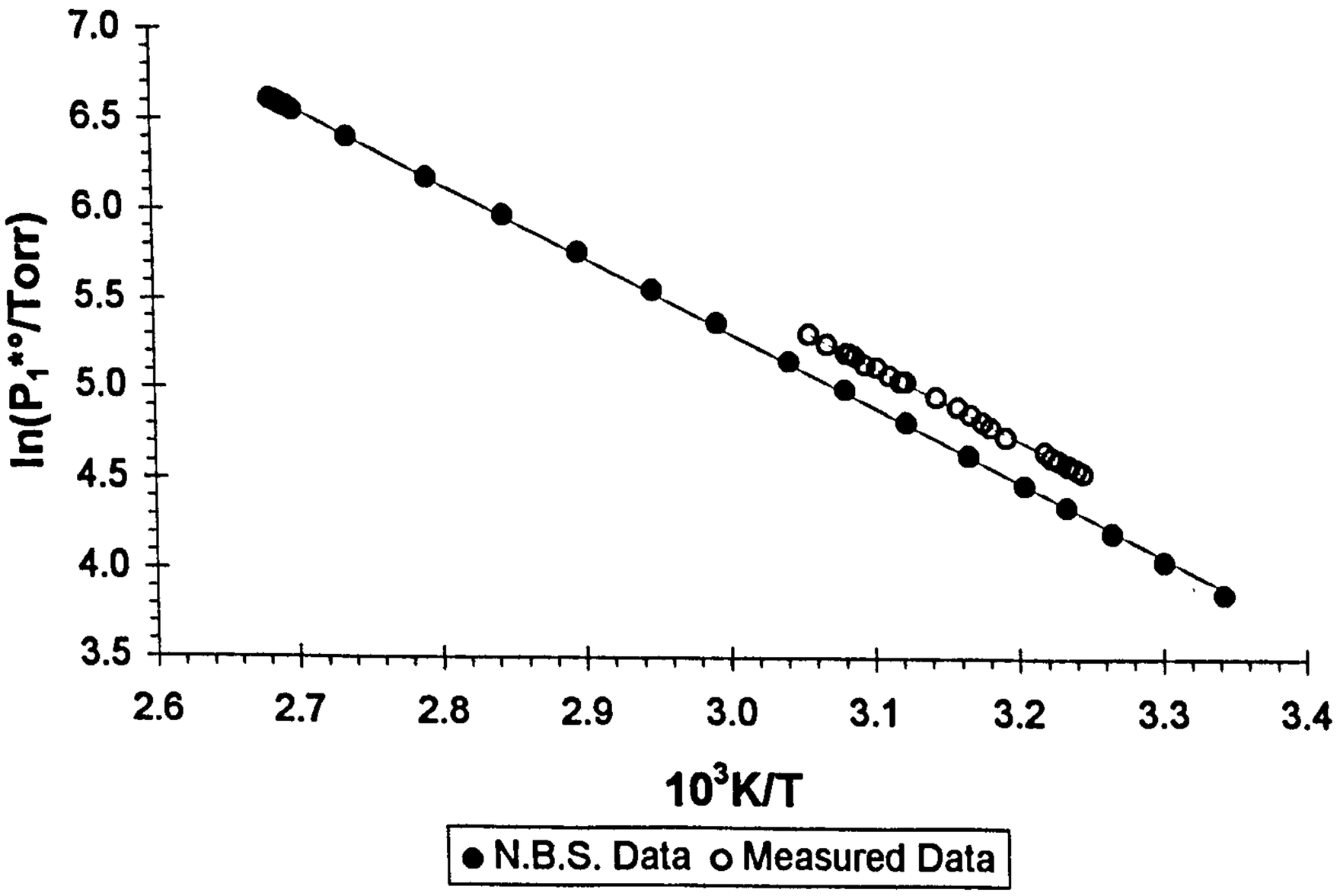

Figure 5.2 *Vapour pressure of pure heptane.*

The red curve in figure 5.1 represents a phase boundary where the saturated solution is in equilibrium with pure solid. The curve passes

through a maximum due to the opposing effects of the temperature dependence of the vapour pressure and of the solubility. On the right hand side the temperature dependence of the vapour pressure is dominant, whereas on the left hand side the change of solubility, and the consequent change in vapour pressure lowering, is dominant.

The cloud point locus for dotriacontane in heptane is calculated from equation 3.1 with the assumption that $w' = 0$. This assumption is easily shown to be justified since, for the points lying on the locus, computational fitting of the data to equation 3.1 leads to a value of $w' = -2 \times 10^{-19}$ J with a residual sum squared of 9×10^{-6}. For this scenario, a plot of $[\ln(x_2)]$ against $(^1/_T)$ gives a value for the enthalpy of fusion of the pure solute ($\Delta_f H_2°$) of 97.7 ± 0.7 kJmol^{-1} and a melting point of 340 ± 5 K. These compare well with values in the literature ranging from 106 to 109 kJmol^{-1} and 339 K[3,4], and the appropriate plot is shown in figure 5.3. It should, however, be noted that, when compared to values obtained from Differential Scanning Calorimetry (D.S.C.)[5] and other techniques[6], the above values approximate to the sum of the heats of pre-melting transition and fusion and the pre-melting transition temperature (see Chapter 6).

In figure 5.1, at high temperatures, we see the expected linear behaviour and the slopes of the lines are constant within experimental error. As the temperature is lowered the vapour pressure falls until the liquid vapour pressure line intersects the saturated solution locus. After phase

separation has occurred, the solid phase being in equilibrium at the specific temperature, the vapour pressure then follows the saturated solution locus.

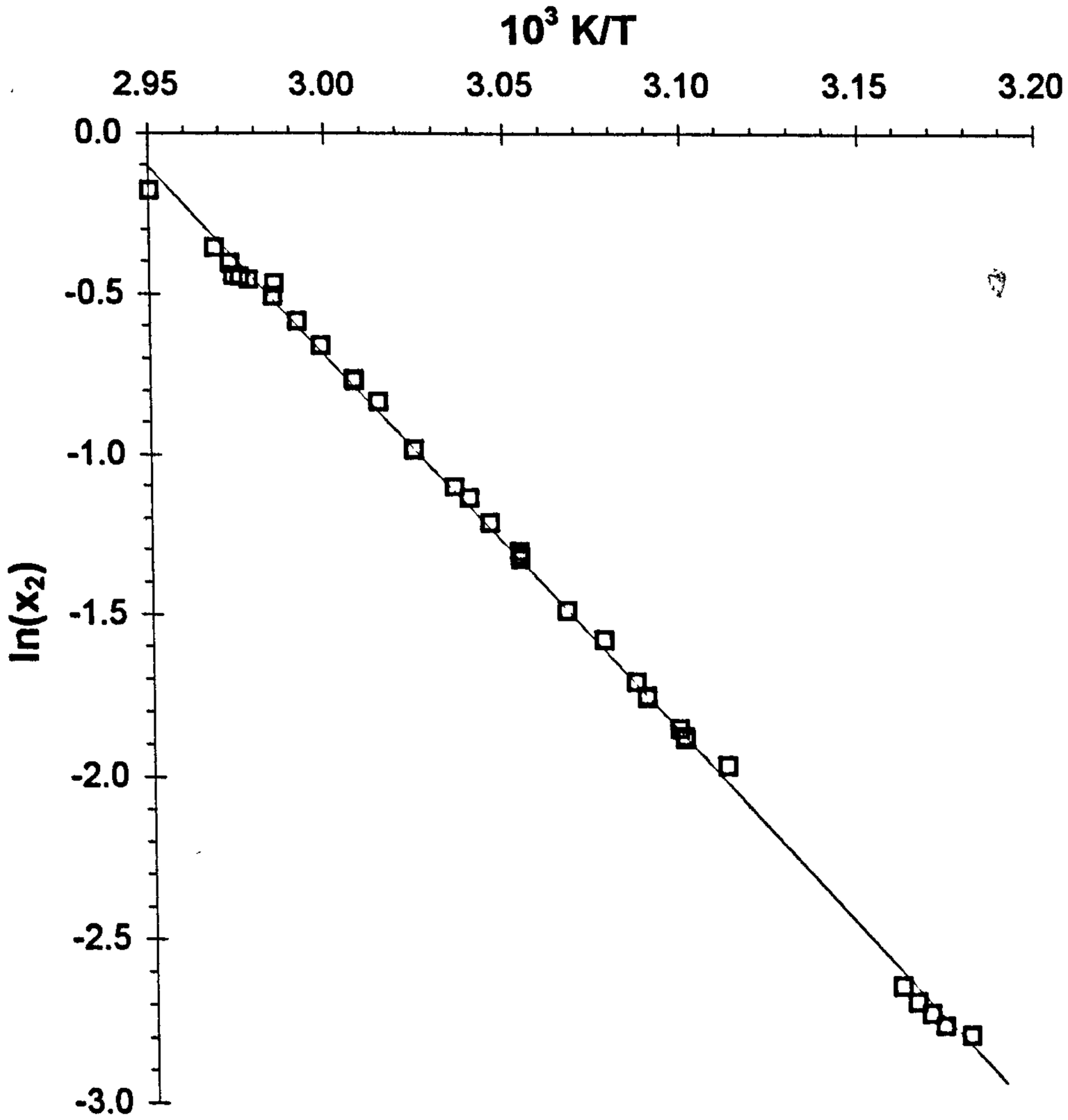

Figure 5.3 *Determination of heat and temperature of fusion for dotriacontane from vapour pressure measurements.*

The fact that the experimental points in figure 5.1 follow the same phase separation locus, no matter what initial liquid composition is used, confirms the assumption that, for this system, the solid phase is impermeable to solvent and, presumably, crystalline.

§ 5.1.2 Heptacosane

The results for heptacosane and heptane at various volume fractions are given in table 5.3, and figure 5.4 shows the natural logarithm of the solvent vapour pressure as a function of reciprocal temperature.

φ_2/%	10^3K/T	ln(P_1*/Torr)
94.2	2.8183	4.4194
	2.8547	4.2968
	2.8759	4.2148
	2.9192	4.0635
	2.9192	4.0609
	2.9417	3.9729
	2.9643	3.8881
	2.9871	3.8185
94.6	2.8567	4.1730
	2.8779	4.0906
	2.9213	3.9212
	2.9661	3.7582
	3.0122	3.5787
	3.0599	3.3484
	3.1091	3.2349
95.0	2.9984	3.5199
	3.0112	3.4783
	3.0348	3.4193

φ_2/%	10^3K/T	ln(P_1*/Torr)
95.0	3.0587	3.2994
93.0	3.0792	3.7996
	3.1124	3.6127
	3.1348	4.0205
	3.1463	4.1085
	3.1582	4.1819
	3.1697	4.2357
	3.1814	4.2631
	3.1931	4.2778
	3.2048	4.2864
	3.2167	4.2827
	3.2407	4.2516
93.0	2.9377	4.3421
	2.9473	4.3273
	2.9575	4.2876
	2.9677	4.2488
	2.9779	4.2000
	2.9885	4.1583

φ_2/%	10^3K/T	ln(P_1*/Torr)
93.0	2.9988	4.1149
	3.0093	4.0835
	3.0197	4.0334
	3.0309	3.9998
	3.0305	4.0003
	3.0412	3.9210
	3.0519	3.8960
	3.0630	3.8584
	3.0739	3.8125
	3.0850	3.7728
	3.0961	3.7246
	3.1074	3.6786
	3.1187	3.6220
	3.1301	3.9458
	3.1415	4.0854
	3.1535	4.1508

Table 5.3 *Vapour pressures of heptane in heptacosane at various compositions.*

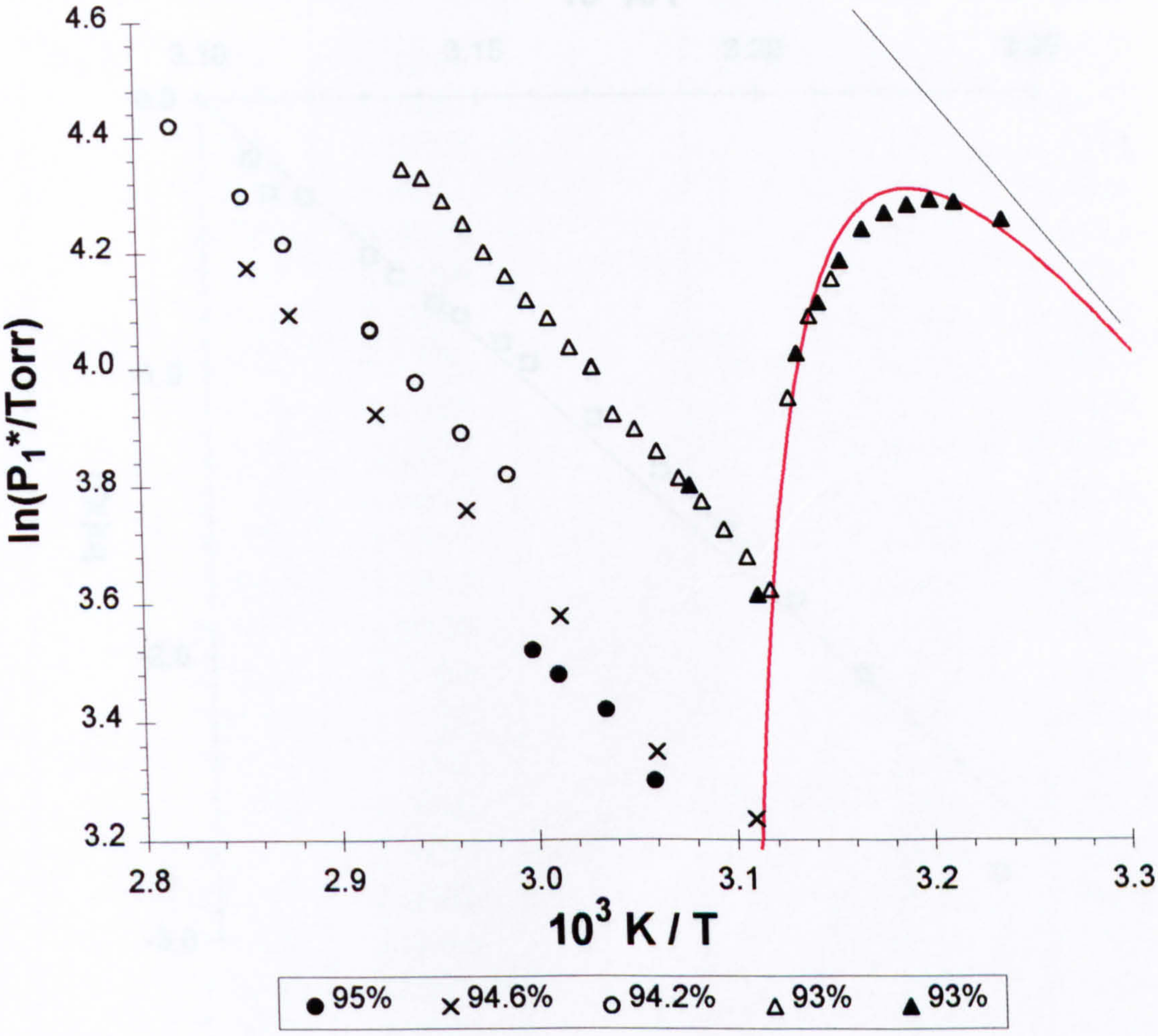

Figure 5.4 *Vapour pressures of heptane in heptacosane at various compositions.*

The red curve in figure 5.4 represents the cloud point locus for heptacosane in heptane and is calculated from equation 3.1 with the assumption that w' = 0. This locus is again reasonable since a plot of $[\ln(x_2)]$ against $(^1/_T)$ gives a value of w' = -3×10^{-19} J with a residual sum squared of 2×10^{-9}. The graph is shown in figure 5.5 and leads to a value for the enthalpy of fusion of the pure solute of 149 ± 6 kJmol^{-1} and a melting point of 323 ± 15 K, which can be compared with values elsewhere[7,8] (~112 kJmol^{-1} and 331 K).

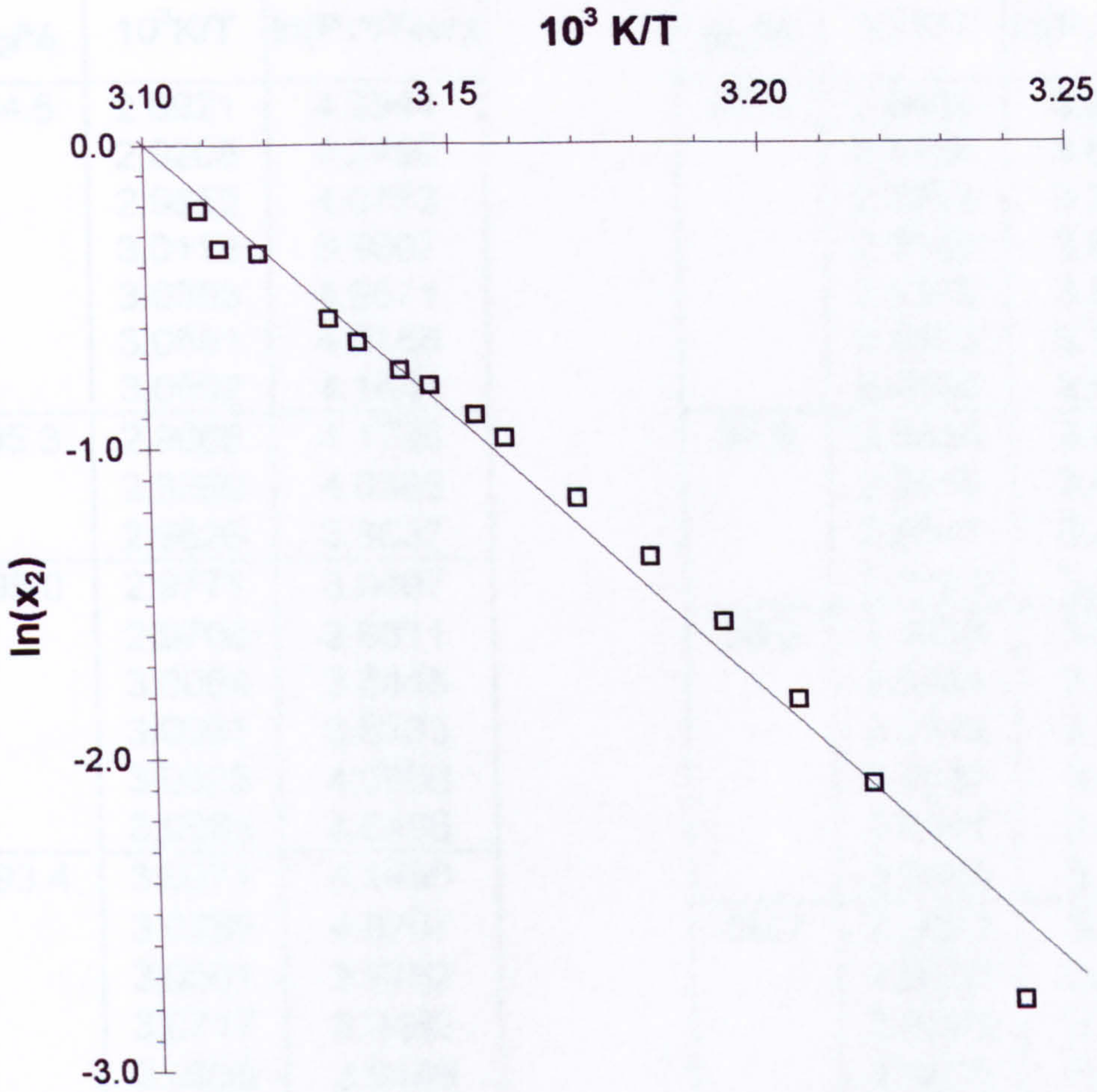

Figure 5.5 *Determination of heat and temperature of fusion for heptacosane from vapour pressure measurements.*

§ 5.2 Equimolar mixture of dotriacontane and heptacosane

An equimolar mixture of dotriacontane and heptacosane was made by melting 0.5422g $C_{32}H_{66}$ with 0.4578g $C_{27}H_{56}$. The results for this binary mixture with heptane at various volume fractions are given in table 5.4, and figure 5.6 shows the temperature dependence of the solvent vapour pressure.

φ_2/%	10^3K/T	ln(P_1*/Torr)
94.5	2.8921	4.3544
	2.9206	4.2450
	2.9652	4.0773
	3.0113	3.9007
	3.0353	4.0571
	3.0591	4.0156
	3.0592	4.1844
95.3	2.9066	4.1726
	2.9399	4.0366
	2.9626	3.9637
95.0	2.9771	3.9497
	2.9706	3.9811
	3.0064	3.8445
	3.0081	3.8333
	3.0325	4.0088
	3.0566	4.0466
93.4	3.0071	4.1456
	3.0289	4.0707
	3.0501	3.9762
	3.0717	3.9480
	3.0935	3.9449
	3.0935	3.9578
	3.0936	3.9831
	3.0935	4.0102
	3.0935	4.1018

φ_2/%	10^3K/T	ln(P_1*/Torr)
97.4	2.8466	3.8993
	2.8726	3.8057
	2.8928	3.7214
	2.9149	3.6504
	2.9375	3.5948
	2.9603	3.5131
	2.9835	3.4517
97.9	2.9634	3.4402
	2.9610	3.4632
	2.9841	3.4062
	3.0119	3.3879
98.3	2.8838	3.6632
	2.9084	3.5943
	2.9313	3.5202
	2.9637	3.4402
	2.9614	3.4733
	2.9845	3.3667
98.7	2.9022	3.5203
	2.9165	3.4387
	2.9393	3.3986
	2.9619	3.3460
	2.9852	3.2744
	3.0087	3.1704
	3.0205	3.6738

Table 5.4 *Vapour pressures of heptane in an equimolar mixture of dotriacontane and heptacosane at various compositions.*

The blue and red curves in figure 5.6 represent the cloud point loci for both pure dotriacontane and heptacosane respectively in heptane. The green curve is the corresponding curve calculated from equation 3.1 with the values for the heat of fusion and melting point given by

$$\Delta_f H^{\circ}_{\text{equimolar mixture}} = \tfrac{1}{2}\Delta_f H^{\circ}_{C_{32}H_{66}} + \tfrac{1}{2}\Delta_f H^{\circ}_{C_{27}H_{56}} \qquad (5.1)$$

$$\text{and } T_M(\text{equimolar mixture}) = T_M(C_{32}H_{66})^{\frac{1}{2}} \times T_M(C_{27}H_{56})^{\frac{1}{2}}. \qquad (5.2)$$

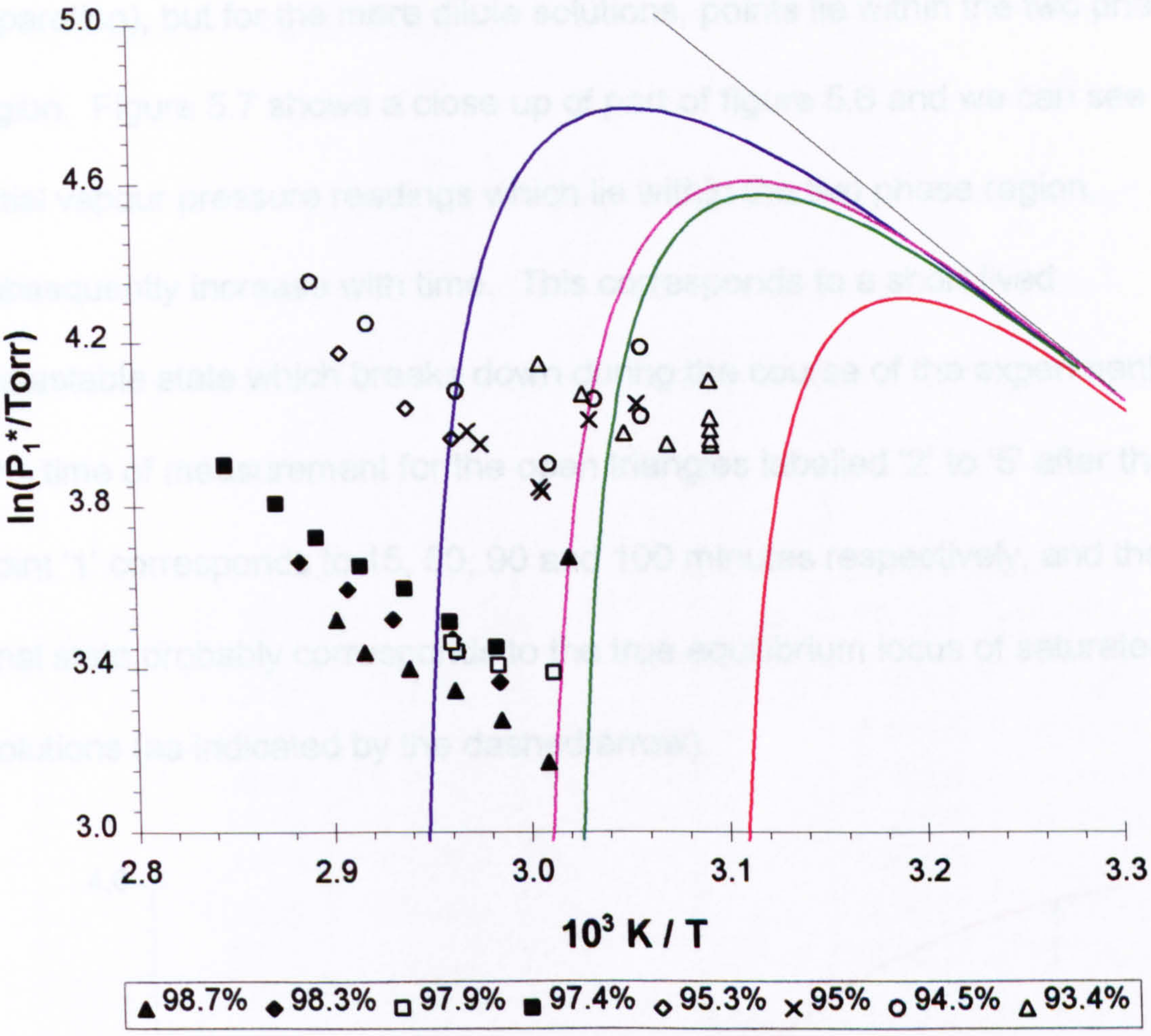

Figure 5.6 *Vapour pressures of heptane in an equimolar mixture of dotriacontane and heptacosane at various compositions.*

Clearly, this does not represent a good fit and the system no longer behaves ideally. Indeed, if we note that an equimolar mixture of dotriacontane and heptacosane corresponds to a 32:27 mixture by volume, and use the following parameters in equation 2.41,

$$\Delta_f H^{\circ}_{\text{equimolar mixture}} = \frac{32}{59}\Delta_f H^{\circ}_{C_{32}H_{66}} + \frac{27}{59}\Delta_f H^{\circ}_{C_{27}H_{56}} \qquad (5.3)$$

$$\text{and } T_M(\text{equimolar mixture}) = T_M(C_{32}H_{66})^{\frac{32}{59}} \times T_M(C_{27}H_{56})^{\frac{27}{59}} \qquad (5.4)$$

then we obtain the purple curve shown. For the most concentrated solutions, the points fall on the phase boundary (indicating immediate phase

separation), but for the more dilute solutions, points lie within the two phase region. Figure 5.7 shows a close up of part of figure 5.6 and we can see that initial vapour pressure readings which lie within the two phase region, subsequently increase with time. This corresponds to a short lived metastable state which breaks down during the course of the experiment. The time of measurement for the open triangles labelled '2' to '5' after that of point '1' corresponds to 15, 50, 90 and 100 minutes respectively, and the final state probably corresponds to the true equilibrium locus of saturated solutions (as indicated by the dashed arrow).

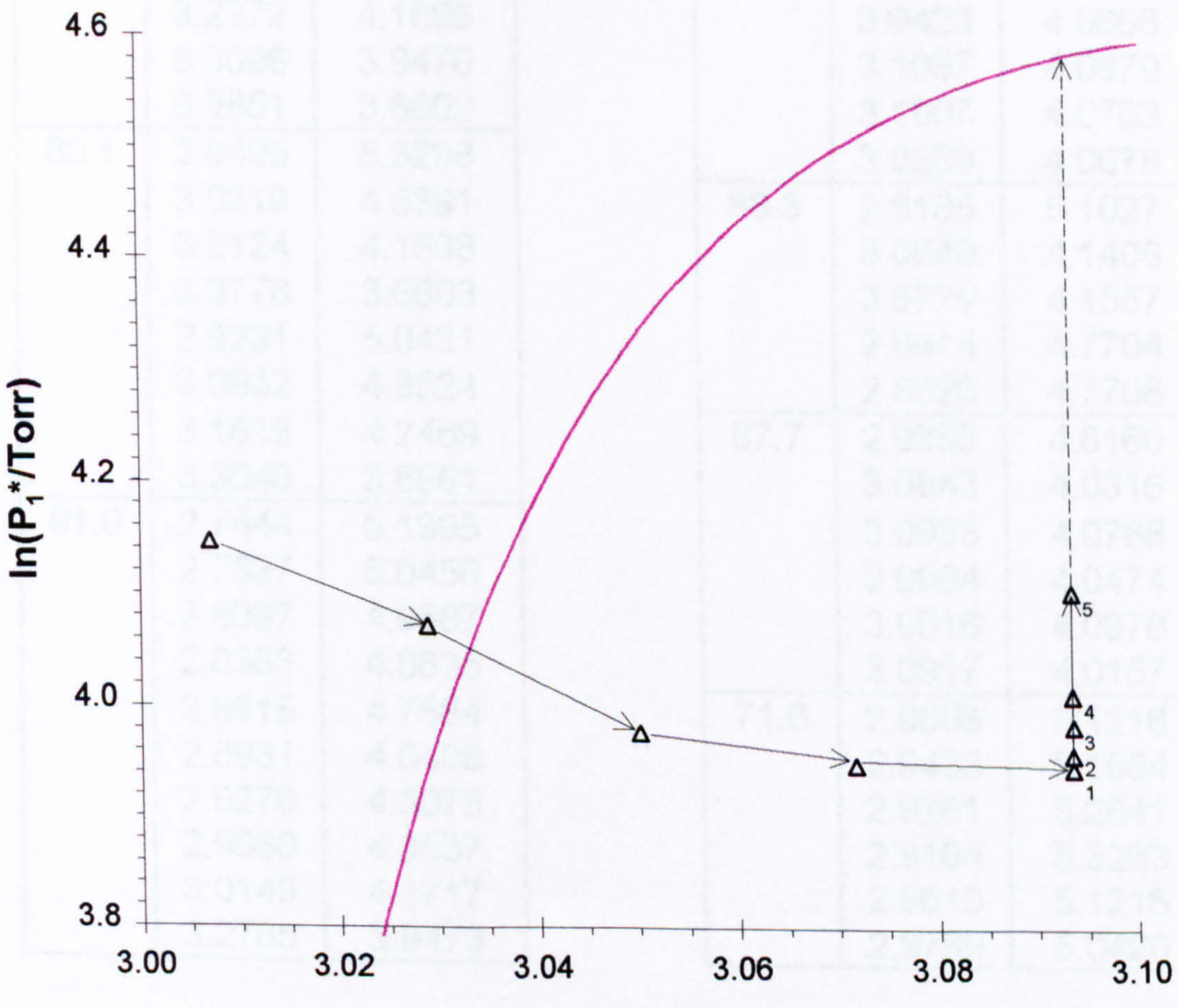

Figure 5.7 *Change in vapour pressure of heptane in an equimolar mixture of dotriacontane and heptacosane at fixed temperature and composition.*

§ 5.3 Nippon Seiro (140/145°F)

The results for Nippon Seiro paraffin wax and heptane at various volume fractions are presented in table 5.5, and figure 5.8 shows the temperature dependence of the solvent vapour pressure for some of these data.

φ_2/%	10^3K/T	ln(P_1*/Torr)
69.8	3.1003	4.6380
	2.9370	5.3276
	3.0248	4.9549
	3.1618	4.3516
	3.2372	4.1696
	3.3096	3.9470
	3.3851	3.6602
80.1	2.8498	5.3298
	3.0210	4.6391
	3.2124	4.1698
	3.3778	3.6603
	2.9231	5.0431
	3.0932	4.3524
	3.1616	4.2469
	3.3046	3.8961
91.0	2.7444	5.1995
	2.7837	5.0456
	2.8097	4.9587
	2.8363	4.8635
	2.8615	4.7584
	2.8931	4.6408
	2.9276	4.5075
	2.9660	4.3537
	3.0149	4.1717
	3.2765	3.9473

φ_2/%	10^3K/T	ln(P_1*/Torr)
91.0	3.3362	3.7852
	2.8965	4.6408
	2.9709	4.3537
	3.0321	4.1205
	3.0423	4.0666
	3.1067	4.0879
	3.1907	4.0763
	3.2589	4.0078
88.3	2.8185	5.1027
	3.0840	4.1408
	3.0779	4.1557
	2.8914	4.7704
	2.8923	4.7706
87.7	2.9353	4.8166
	3.0843	4.0316
	3.0883	4.0768
	3.0964	4.0474
	3.0816	4.0978
	3.0917	4.0167
71.6	2.9608	5.1216
	2.9433	5.1954
	2.9261	5.2641
	2.9104	5.3283
	2.9610	5.1216
	2.9799	5.0420

Table 5.5 *Vapour pressures of heptane in Nippon Seiro (140/145°F) paraffin wax at various compositions.*

φ_2/%	10^3K/T	ln(P_1*/Torr)
71.6	2.9882	5.0082
	2.9965	4.9733
	3.0054	4.9371
	3.0143	4.8995
	3.0239	4.8605
	3.0337	4.8198
	3.0439	4.7775
	3.0548	4.7332
	3.0659	4.6869
	3.0773	4.6383
	3.0960	4.5607
	3.1158	4.4764
57.8	2.9818	5.2627
	3.0350	5.0408
	3.0783	4.8595
	3.0879	4.8189
	3.1034	4.7547
	3.1140	4.7094
	3.1310	4.6375
	3.1492	4.5599
	3.1623	4.5046
	3.1797	4.4308
	3.1950	4.3643
89.6	3.0092	4.2846
	3.0265	4.2187
	3.0487	4.1354
	3.0487	4.1448
89.0	2.9541	4.5072
	2.9551	4.5072
	2.9797	4.4097
	2.9798	4.4194
	2.9797	4.4194
	2.9796	4.4175
	2.9797	4.4256
	2.9972	4.3561
	3.0149	4.2835
	3.0325	4.2133
	3.0505	4.1370

φ_2/%	10^3K/T	ln(P_1*/Torr)
76.5	2.8981	5.2521
	2.9110	5.1961
	2.9488	5.0426
	2.9937	4.8610
	3.0476	4.6387
	3.1308	4.3519
	3.1703	4.2829
	3.1324	4.3519
	3.2079	4.1902
90.4	2.8966	4.6408
	2.9756	4.3536
	3.0250	4.1717
	3.0465	4.0884
	3.2390	3.9962
	3.2290	4.0197
	3.2180	4.0427
	3.2058	4.0651
	3.1907	4.0871
	3.1761	4.1087
	3.0403	4.1309
89.6	3.1913	4.1357
	3.0290	4.2107
	3.0309	4.2106
	3.0251	4.2315
	3.0428	4.1619
	3.0474	4.1460
	3.0519	4.1287
	3.0564	4.1291
	3.0611	4.1156
	3.0655	4.1290
	3.0701	4.1483
	3.0793	4.1519
	3.0884	4.1457
	3.0982	4.1634
	3.1074	4.1625
	3.1166	4.1688
	3.1262	4.1591
	3.1357	4.1746

Table 5.5 *continued.*

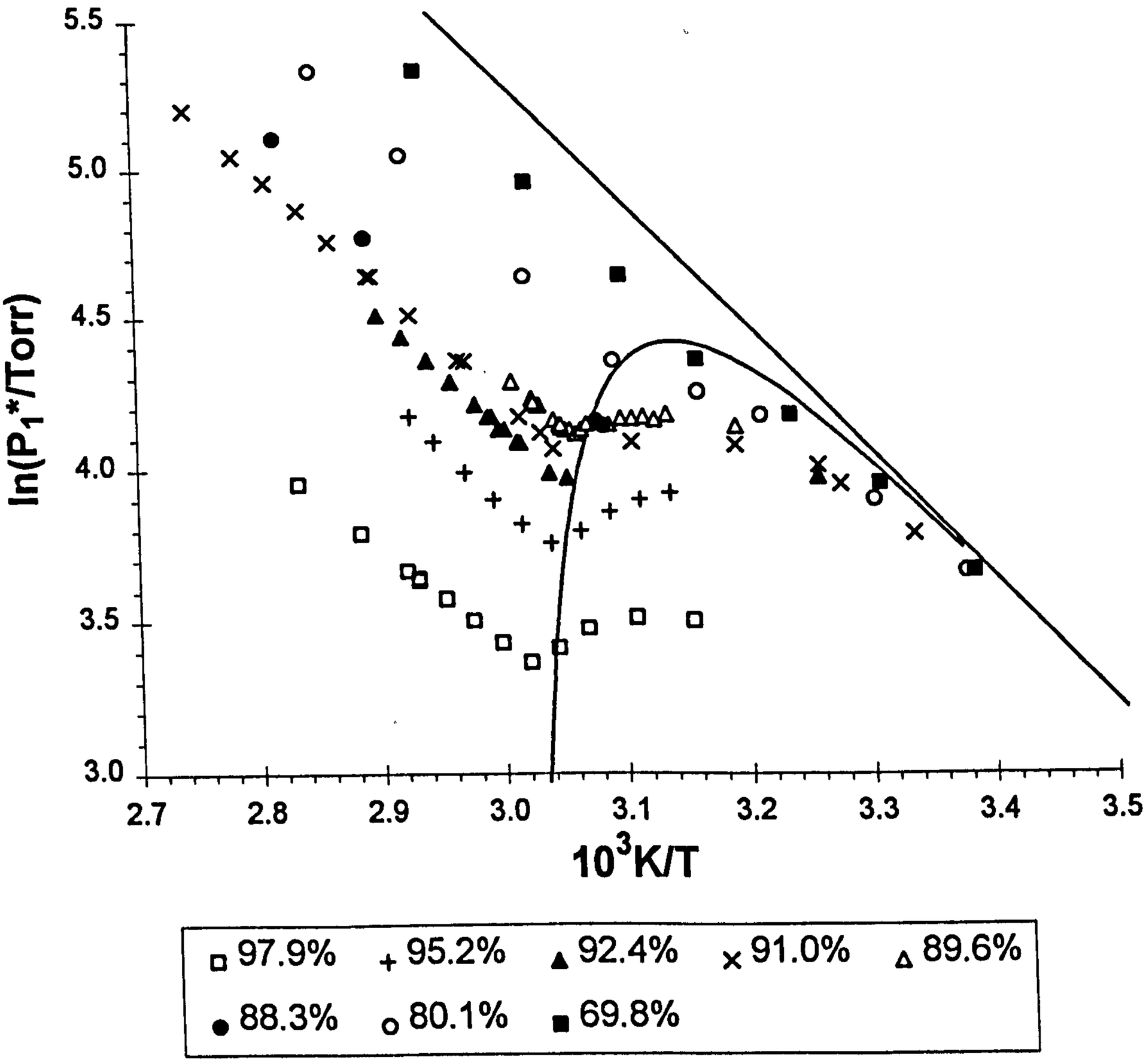

Figure 5.8 *Vapour pressures of heptane in Nippon Seiro (140/145°F) paraffin wax at various compositions.*

It can be inferred from the solubility results in chapter 3 that the approximation of w'=0 applies to the Nippon Seiro / heptane system. This assumption is included in the calculation of the blue cloud point locus in figure 5.8. Again, we see the expected linear behaviour at high temperatures and on lowering the temperature, the vapour pressure falls until the liquid vapour pressure line intersects the saturated solution locus. Upon phase separation, if the solid phase was pure wax at equilibrium, we

would expect the vapour pressure to follow the saturated solution locus. The results suggest, however, that a lower vapour pressure than that calculated for the saturated solution is obtained.

§ 5.4 BD887 microcrystalline wax

BD887 is a commercial microcrystalline wax which melts in the temperature range 45–90°C. It consists mainly of straight chain alkanes (~72%) in the carbon number range 25–45, with the main impurities being simple methyl substituted derivatives. G.C. leads to an average carbon number ($\bar{n}$) of 36.32 and hence a mean molecular weight of 511.44 $gmol^{-1}$ (assuming an overall stoichiometry of $C_{\bar{n}}H_{2\bar{n}\ 2}$).

The results for BD887 microcrystalline wax and heptane at various weight fractions are presented in table 5.6, and figure 5.9 shows the temperature dependence of the solvent vapour pressure for some of these data.

The purple curve in figure 5.9 is calculated using values for the heat of fusion and melting point obtained by D.S.C.[9] in equation 2.41 with the usual assumption that w' = 0 and only serves as a very approximate phase boundary. Here, no sharp rise in vapour pressure is observed when the temperature of the liquid mixture is lowered and points are obtained within the two phase region. This indicates that a metastable network is formed which gives rise to lower vapour pressures than expected and it has a

lifetime at least of the order of the duration of the experiment (~30 minutes between points).

w_2/%	10^3K/T	ln(P_1*/Torr)
95.1	2.9327	4.5345
	2.9511	4.4643
	2.9379	4.5146
	2.9558	4.4643
	2.9750	4.4333
	2.9944	4.3854
	3.0137	4.3658
	2.9526	4.4622
	2.9709	4.4549
94.1	2.9906	4.4742
	3.0096	4.4502
	3.0095	4.4472
	3.0297	4.4123
95.4	2.9335	4.4754
	2.9332	4.4465
	2.9519	4.4696
	2.9711	4.4730
	2.9711	4.4747
	2.9904	4.4347
93.8	2.9335	4.5506
	2.9518	4.5375
	2.9709	4.5553
	2.9904	4.4960
95.0	2.9544	4.4351
	2.9734	4.5048
	2.9733	4.5444
	2.9919	4.5000
	2.9916	4.5634
93.4	2.9077	4.6538
	2.8695	4.7849
	2.8323	4.9320
	2.7960	5.0766

w_2/%	10^3K/T	ln(P_1*/Torr)
93.8	2.9673	4.5866
	2.9472	4.5826
	2.9472	4.5911
	2.9273	4.5915
	2.9078	4.6244
	2.8887	4.6739
	2.8699	4.7423
	2.8333	4.8950
92.5	3.0505	4.4958
	3.0291	4.5300
	3.0289	4.5388
	3.0082	4.5565
	2.9878	4.5871
	2.9674	4.6109
	2.9479	4.6170
	2.9265	4.6376
93.4	2.9888	4.5325
	3.0091	4.5066
	3.0296	4.4679
	3.0506	4.4329
	3.0716	4.4183
	3.0934	4.3864
	3.1153	4.3398
	3.1376	4.2851
	3.1604	4.2287
	3.1834	4.1640
	3.2067	4.0948
	3.2305	4.0380
	3.2545	3.9310
	3.2792	3.8617
	3.3040	3.7590
	3.3294	3.6590

Table 5.6 *Vapour pressures of heptane in BD887 microcrystalline wax.*

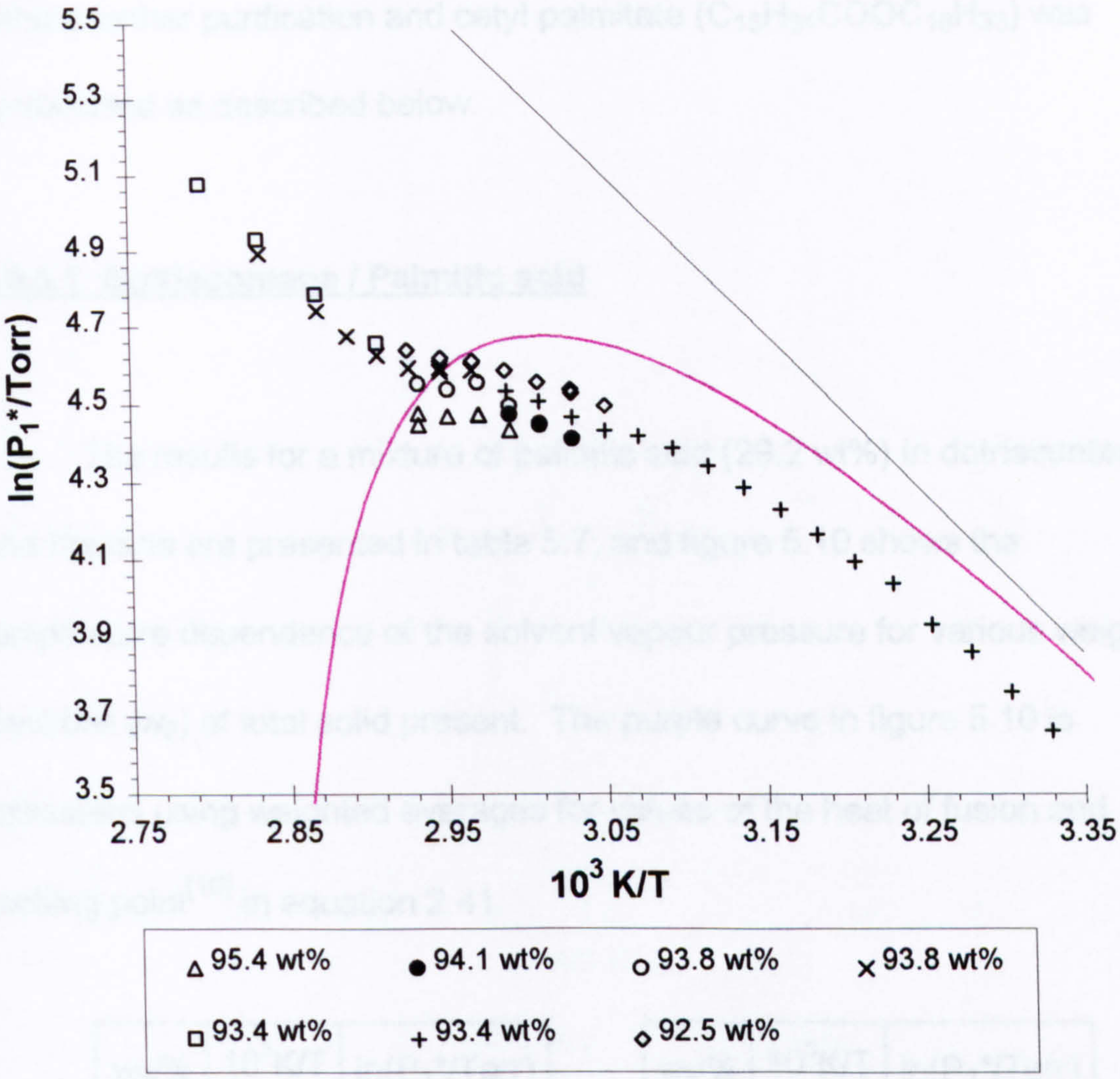

Figure 5.9 *Vapour pressures of heptane in BD887 microcrystalline wax.*

§ 5.5 Doped dotriacontane systems

It is clear from the results presented so far that additives to a pure long chain hydrocarbon / heptane system show some degree of introducing 'gel-like' behaviour. For this reason it was seen to be useful to try and identify any component(s) in polish pastes which would induce gelation.

Samples of palmitic acid ($C_{15}H_{31}COOH$ - Aldrich Chemical Co., 99%) and hexadecanol ($C_{16}H_{33}OH$ - Aldrich Chemical Co., 99%) were used

without further purification and cetyl palmitate ($C_{15}H_{31}COOC_{16}H_{33}$) was synthesised as described below.

§ 5.5.1 Dotriacontane / Palmitic acid

The results for a mixture of palmitic acid (29.2 wt%) in dotriacontane and heptane are presented in table 5.7, and figure 5.10 shows the temperature dependence of the solvent vapour pressure for various weight fractions (w_2) of total solid present. The purple curve in figure 5.10 is calculated using weighted averages for values of the heat of fusion and melting point[10] in equation 2.41.

w_2/%	10^3K/T	ln(P_1*/Torr)
90.5	2.9684	4.3551
	3.0080	4.1678
	3.0286	4.0799
	3.0492	4.1327
	3.0705	4.2255
	3.0921	4.2673
	3.1141	4.2768
	3.1361	4.2323

w_2/%	10^3K/T	ln(P_1*/Torr)
90.5	3.1730	4.2259
	3.1818	4.1906
91.9	2.9871	4.1909
	3.0075	4.0991
	3.0282	4.0140
	3.0492	4.0860
	3.0708	4.2088
	3.0925	4.2432

Table 5.7 *Vapour pressures of heptane in palmitic acid / dotriacontane.*

Clearly, this is not a good fit for this system and a more representative fit would be given by the dashed curve. The sharp rise in vapour pressure observed when lowering the temperature of the liquid mixture is indicative of phase separation and no gel formation occurs.

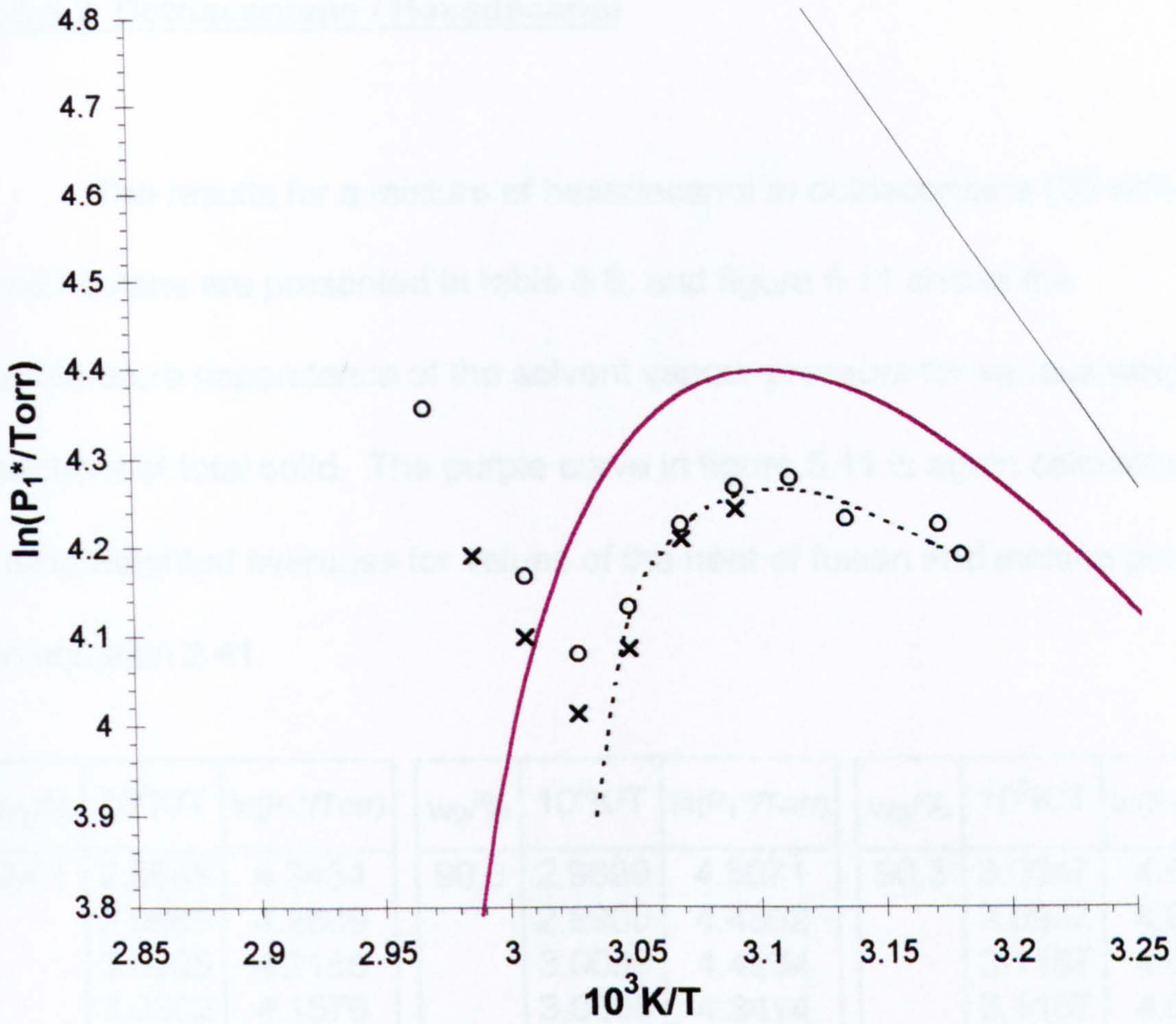

Figure 5.10 *Vapour pressures of heptane in palmitic acid / dotriacontane.*

As pointed out in chapter 3, determination of the solubility in the usual sense is not meaningful for wax mixtures since the use of solvent results in fractionation. Hence a more accurate estimate of the phase boundary from solubility measurements is not possible. It is known, however, from complementary test-tube studies that these systems do in fact phase separate (see chapter 6).

§ 5.5.2 Dotriacontane / Hexadecanol

The results for a mixture of hexadecanol in dotriacontane (25 wt%) and heptane are presented in table 5.8, and figure 5.11 shows the temperature dependence of the solvent vapour pressure for various weight fractions of total solid. The purple curve in figure 5.11 is again calculated using weighted averages for values of the heat of fusion and melting point[10] in equation 2.41.

w_2/%	10^3K/T	ln(P_1*/Torr)
94.1	2.9685	4.3454
	2.9888	4.2889
	3.0095	4.2185
	3.0302	4.1576
	3.0515	4.3680
	3.0684	4.4489
	3.0961	4.4796
	3.1245	4.4512

w_2/%	10^3K/T	ln(P_1*/Torr)
90.3	2.9699	4.5071
	2.9900	4.4362
	3.0099	4.4234
	3.0305	4.3414
	3.0518	4.4257
	3.0518	4.4266
	3.0730	4.5669
	3.0730	4.5648
	3.0838	4.6034
	3.0838	4.5998

w_2/%	10^3K/T	ln(P_1*/Torr)
90.3	3.0947	4.6231
	3.0947	4.6231
	3.1167	4.6303
	3.1167	4.6283
	3.1388	4.6082
	3.1388	4.6077
	3.1616	4.5648
	3.1846	4.4926
	3.1844	4.5097
	3.2079	4.4435

Table 5.8 *Vapour pressures of heptane in hexadecanol / dotriacontane.*

This is a much better fit for this system, although when attempting to increase the set point of the solvent for the more dilute solution run a different saturated solution locus was followed. This is attributed to loss of solute form the thermometer element and hence a shift in overall composition making the recorded concentration of 90.3 wt% somewhat questionable. Test-tube studies confirm that phase separation occurs.

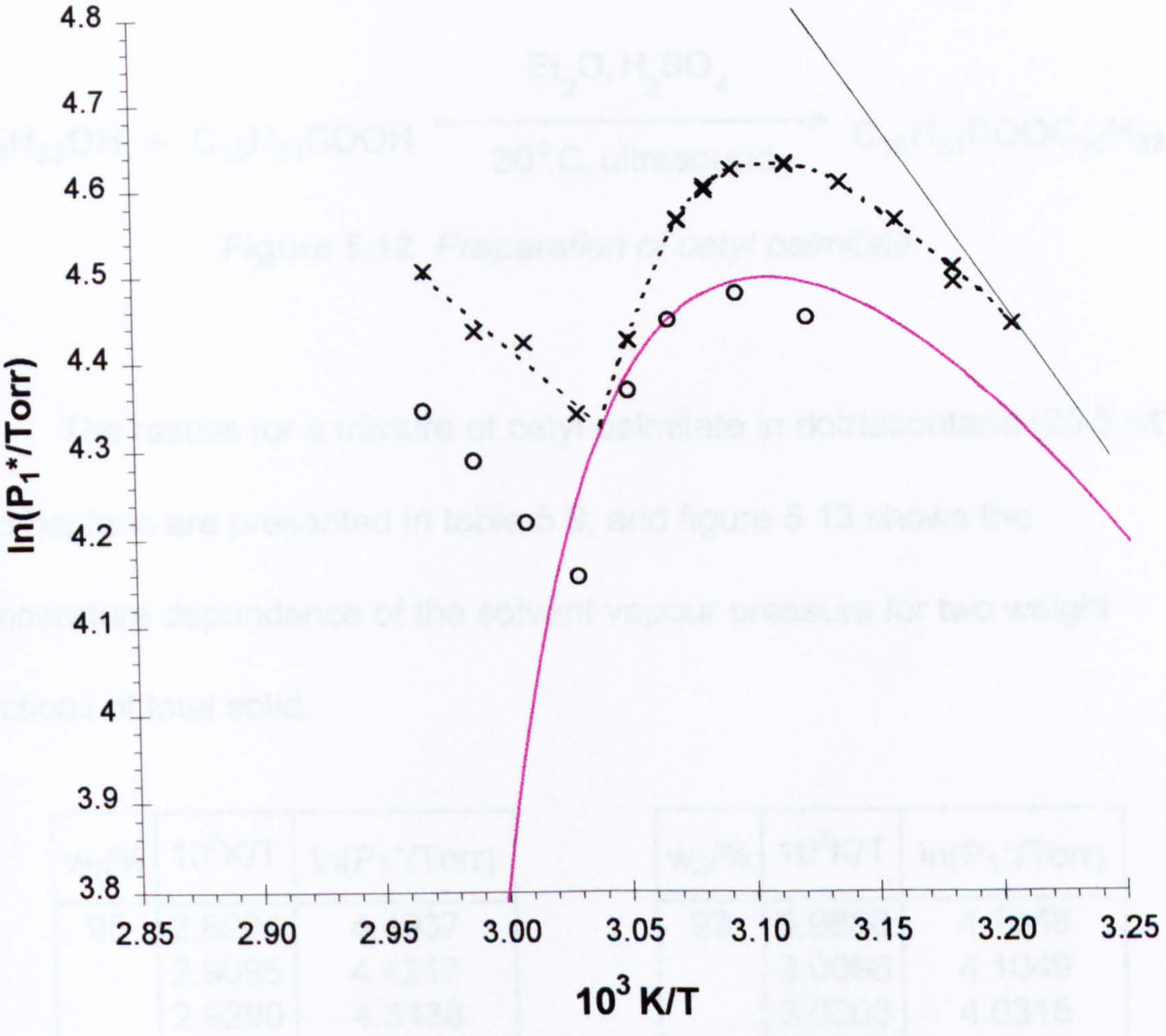

Figure 5.11 *Vapour pressures of heptane in hexadecanol / dotriacontane.*

§ 5.5.3 Dotriacontane / Cetyl palmitate

Cetyl palmitate was prepared by simple acid catalysed esterification of palmitic acid with hexadecanol as shown in figure 5.12. It was found that use of a conventional heating mantle resulted in a low yield, presumably due to folding over of the long chains which hinder the reaction centres. The yield was enhanced greatly by use of ultrasound heating techniques[11].

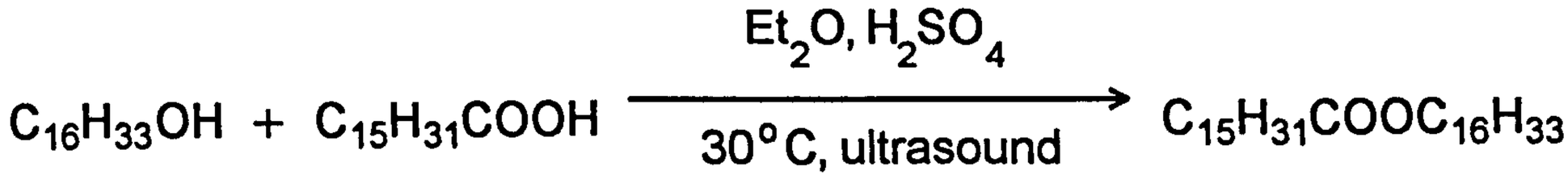

Figure 5.12 *Preparation of cetyl palmitate.*

The results for a mixture of cetyl palmitate in dotriacontane (25.5 wt%) and heptane are presented in table 5.9, and figure 5.13 shows the temperature dependence of the solvent vapour pressure for two weight fractions of total solid.

w_2/%	10^3K/T	ln(P_1*/Torr)
95	2.8904	4.4937
	2.9095	4.4217
	2.9290	4.3438
	2.9485	4.2687
	2.9686	4.1884
	2.9888	4.1255
	3.0094	4.0183
	3.0304	3.9312

w_2/%	10^3K/T	ln(P_1*/Torr)
93	2.9898	4.1848
	3.0098	4.1049
	3.0303	4.0315
	3.0514	4.1831
	3.0728	4.3143
	3.0944	4.3691
	3.1167	4.3809
	3.1387	4.3655
	3.1615	4.3145

Table 5.9 *Vapour pressures of heptane in cetyl palmitate / dotriacontane.*

The data again indicates that phase separation occurs and parallels the general trend as predicted by the purple curve[9].

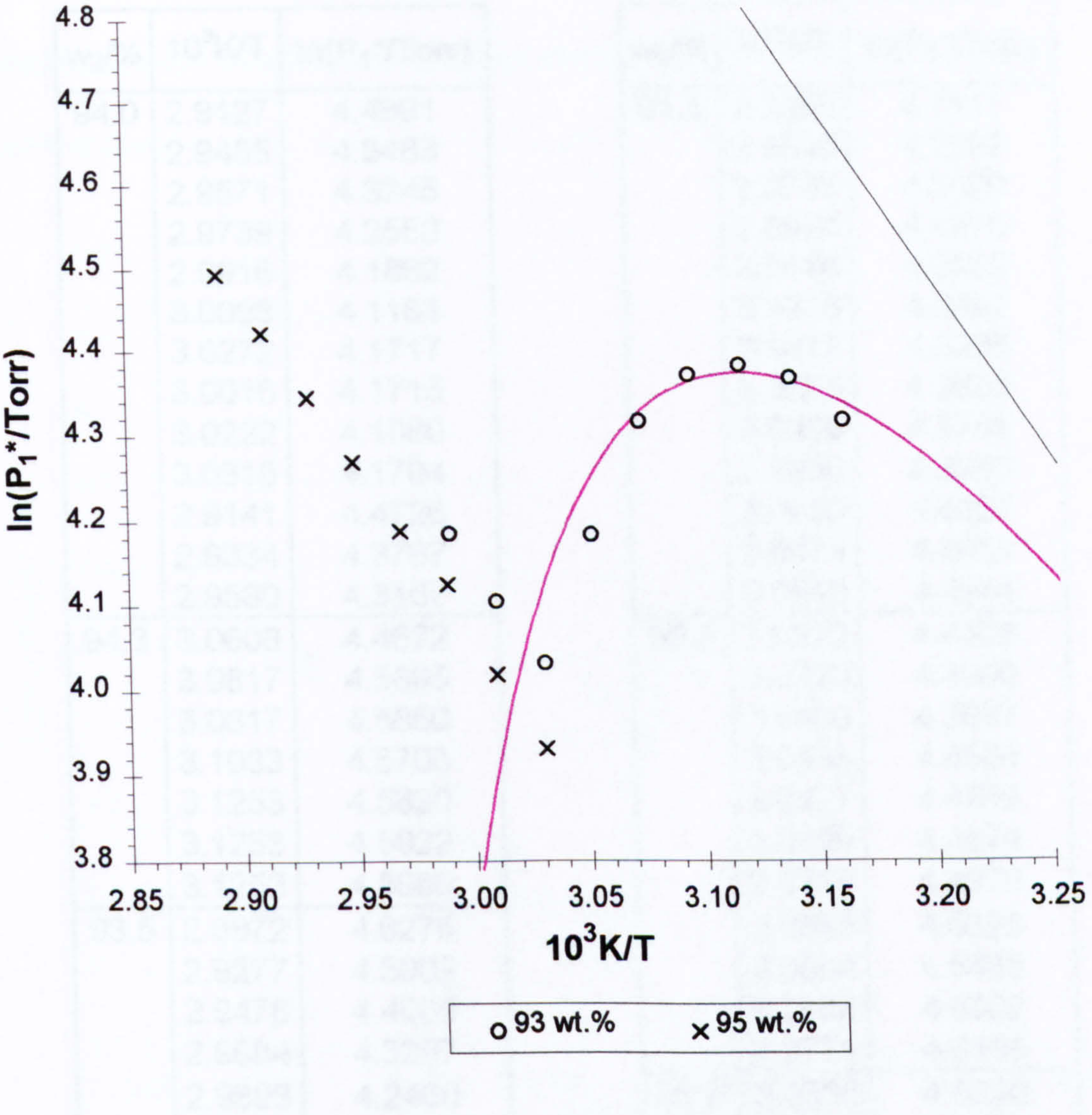

Figure 5.13 *Vapour pressures of heptane in cetyl palmitate / dotriacontane.*

§ 5.5.4 Dotriacontane / BD887 microcrystalline wax

The results for a mixture of BD887 microcrystalline wax in dotriacontane (9.1 wt%) and heptane are presented in table 5.10, and figure 5.14 shows the temperature dependence of the solvent vapour pressure for various weight fractions of total solid.

The red curve in figure 5.14 is the cloud point locus for dotriacontane as shown in figure 5.1.

w_2/%	10^3K/T	ln(P_1*/Torr)
94.0	2.9127	4.4891
	2.9455	4.3483
	2.9571	4.3245
	2.9739	4.2558
	2.9916	4.1862
	3.0098	4.1161
	3.0272	4.1717
	3.0016	4.1715
	3.0222	4.1080
	3.0315	4.1704
	2.9141	4.4726
	2.9334	4.3767
	2.9530	4.3167
94.3	3.0608	4.4672
	3.0817	4.5895
	3.0817	4.5850
	3.1033	4.5705
	3.1253	4.5820
	3.1253	4.5922
	3.1253	4.5966
93.5	2.8972	4.6278
	2.9277	4.5002
	2.9478	4.4069
	2.9684	4.3207
	2.9893	4.2460
	3.0222	4.1352
90.0	2.9769	4.7121
	2.9873	4.6259
	2.9978	4.5945
	3.0083	4.5247
	3.0190	4.4582
	3.0297	4.4355

w_2/%	10^3K/T	ln(P_1*/Torr)
91.1	2.9340	4.7111
	2.9340	4.7237
	2.9743	4.5520
	2.9924	4.4815
	3.0118	4.3862
	3.0318	4.3282
	3.0317	4.3286
	3.0355	4.3623
	3.0396	4.3785
	3.0436	4.3910
	3.0453	4.4307
	3.0473	4.4659
	3.0513	4.4944
90.0	3.0222	4.4428
	3.0320	4.4000
	3.0400	4.3837
	3.0438	4.4534
	3.0477	4.4756
	3.0499	4.4874
	3.0519	4.4970
	3.0560	4.5329
	3.0604	4.5488
	3.0688	4.5802
	3.0771	4.6196
90.0	3.0536	4.5230
	3.0639	4.5952
	3.0742	4.6384
	3.0804	4.6679
	3.0865	4.6671
	3.0948	4.7033
	3.1053	4.7085
	3.1159	4.6918
	3.1267	4.6829

Table 5.10 *Vapour pressures of heptane in BD887 microcrystalline wax / dotriacontane.*

For all of the runs except the most concentrated one, a sharp rise in vapour pressure is observed when the temperature of the liquid mixture is

lowered and the points trace a rather well defined two phase boundary (dashed line).

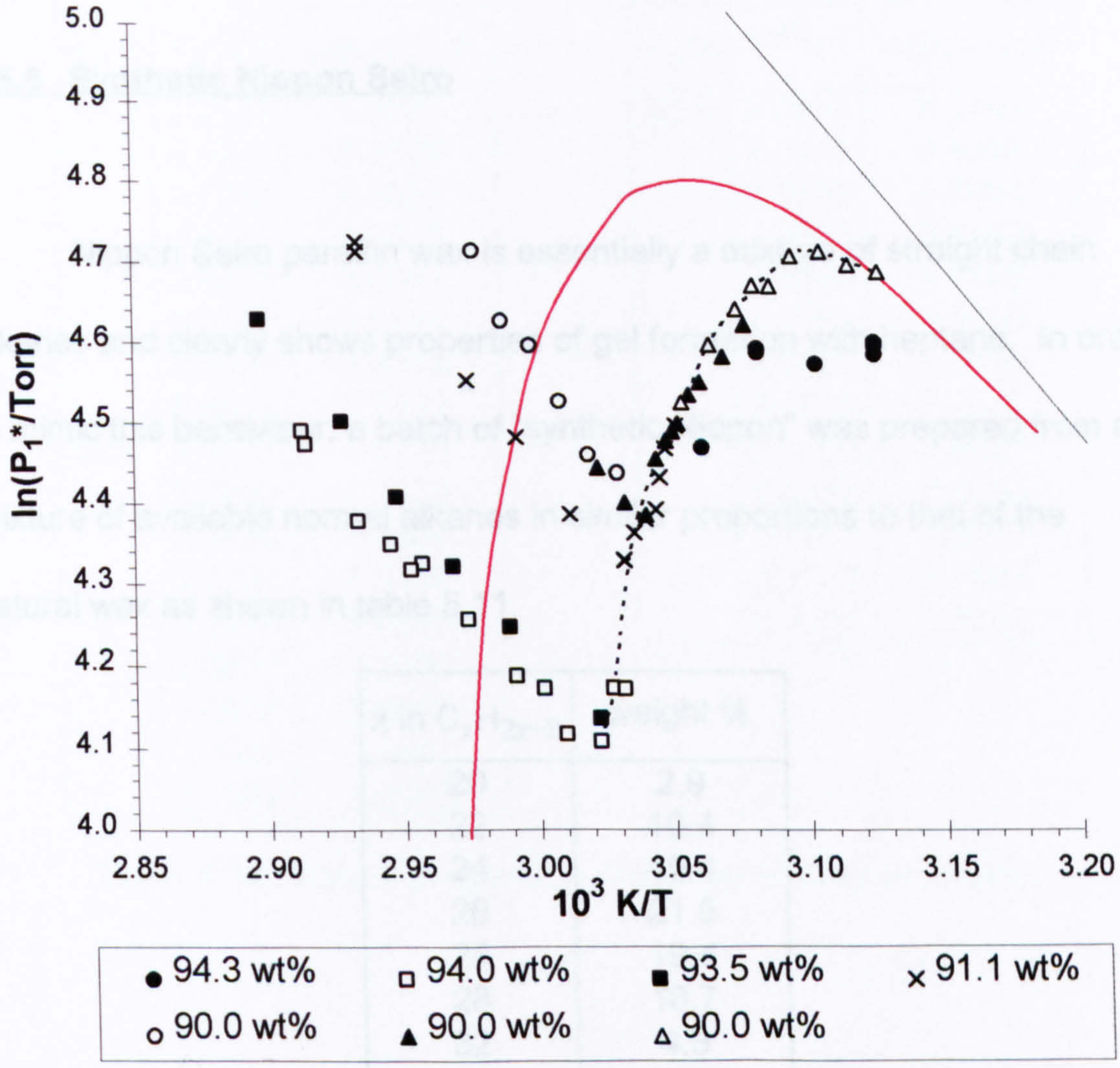

Figure 5.14 *Vapour pressures of heptane in BD887 microcrystalline wax / dotriacontane.*

The abrupt change in vapour pressure is an indication that during the course of the experiment phase separation occurs for this system at equilibrium. The cloud point locus is obviously shifted from the ideal values for pure dotriacontane due to the addition of the microcrystalline wax. The data shown by the black circles was obtained by rapid quenching of the

liquid mixture and represents a non-equilibrium metastable gel state since the vapour pressure increases very slowly with time at constant temperature.

§ 5.6 Synthetic Nippon Seiro

Nippon Seiro paraffin wax is essentially a mixture of straight chain alkanes and clearly shows properties of gel formation with heptane. In order to mimic this behaviour, a batch of "synthetic Nippon" was prepared from a mixture of available normal alkanes in similar proportions to that of the natural wax as shown in table 5.11.

x in C_xH_{2x+2}	weight %
20	2.9
22	10.4
24	19.4
26	21.5
27	19.4
28	18.7
32	4.3
33	2.0
36	1.3

Table 5.11 *Composition of "synthetic Nippon".*

The results for "synthetic Nippon" in heptane are presented in table 5.12, and figure 5.15 shows the temperature dependence of the solvent vapour pressure for various weight fractions of total solid.

The blue curve is the locus of saturated solutions calculated for pure Nippon and the red one that of synthetic Nippon. The latter is calculated

using average values for the synthetic sample. Namely, $\bar{n} = 26.12$, $\overline{M_W} = 368.42\ gmol^{-1}$, $\overline{\Delta_f H_2^o} = 93.86\ kJmol^{-1}$ and $\overline{T_M} = 329.0\ K$.

w_2/%	$10^3K/T$	$\ln(P_1^*/Torr)$
93.2	2.9131	4.3399
	2.9324	4.2528
	2.9519	4.1653
	2.9717	4.0838
	2.9918	4.0044
	3.0122	3.9129
	3.0330	3.8315
	3.0541	3.7422
92.3	2.9613	4.1710
	2.9800	4.1070
	2.9999	4.0304
	3.0203	3.9454
	3.0410	3.8520
	3.0617	3.7807
	3.0833	3.6862
	3.1047	3.5947
	3.1053	3.6060

w_2/%	$10^3K/T$	$\ln(P_1^*/Torr)$
92.3	3.0237	3.9469
	3.0440	3.8486
	3.0646	3.7694
	3.0855	3.6862
	3.1068	3.5958
	3.1284	3.5058
	3.1505	3.5736
	3.1725	3.7147
	3.1952	3.8037
	3.2273	3.8265
	3.2501	3.8257
	3.2732	3.7647
	3.3207	3.6791

Table 5.12 *Vapour pressures of heptane in synthetic Nippon.*

The important difference is the almost temperature independence of the vapour pressure inside the locus for the Nippon (indicating gelation) as compared with the maximum seen for the synthetic mixture (due to phase separation and crystallisation). This suggests that the alkane mixture is not responsible alone for the formation of a gel.

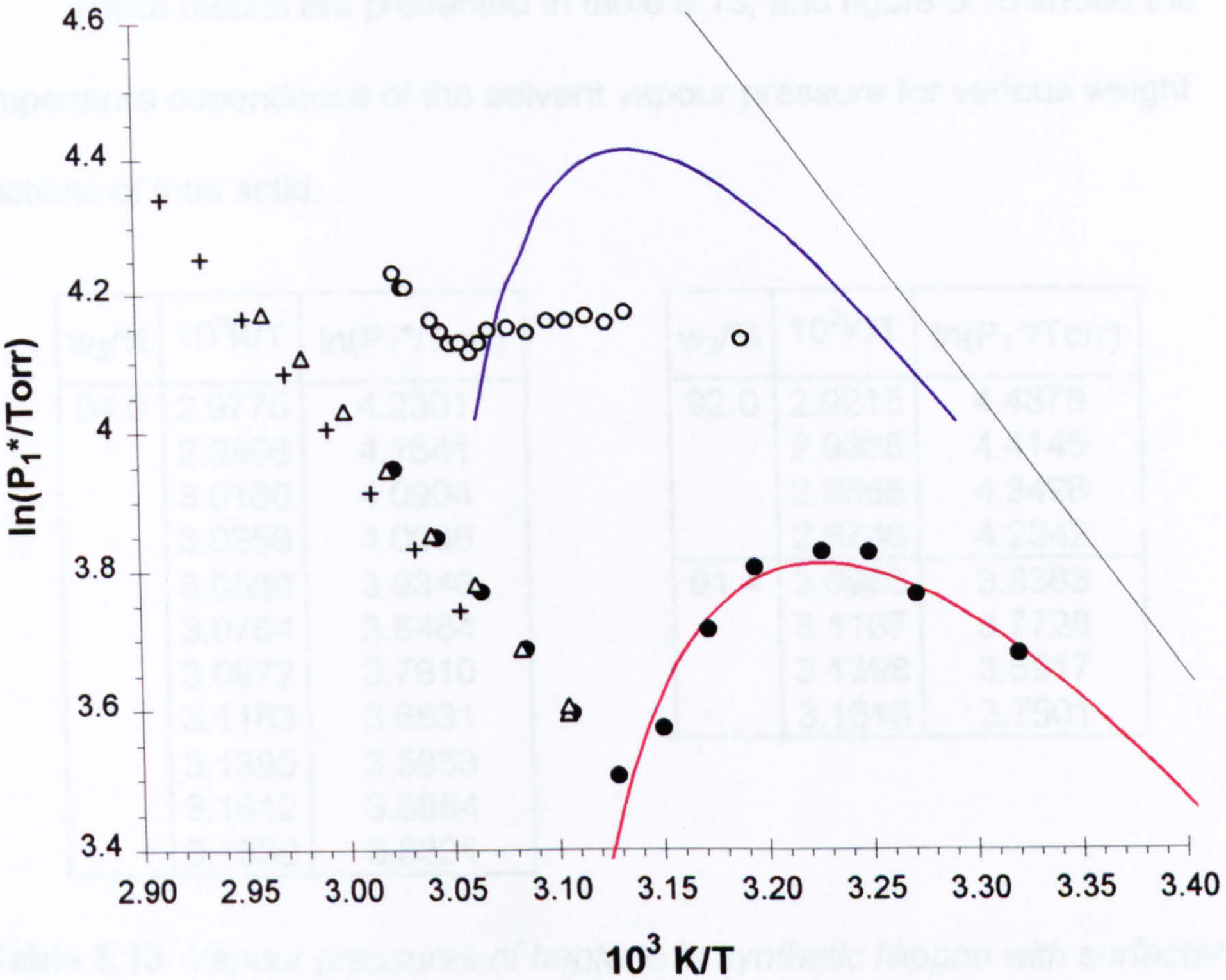

Figure 5.15 *Vapour pressures of heptane in synthetic Nippon.*

§ 5.6.1 Synthetic Nippon Seiro + surfactant

In the manufacture of certain paste polishes, a surfactant mixture of lime / stearin is sometimes added to the melt in order to improve the setting characteristics of the gel. For this reason, a mixture of synthetic Nippon doped with an organic surfactant (21.6 wt.% Aerosol OT : sodium bis-2-ethylhexyl sulphosuccinic acid) was tried.

These results are presented in table 5.13, and figure 5.16 shows the temperature dependence of the solvent vapour pressure for various weight fractions of total solid.

w_2/%	10^3K/T	ln(P_1*/Torr)
94.0	2.9775	4.2301
	2.9966	4.1641
	3.0160	4.0904
	3.0359	4.0036
	3.0560	3.9346
	3.0764	3.8484
	3.0972	3.7810
	3.1183	3.6831
	3.1395	3.5953
	3.1612	3.6854
	3.1830	3.8321

w_2/%	10^3K/T	ln(P_1*/Torr)
92.0	2.9215	4.4879
	2.9388	4.4145
	2.9566	4.3498
	2.9746	4.2842
91.4	3.0986	3.8383
	3.1187	3.7726
	3.1398	3.6917
	3.1616	3.7501

Table 5.13 *Vapour pressures of heptane in synthetic Nippon with surfactant Aerosol OT (21.6 wt.%).*

The red curve represents the locus of saturated solutions calculated as in the previous section for synthetic Nippon Seiro paraffin wax and the data shows that Aerosol OT is not effective enough to cause gelation of a mixture of long chain alkanes.

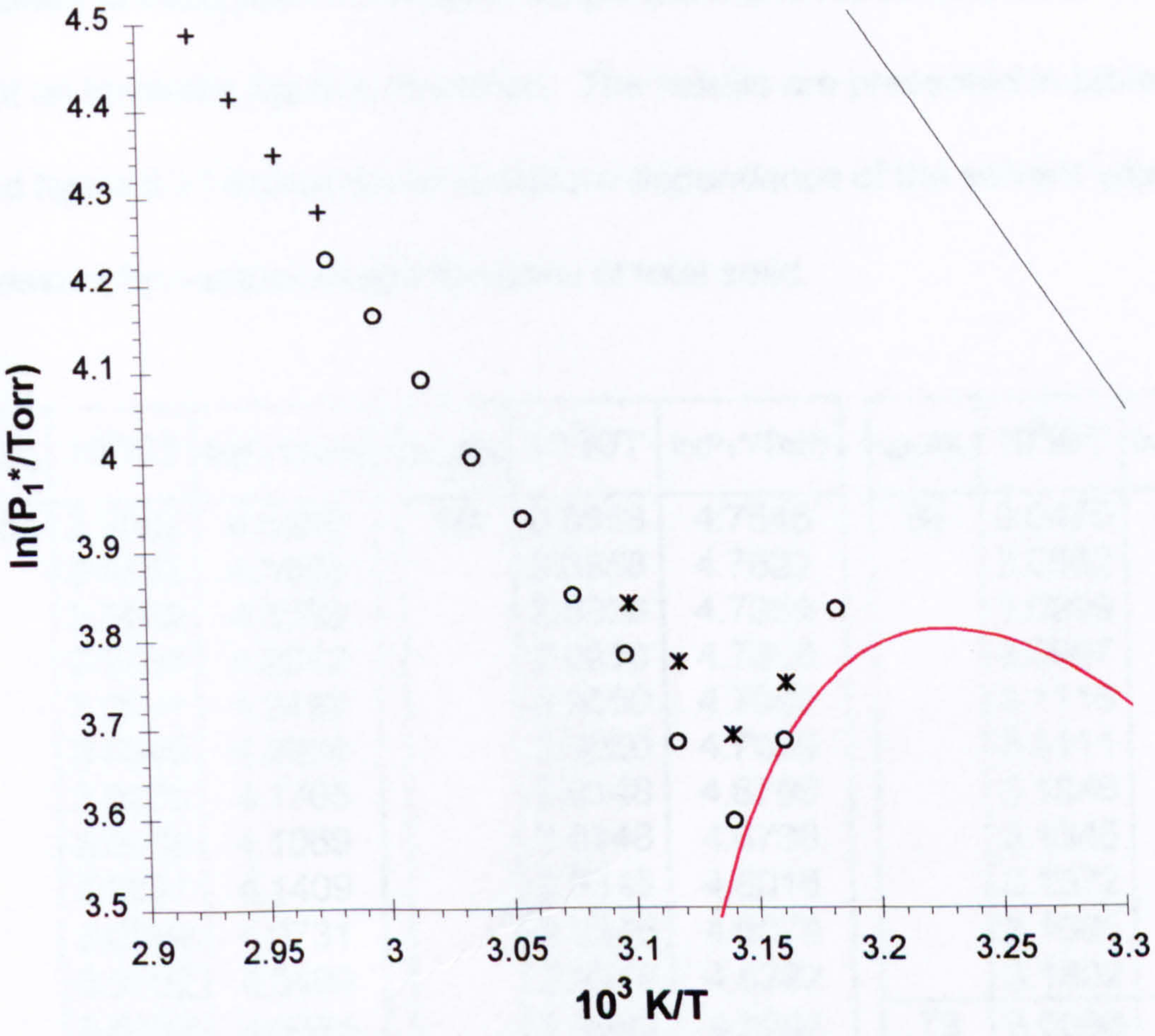

Figure 5.16 *Vapour pressures of heptane in synthetic Nippon with surfactant Aerosol OT.*

§ 5.7 Cherry Blossom

Reckitt and Colman produce a wide range of polish formulations for different applications. The one of main interest in this investigation is the non-aqueous "Cherry Blossom" range of paste polishes. This system has been modelled using simple hydrocarbon mixtures with pure organic additives. In order to investigate the properties of the commercial product, a batch of polish was made using conventional conditions and then the solvent

allowed to evaporate at elevated temperature and reduced pressure such that an involatile residue remained. The results are presented in table 5.14, and figure 5.17 shows the temperature dependence of the solvent vapour pressure for various weight fractions of total solid.

w_2/%	10^3K/T	ln(P_1*/Torr)
95	2.9585	4.3428
	2.9583	4.3555
	2.9583	4.3588
	2.9834	4.2912
	3.0041	4.2193
	3.0040	4.2200
	3.0253	4.1705
	3.0465	4.1069
	3.0281	4.1409
	3.0594	4.0731
	3.0702	4.0489
	3.0702	4.0575
	3.0812	4.0498
	3.0921	4.0815
	3.1031	4.0696
86	3.0040	4.3769
	3.0250	4.3168
	3.0745	4.2522
	3.0677	4.2317
	3.0895	4.2279
	3.1115	4.2441
	3.1339	4.2676
	3.1339	4.2556

w_2/%	10^3K/T	ln(P_1*/Torr)
86	2.8858	4.7545
	2.8858	4.7622
	2.8953	4.7369
	2.8953	4.7358
	2.9050	4.7089
	2.9050	4.7059
	2.9148	4.6795
	2.9148	4.6736
	2.9345	4.6018
	2.9345	4.6079
	2.9544	4.5292
	2.9543	4.5247
	2.9744	4.4732
	2.9744	4.4664
	2.9744	4.4623
	2.9951	4.4032
	3.0157	4.3466
82	2.9500	4.5825
	2.9603	4.5503
	2.9706	4.5315
	2.9811	4.5044
	2.9916	4.4699

w_2/%	10^3K/T	ln(P_1*/Torr)
86	3.0475	4.2594
	3.0682	4.2251
	3.0899	4.2524
	3.0897	4.2476
	3.1116	4.2496
	3.1111	4.2609
	3.1346	4.2581
	3.1345	4.2647
	3.1572	4.2725
	3.1685	4.2652
	3.1802	4.2443
79	3.0068	4.5114
	3.0280	4.4322
	3.0280	4.4321
	3.0491	4.3750
	3.0704	4.3051
	3.0705	4.3103
	3.0921	4.2640
	3.1032	4.2574
90	2.9819	4.3935
	3.0237	4.2665
	3.0667	4.1701

Table 5.14 *Vapour pressures of heptane in "Cherry Blossom".*

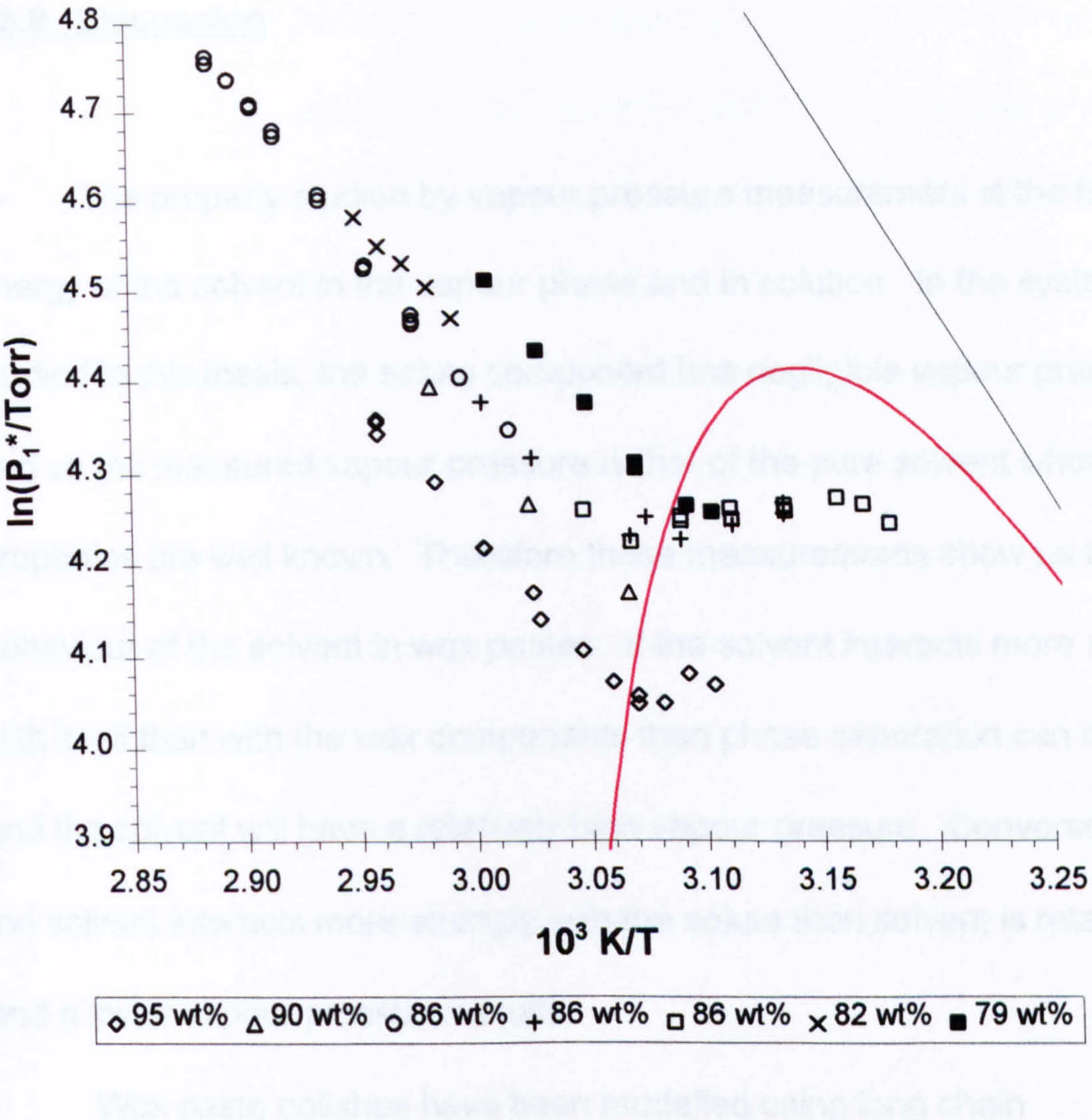

Figure 5.17 *Vapour pressures of heptane in "Cherry Blossom".*

The red curve is the locus of saturated solutions for Nippon Seiro paraffin wax since this is the major component in Cherry Blossom shoe polish. The data clearly show that gel formation does occur for this system since points are obtained within the two phase region.

§ 5.8 Discussion

The property studied by vapour pressure measurement is the free energy of the solvent in the vapour phase and in solution. In the systems studied in this thesis, the solute component has negligible vapour pressure and so the measured vapour pressure is that of the pure solvent whose properties are well known. Therefore these measurements show us the behaviour of the solvent in wax pastes. If the solvent interacts more strongly with itself than with the wax components then phase separation can occur and the solvent will have a relatively high vapour pressure. Conversely, if the solvent interacts more strongly with the solute then solvent is retained and a lower vapour pressure results.

Wax paste polishes have been modelled using long chain hydrocarbon solids with pure hydrocarbon solvent. Normal behaviour is the formation of a homogenous solution at high temperature, with separation into saturated solution and a crystalline solid phase on cooling. The addition of natural material such as microcrystalline paraffin wax induces the formation of a gel-like phase having a remarkably low solvent vapour pressure at low solvent concentration. Pure materials do not readily form this gel-like structure and for a mixture of dotriacontane and heptacosane the metastable state is very short lived.

From these vapour pressure measurements we can identify three classes of behaviour :

Class 1 behaviour - On lowering the temperature of the liquid mixture, phase separation occurs giving crystals of pure solid which is impermeable to solvent and in equilibrium with saturated solution.

Class 2 behaviour - On lowering the temperature of the liquid mixture, the two phase envelope is penetrated and gives a vapour pressure nearly independent of temperature due to the solvent being entangled within the gel.

Class 3 behaviour - For the doped systems, a new two phase envelope is produced at lower vapour pressures. This is probably due to the formation of mixed crystals (see § 6.4.2).

§ 5.9 References

1 C.B. Willingham, W.T. Taylor, J.M. Pignocco and F.D. Rossini, **J.Res.Nat.Bur.Stand.(US)**, 35,219,(1945).

2 A.F.M. Barton, "Handbook of Solubility Parameters and Other Cohesion Parameters", pp 9-11, 2nd Edition, CRC Press Inc., (1985) – quotes values of 36.6 $kJmol^{-1}$ at 25°C and 31.85 $kJmol^{-1}$ at 98.4°C.

3 J.H. Hildebrand and A.J. Wachter, **J.Phys.Coll.Chem.**, 53,886,(1949) – gives values of 106 ± 4 $kJmol^{-1}$ and 339 ± 1 K.

4 H.E. Lundager Madsen and R. Boistelle, **J.Chem.Soc.-Farad.Trans.I**, 72,1078,(1976) – gives values of ~109 $kJmol^{-1}$ and 339 K.

5 D.S.C. thermograms performed at Hull University give :

$$\beta_M \xrightarrow[34.6\,kJmol^{-1}]{337\,K} \alpha_H \xrightarrow[77.1\,kJmol^{-1}]{341\,K} L$$ in the notation of Broadhurst[6].

6 M.G. Broadhurst, **J.Res.Nat.Bur.Stand.**, 66A(3),241,(1962) – gives

$$\beta_M \xrightarrow[40.2\,kJmol^{-1}]{339\,K} \alpha_H \xrightarrow[76.6\,kJmol^{-1}]{343\,K} L.$$

7 D.S.C. thermograms performed at Hull University give :

$$\beta_O \xrightarrow[37.2\,kJmol^{-1}]{327\,K} \alpha_H \xrightarrow[74.7\,kJmol^{-1}]{331\,K} L.$$

8 M.G. Broadhurst, **J.Res.Nat.Bur.Stand.**, 66A(3),241,(1962) – gives

$$\beta_O \xrightarrow[29.0\,kJmol^{-1}]{326\,K} \alpha_H \xrightarrow[60.4\,kJmol^{-1}]{332\,K} L.$$

9 D.S.C. thermograms performed at Hull University give $\Delta_f H_2^\circ$ = 74.84 kJmol^{-1} and T_m = 49°C.

10 "Handbook of Chemistry and Physics", 56th edition, Chemical Rubber Company (C.R.C.) Press Inc., (1975).

11 R. Denman, private communication, University of Hull.

Chapter Six

Other Techniques

§ 6.1 Chain packing in n-alkanes.

The minimum energy conformation of a normal alkane molecule in the solid phase is typified below in figure 6.1. Here we can see that, for example with heptane, the carbon chain adopts a planar zigzag arrangement with the units in an all trans conformation and the hydrogens on the non-terminal carbon atoms lying in perpendicular planes.

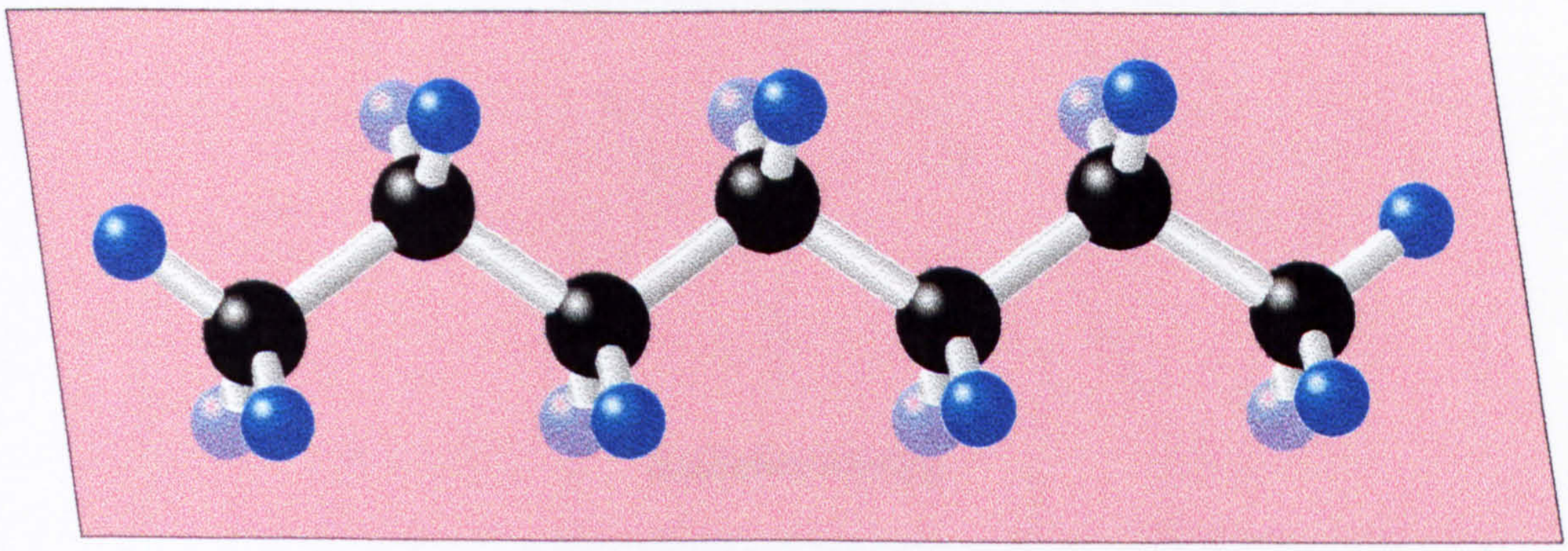

Figure 6.1 *Minimum energy conformation for a heptane molecule.*

The crystal structures of the n-alkane homologous series have been well studied[1,2]. This series of hydrocarbons, like many others, can be divided into two sub-series with regards to the adopted conformations in their crystalline modifications. These series differ in the respect that one contains an odd number of carbon atoms in the molecule and the other contains an even number. Clearly the disposition of the terminal methyl group will be different for each series and the four most common packing geometries are Orthorhombic, Hexagonal, Monoclinic and Triclinic, some of which are illustrated in figure 6.2.

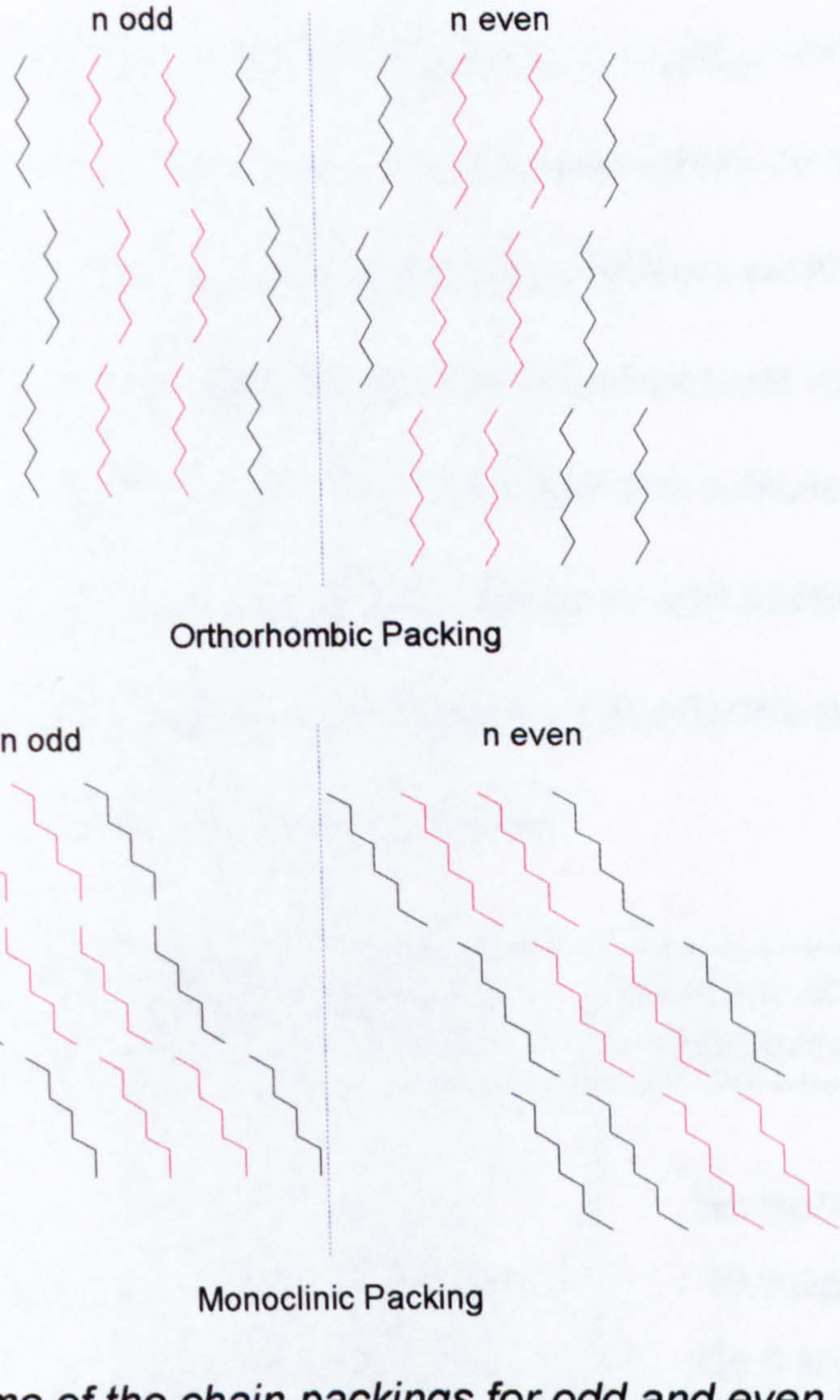

Figure 6.2 *Some of the chain packings for odd and even n-alkanes.*

§ 6.2 Phase transitions in n-alkanes and paraffin waxes.

§ 6.2.1 n-Alkanes

This subject has been reviewed more recently by Turner[3] and an indication of the purity of n-alkanes is given by their temperatures of transition and melting. The useful article by Broadhurst[1] lists transition and melting temperatures, heats of transition and melting, and X-ray long spacing data, known at the time.

Most of the n-alkanes in the region $C_{11}H_{24}$ to $C_{44}H_{90}$ show a pre-melting transition which is reflected in X-ray measurements by a change of symmetry. On cooling from the liquid, long range order is established by alignment of the alkane molecules along their long molecular axis. However, a degree of disorder remains since the molecules have sufficient energy to rotate about this axis. This "rotator phase" has been well studied[1,4] and further cooling eventually results in structures of more dense geometry. These can be summarised as in table 6.1 below.

n = No. of C atoms per molecule	Structure below pre-melting transition	Structure above pre-melting transition(s)
n odd		
$n \leq 9$	Triclinic	No transition
$11 \leq n \leq 43$	Orthorhombic	Hexagonal
$n > 43$	Orthorhombic	No transition
n even		
$n \leq 20$	Triclinic	No transition
$22 \leq n \leq 32$	Monoclinic	Hexagonal
$34 \leq n \leq 38$	Monoclinic	Orthorhombic (and Hexagonal)
$40 \leq n \leq 42$	Orthorhombic	Hexagonal
$n \geq 44$	Orthorhombic	No transition

Table 6.1 *Crystal geometries favoured by n-alkane molecules.*

§ 6.2.2 Mixtures of n-alkanes

When binary mixtures of pure n-alkanes are investigated, a whole range of behaviour is observed[5-7] from which general conclusions can be drawn.

When the difference in carbon number chain length is small ($\lesssim 4$) mixtures of n-alkanes tend to give a continuous series of solid solutions[8], independent of whether the mixtures are odd-odd, even-even or odd-even combinations of carbon atoms. This can vary from the relatively simple phase behaviour of $C_{46}H_{94}/C_{50}H_{102}$[9] and $C_{21}H_{44}/C_{23}H_{48}$ or $C_{35}H_{72}/C_{36}H_{74}$[5] to phase diagrams which are complicated by partial miscibility in the solid phase; for example, $C_{17}H_{36}/C_{18}H_{38}$, $C_{19}H_{40}/C_{20}H_{42}$ and $C_{16}H_{34}/C_{18}H_{38}$[5] or $C_{32}H_{66}/C_{36}H_{74}$ and $C_{33}H_{68}/C_{36}H_{74}$[6] or $C_{12}H_{26}/C_{13}H_{28}$, $C_{13}H_{28}/C_{14}H_{30}$ and $C_{14}H_{30}/C_{15}H_{32}$[7]. However, for much larger differences in chain length[10], for example with $C_{21}H_{44}/C_{31}H_{64}$[5] , $C_{30}H_{62}/C_{40}H_{82}$[11] and $C_{22}H_{46}/C_{30}H_{62}$[12], where the free energies of the pure components are both less than that of the co-crystallised state, independent crystallisation predominates and eutectic behaviour is observed.

§ 6.2.3 Hydrocarbon waxes

Paraffin waxes which melt in the temperature range 60 - 75°C tend to show a single first order pre-melting transition which is due to a change in

lattice parameters from orthorhombic to hexagonal symmetry[13].

Microcrystalline wax, on the other hand, does not show a pre-melting transition.

§ 6.3 Optical Microscopy

As indicated above, many of the pure alkanes are known to give solid-solid pre-melting transitions, as can mixtures of two or more of the individual components. This behaviour is not unlike that observed with some liquid crystalline materials and so techniques, such as optical microscopy, which are useful for the assignment of a particular mesophase[14], can also be employed here.

A small amount of sample is molten and secured between a glass microscope slide and cover slip. This is then mounted on a hot stage and can be viewed on a microscope using illumination from a fine beam of light.

Figure 6.3 shows the optical micrograph for dotriacontane at 25°C as viewed without cross-polarisers, with a 530 nm filter and at a magnification of X50. Here we can see quite clear distinctions between folded plate like crystals in the foreground, which appear to have a striated texture, and the larger regions in the background, which are slightly out of focus and given extra contrast by the use of the 530 nm filter.

Figure 6.3 *Optical micrograph of $C_{32}H_{66}$ (X50, 25°C).*

When the hot stage is taken to a temperature above the solid-solid transition temperature but below that of fusion ($T_{\beta M \rightarrow \alpha H}$ = 65.5°C and $T_{\alpha H \rightarrow L}$ = 69.3°C), as shown in figure 6.4, we see a noticeable enhancement in texture for the two regions.

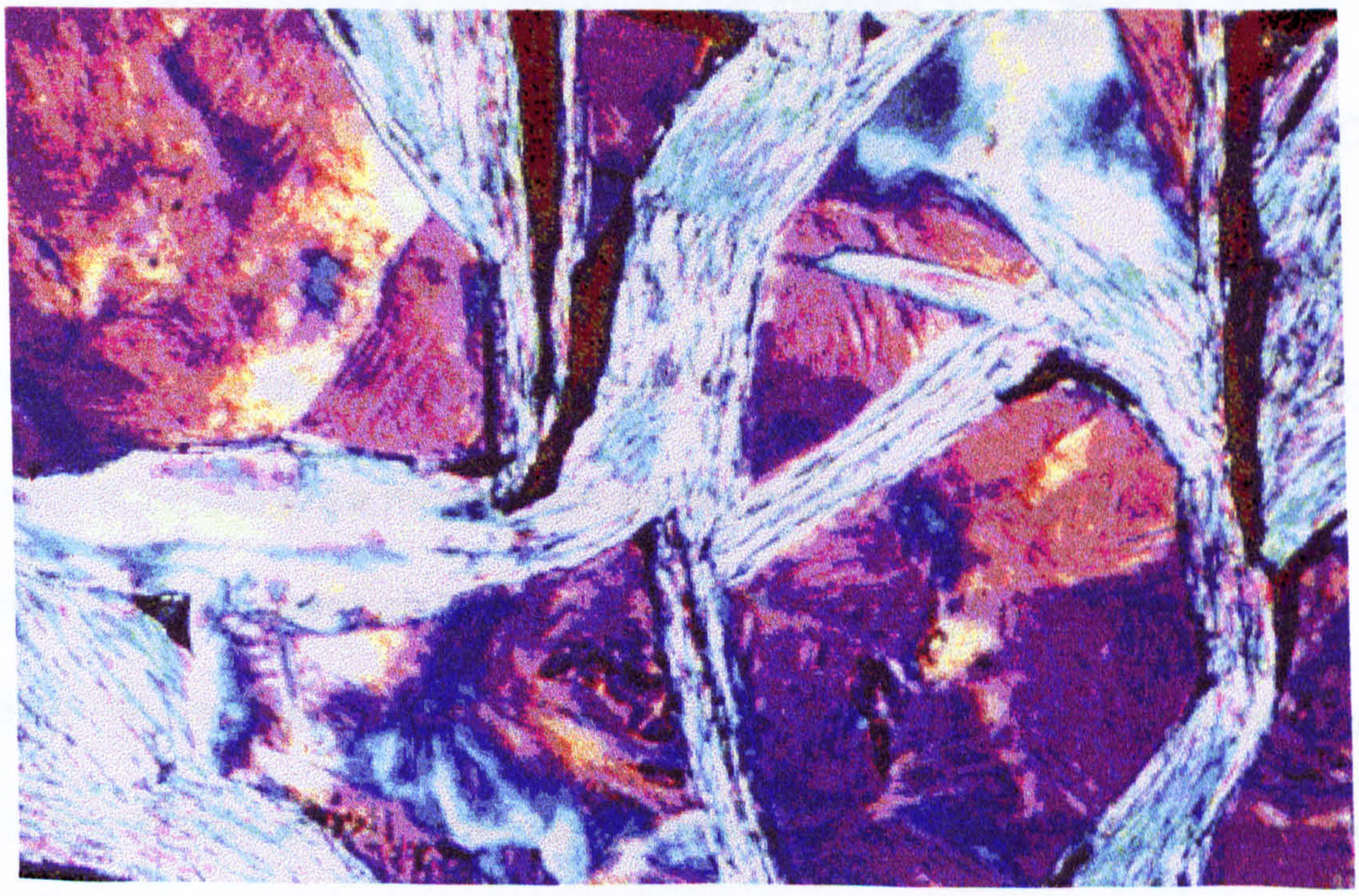

Figure 6.4 *Optical micrograph of $C_{32}H_{66}$ (X50, 67°C).*

Figure 6.5 shows the optical micrograph for a 50:50 wt.% mixture of dotriacontane and heptacosane at 25°C, viewed under the same conditions as above. A much more densely packed mass of smaller crystallites is seen, and on slowly raising the temperature, the smaller crystals melt first, leaving voids between the larger ones, with no noticeable change in texture, even under higher magnification.

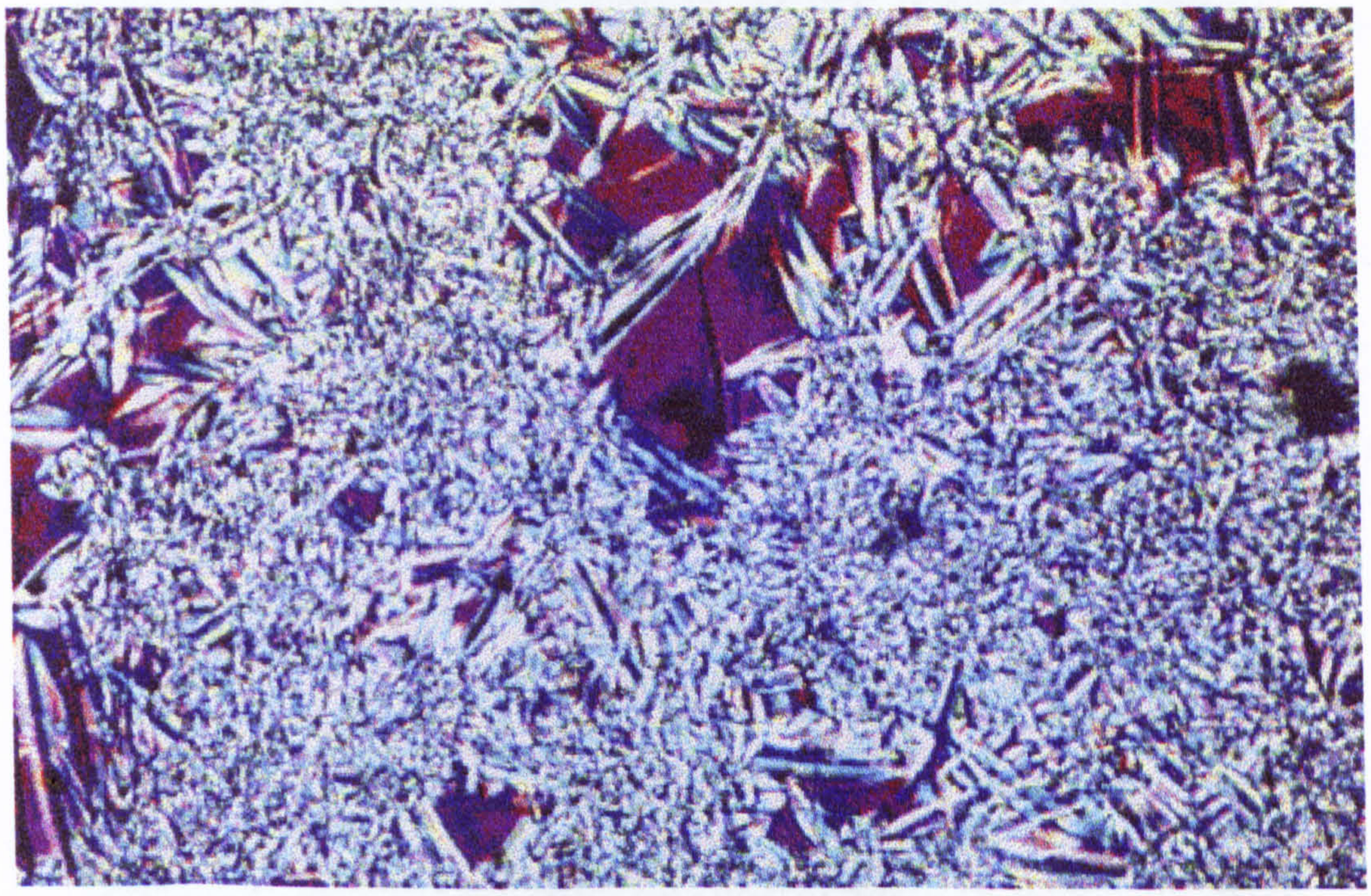

Figure 6.5 *Optical micrograph of 50:50 wt.% $C_{27}H_{56}/C_{32}H_{66}$ (X50, 25°C).*

When Nippon Seiro paraffin wax is viewed in the same manner a similar collection of crystallites is seen. This is shown in figures 6.6 and 6.7. The lower temperature micrograph shows another aggregation of mixed crystal types, however on heating to 58°C (i.e. within the rotator phase region), the smaller crystallites melt to leave a more uniform region of curved crystals. Indeed under higher magnification (X140), on cooling Nippon Seiro from the melt, we see the formation of structures as shown in figure 6.8.

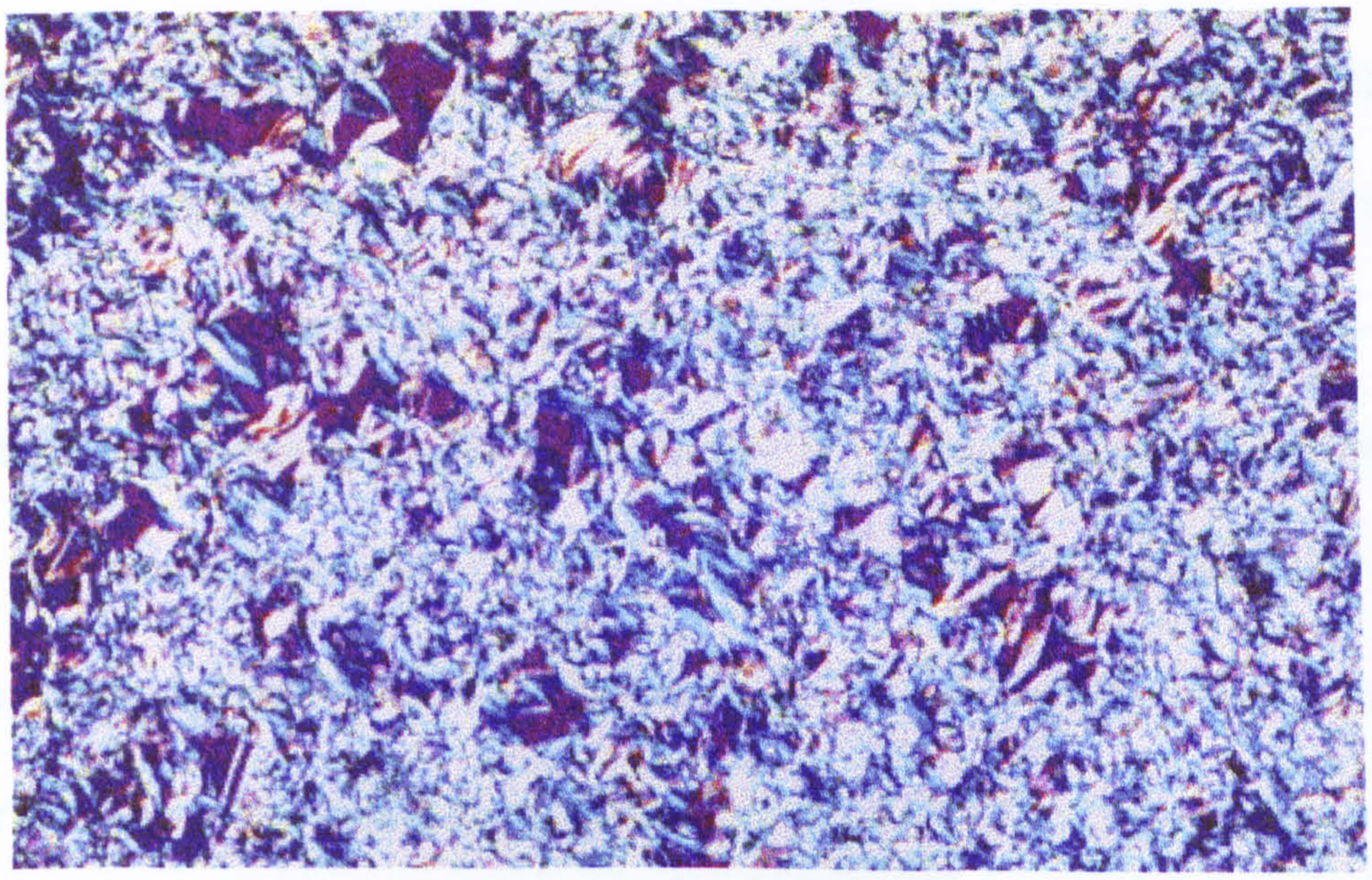

Figure 6.6 *Optical micrograph of Nippon Seiro (X50, 25°C).*

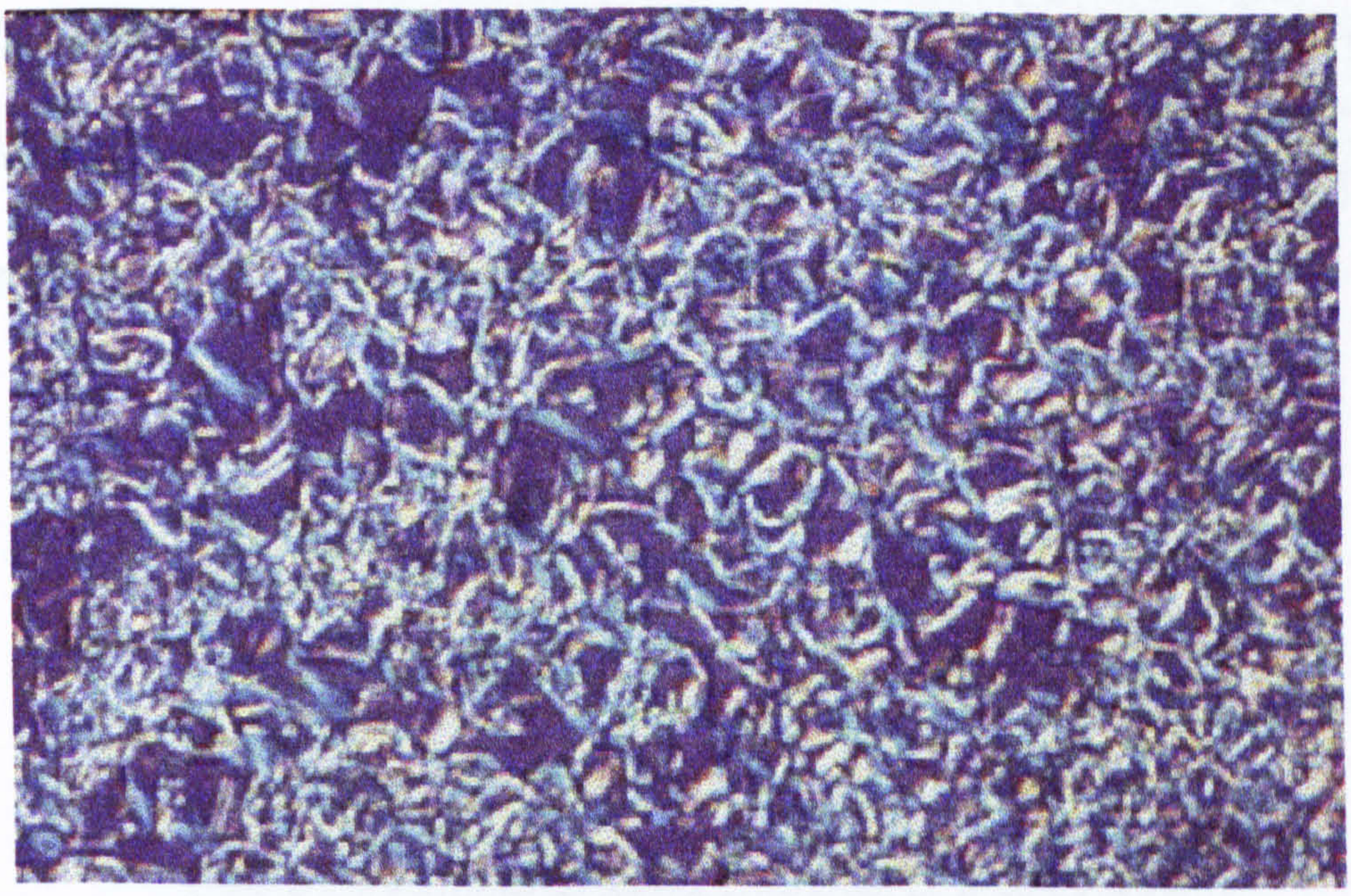

Figure 6.7 *Optical micrograph of Nippon Seiro (X50, 58°C).*

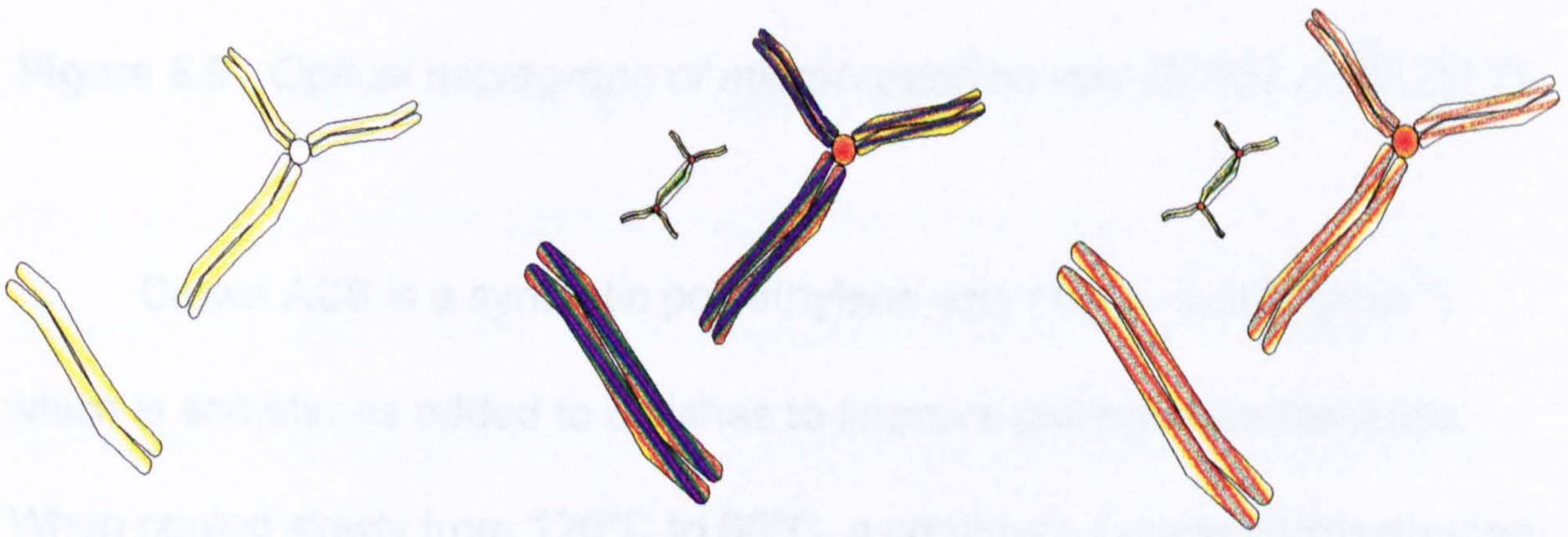

Figure 6.8 *Cooling of Nippon Seiro (X140).*

The first thing to be noticed is the formation of rolled plate crystals which give the appearance of consisting of two faint yellow strands which tend to be aligned in one particular direction or perpendicular to this orientation. On cooling to ~50°C, the existing structures become thicker and start to darken to have purple and blue/green centres with brown on the outside. Also, smaller structures start to appear with similar characteristics. Further cooling leads not only to eventual thickening and formation of new structures such that physical contact is established between some, but also the darker colours eventually fade to give way to pale greens and yellows.

Microcrystalline waxes, on the other hand, tend to form much smaller needles or mis-shaped crystals as shown in figure 6.9.

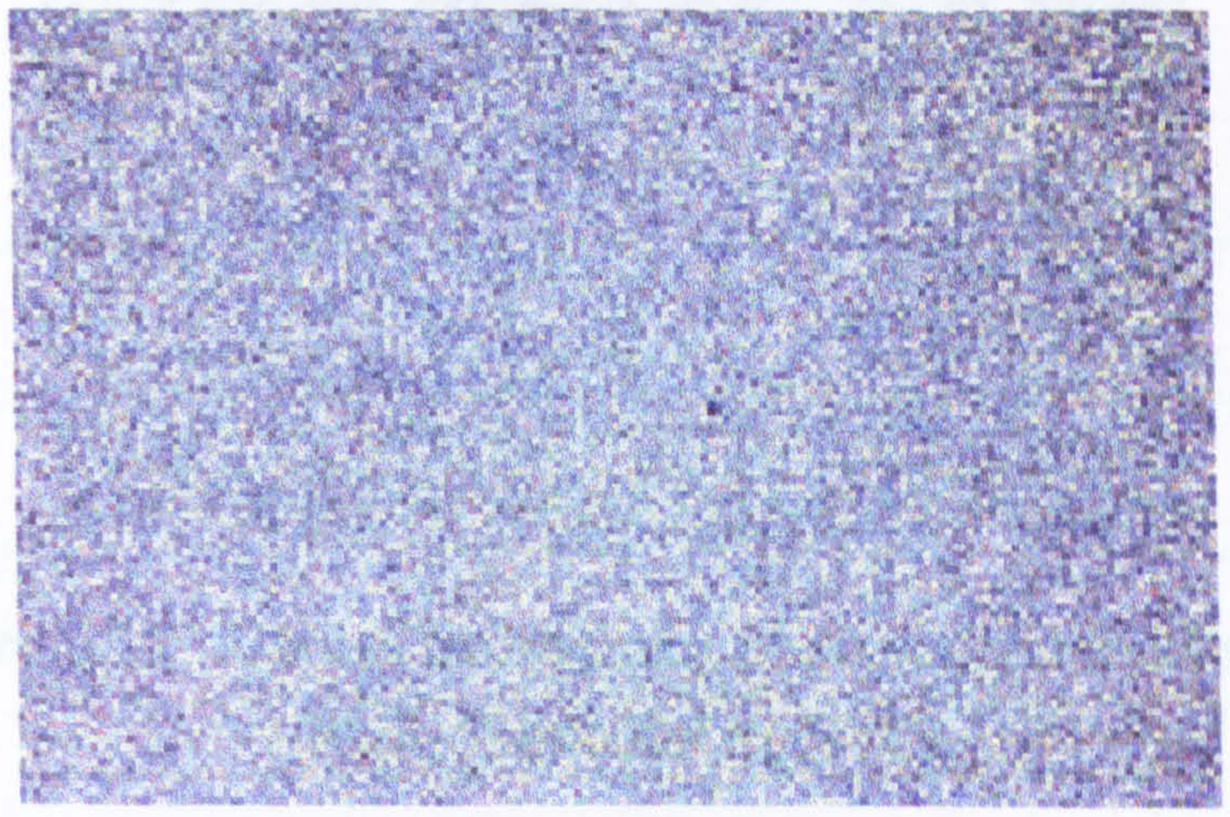

Figure 6.9 *Optical micrograph of microcrystalline wax BD887 (X50, 25°C).*

Crown AC8 is a synthetic polyethylene wax ($\overline{M}_n \approx 2{,}500\ gmol^{-1}$) which is sometimes added to polishes to improve gelling characteristics. When cooled slowly from 120°C to 60°C, a continuous mass of mis-shaped crystals is formed, as shown in figure 6.10. If, however, the melt is

quenched to 60°C then we see the appearance of more larger and regular, almost spherulitic, structures (see figure 6.11).

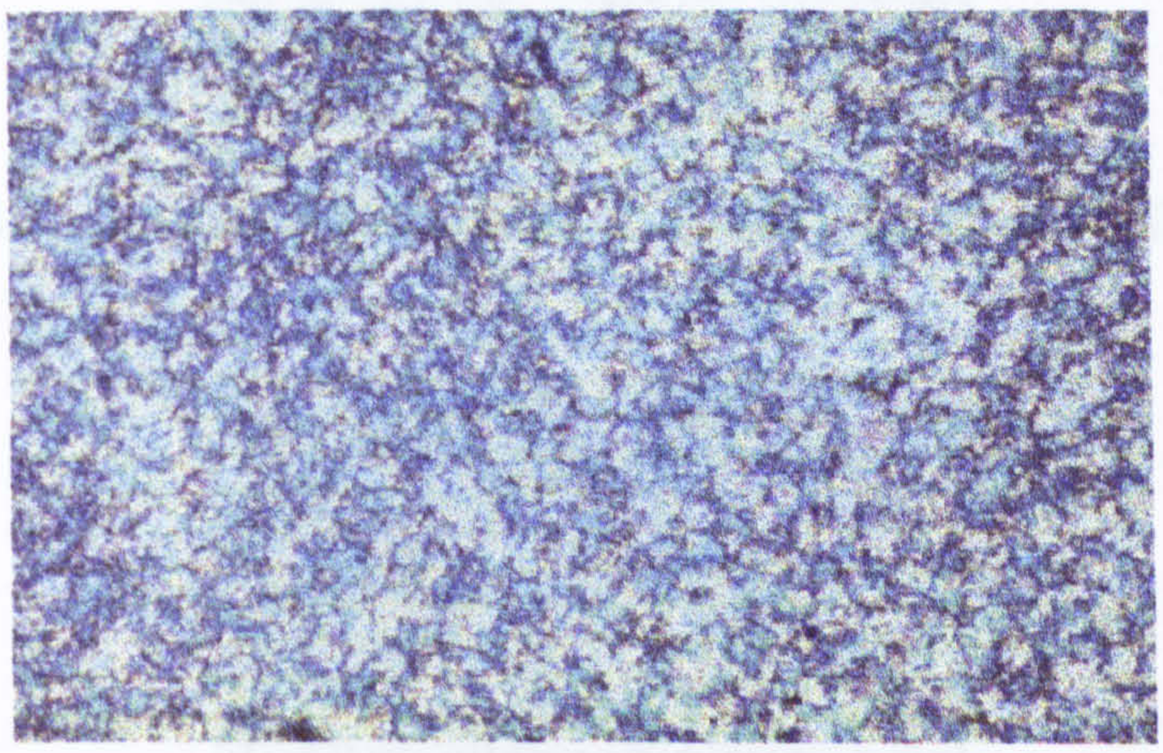

Figure 6.10 *Optical micrograph of polyethylene wax AC8 (X50, slow cooled to 60°C).*

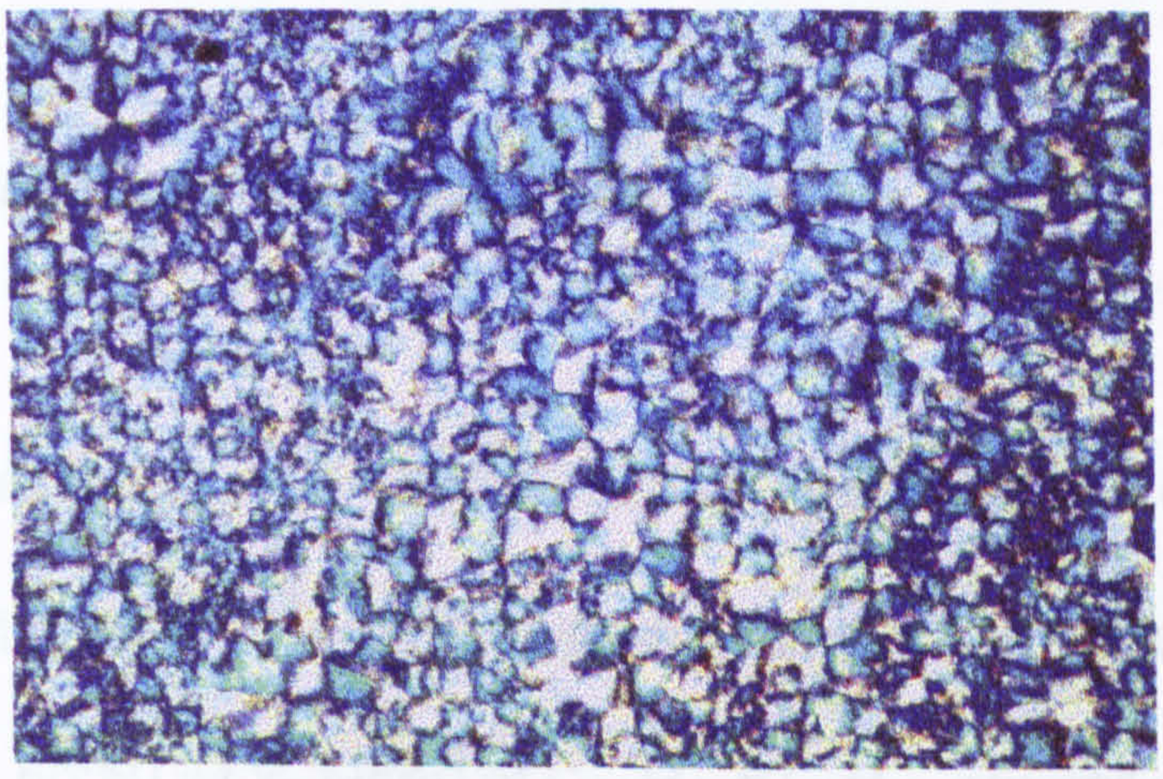

Figure 6.11 *Optical micrograph of polyethylene wax AC8 (X50, quenched to 60°C).*

When a sample of Cherry Blossom is evaporated to dryness and the remaining solids viewed using optical microscopy, we see that at 100°C (figure 6.12), where many of the components will be liquid, solid black particulate material of varying size exists as a suspension in a mixture of the lower melting waxes. However, at 25°C (figure 6.13), the solid particles become fixed in a matrix of relatively large irregular shaped crystals.

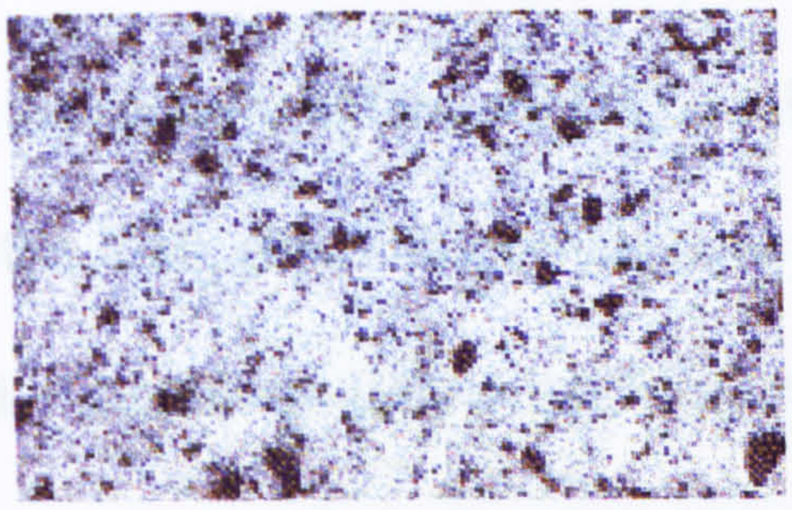

Figure 6.12 *Optical micrograph of Cherry Blossom (X50, 100°C).*

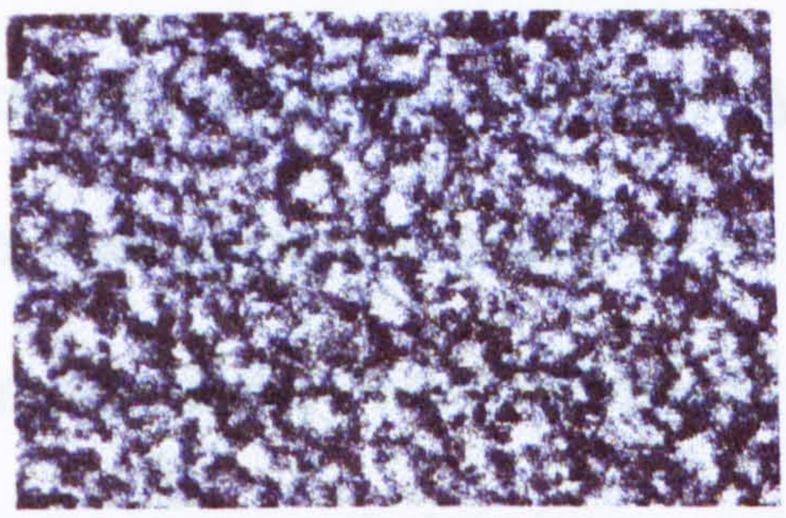

Figure 6.13 *Optical micrograph of Cherry Blossom (X50, 25°C).*

§ 6.3.1 Discussion of crystal structures

It is known that pure n-alkanes can crystallise as thin blades or lozenge shaped plates[15,16]. These alkanes are potent mutual crystal modifiers and a 50:50 wt.% blend of $C_{20}H_{42}/C_{22}H_{46}$ crystallises in the form of spherulites. When small amounts (0.1%) of polymeric ester or hydrocarbon modifier is added to pure n-alkanes the crystal growth is affected such that fibrous, irregular shaped crystals are produced. It is likely that the incorporation of a modifier molecule at the growing interface poisons further growth[15].

Recently, Dorset[17] showed that, for a mixture of $C_{36}H_{74}$ with $C_{18}H_{37}OOCC_{17}H_{35}$, two materials which exhibit very similar crystal forms do

not show solid solution behaviour. When cooling a mixture consisting of 67 mol.% alkane, from the melt, dendrites of the pure alkane appear in equilibrium with a liquid of approximately eutectic composition. On further cooling, the eutectic mixture crystallises on top of the alkane crystals.

For more complex mixtures of alkanes, in the form of paraffin waxes, solidification is known to give combinations of both crystalline structures and amorphous regions; the latter being characteristic for branched alkanes[18]. In the petroleum industry, the ability of a paraffin wax to retain lower molecular weight 'solvent' components has been correlated to crystal structure[19]. A 'good pressing' wax gives solid plate-like crystals whereas a 'good sweating' wax produces interlocking needles.

In general, the purer, high molecular weight fractions of paraffin wax (m.p. 50 - 65°C) crystallise in the form of plates, whereas the more crude, lower molecular weight fractions (m.p. 30 - 40°C) tend to form needles[20,21]. Intermediate fractions give irregular shaped crystals. When cooled rapidly, paraffin waxes can form needles with ribs in the middle due to rolling of the plates, giving rise to characteristic double bands when viewed under the microscope[22].

Like their pure n-alkane analogues, the lath-like crystals of paraffin waxes can also be modified by doping with small amounts of polymer to produce mal-shaped dendrites[23–25].

§ 6.4 Differential Scanning Calorimetry

When used in conjunction with other techniques, D.S.C. is a method of thermal analysis which provides a facile tool for the characterisation of many natural and synthetic waxes. It is a useful technique for the determination of phase transition temperatures and their associated enthalpies[26]. In D.S.C., both sample (typically 5-10 mg) and reference (usually γ-Al_2O_3) are heated differentially in order to maintain isothermal conditions whilst endothermic or exothermic events, such as phase transitions, occur. The heat flow into (or out of) the sample and reference is measured as a function of the sample temperature controlled under a linear programmed rate and the results are plotted as 'Heat Flow' (in units of Power) versus sample temperature. First order transitions are typically observed as peaks and the area beneath such a peak is a direct measure of the enthalpy change for the transition. Second order thermodynamic phenomena, such as glass transitions in polymers, involve no change in enthalpy but manifest themselves as steps in the thermogram due to the difference in heat capacity of the two states.

§ 6.4.1 Pure compounds

Pure samples of organic compounds often show simple thermal profiles in D.S.C. Figures 6.14 to 6.18 show the thermographs for eicosane, dotriacontane, hexadecanol, palmitic acid and cetyl palmitate respectively.

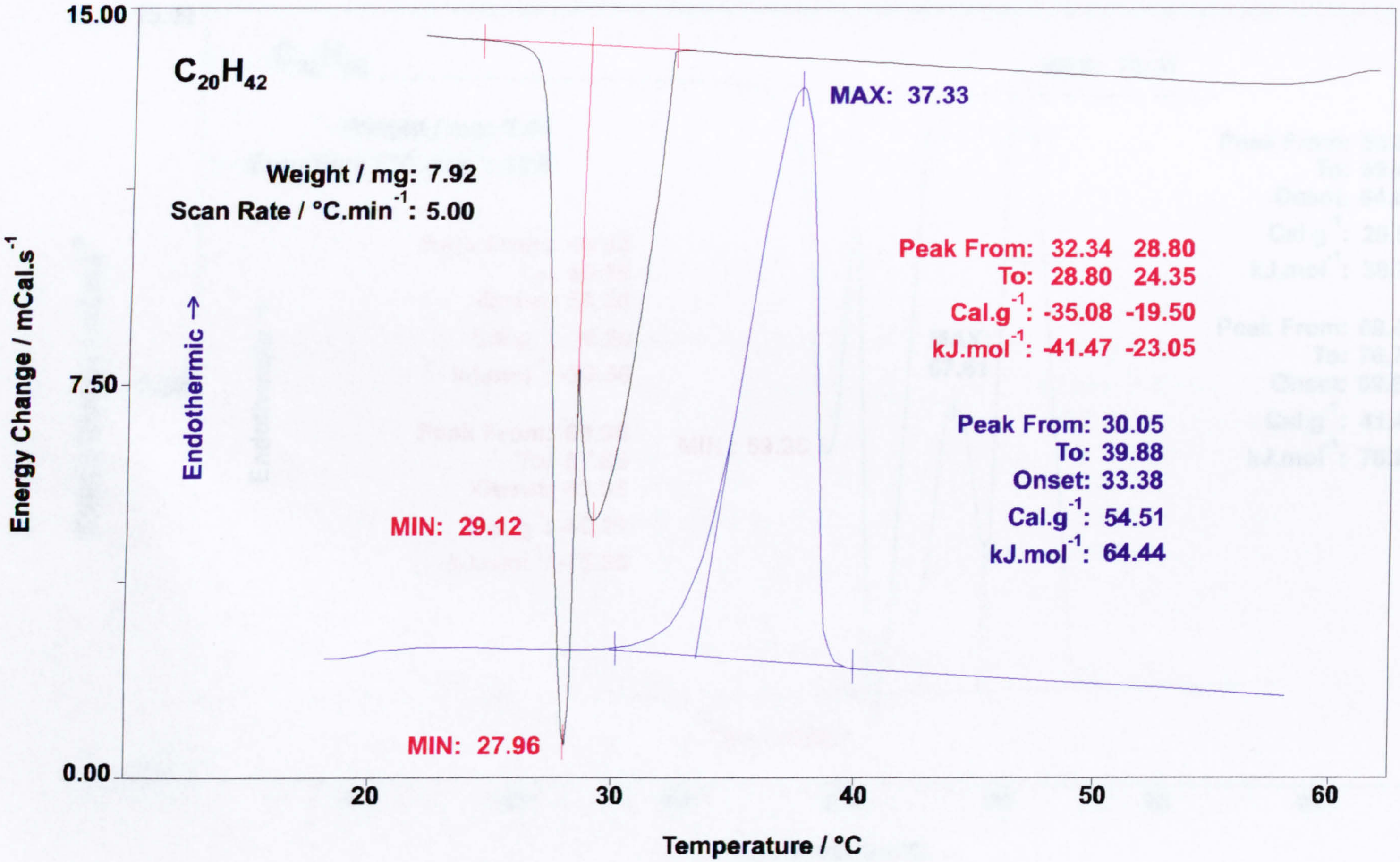

Figure 6.14 *D.S.C. thermogram for eicosane.*

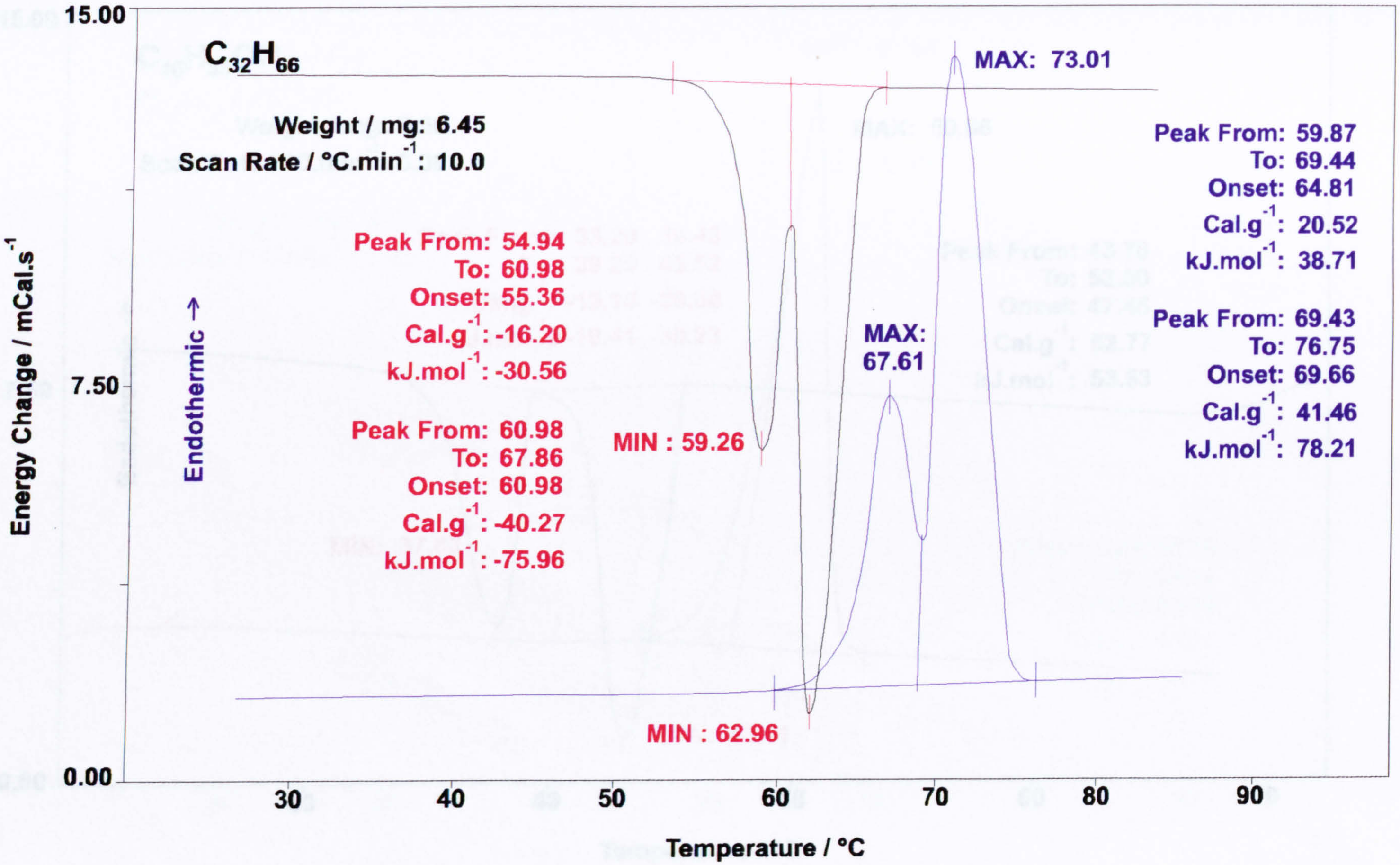

Figure 6.15 *D.S.C. thermogram for dotriacontane.*

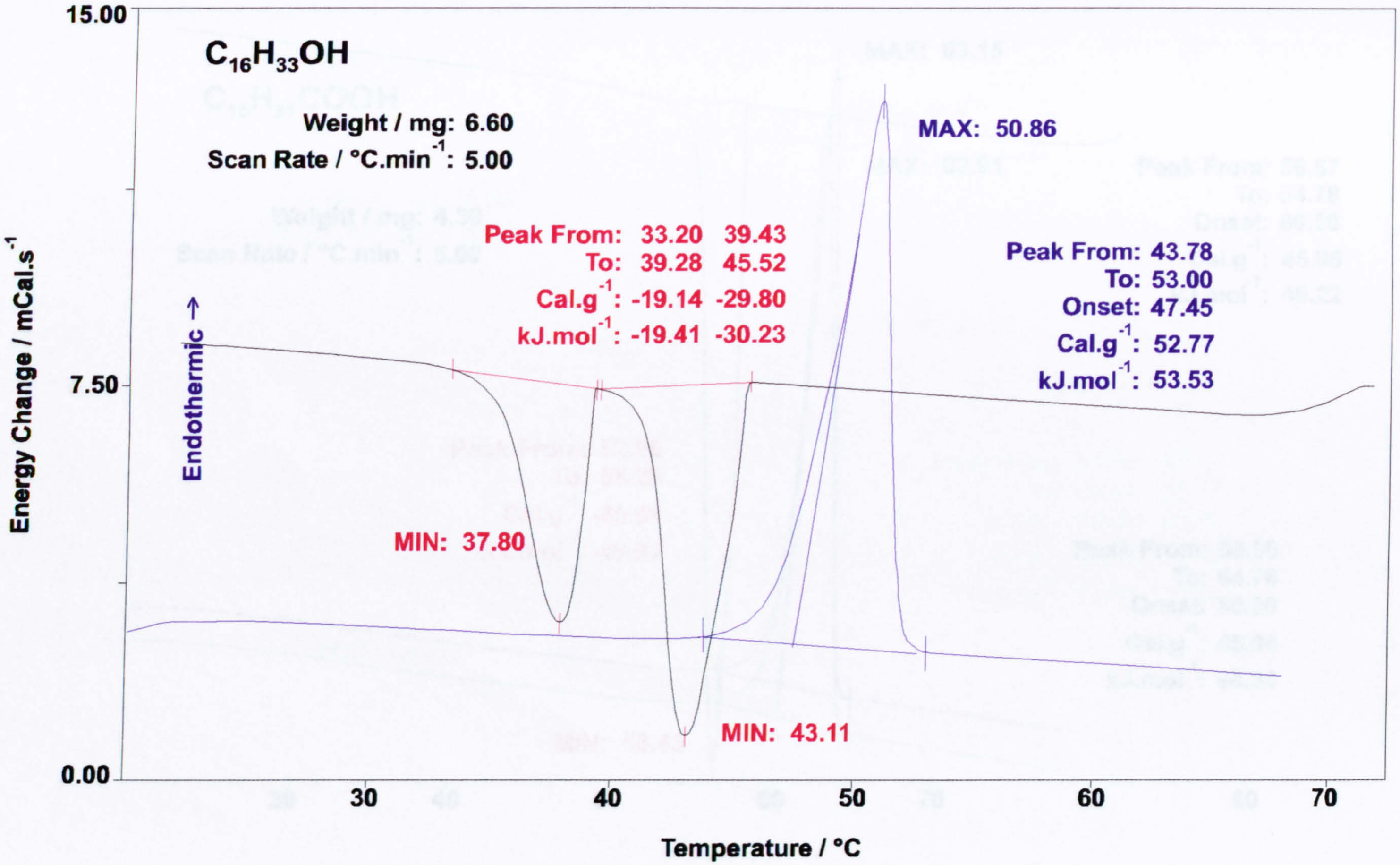

Figure 6.16 *D.S.C. thermogram for hexadecanol.*

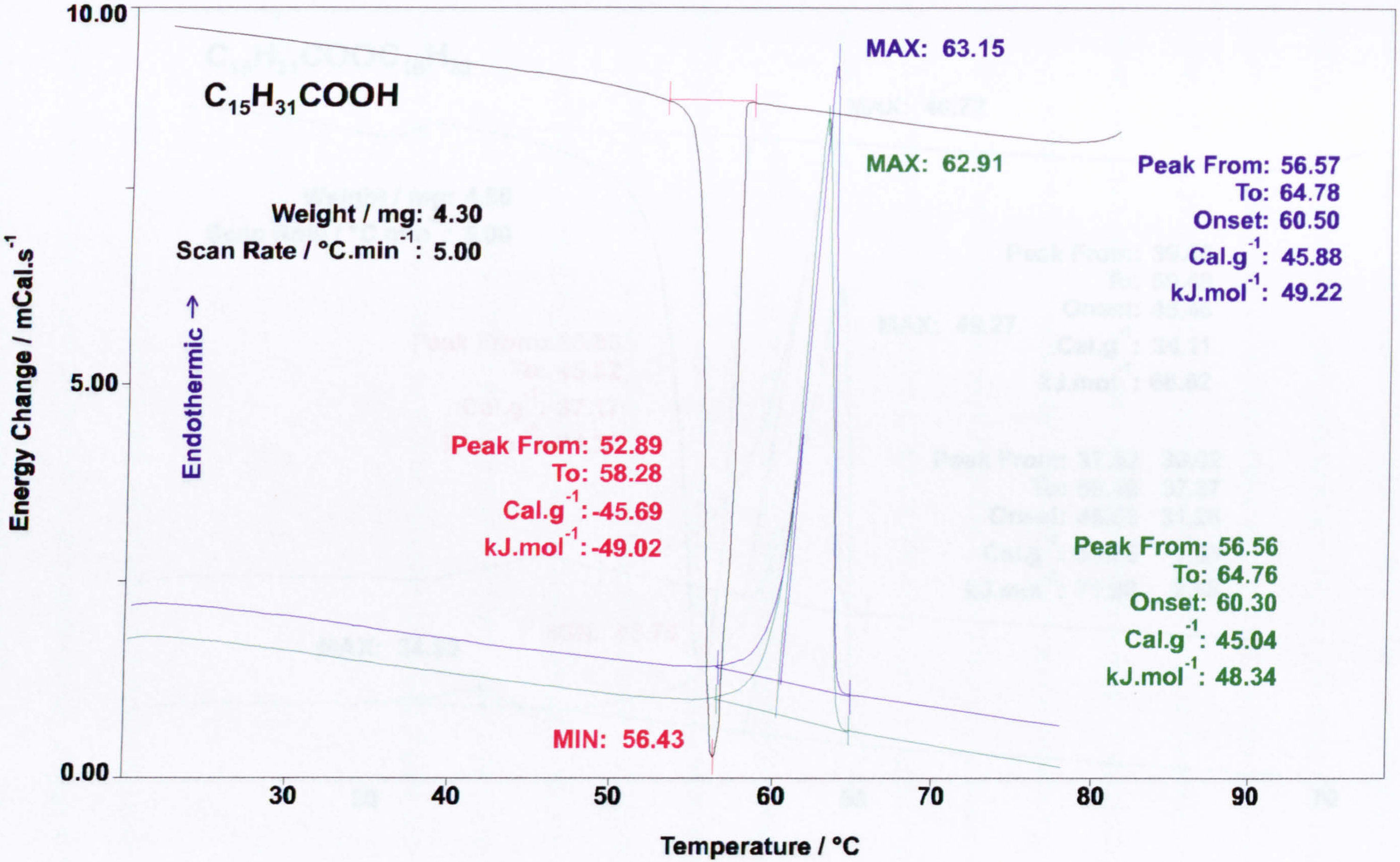

Figure 6.17 *D.S.C. thermogram for palmitic acid.*

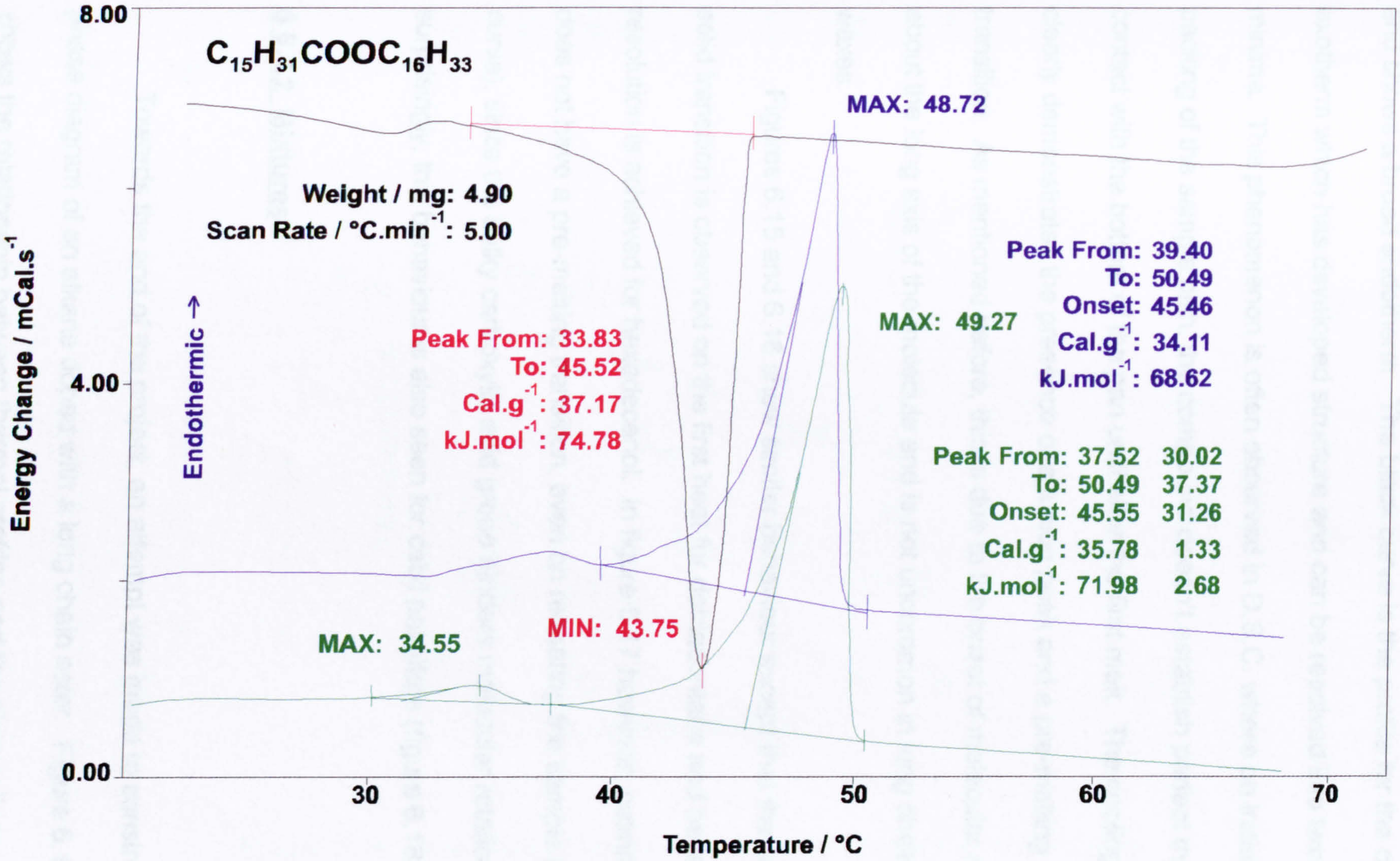

Figure 6.18 *D.S.C. thermogram for cetyl palmitate.*

In figure 6.14 the blue curve represents the first heating of the sample and shows a broad endotherm. The black curve is the profile for the cooling exotherm which has developed structure and can be resolved into two minima. This phenomenon is often observed in D.S.C. where on initial packing of the sample dish, the compound doesn't establish perfect thermal contact with the bottom of the pan until after the first melt. The cooling curve clearly demonstrates the presence of a fusion peak and a pre-melting transition. As mentioned before, this is due to the onset of molecular rotation about the long axis of the molecule and is not uncommon in long chain waxes.

Figures 6.15 and 6.16 show similar behaviour except that the solid-solid transition is observed on the first heat for dotriacontane and base line resolution is achieved for hexadecanol. In figure 6.17 however, palmitic acid does not have a pre-melting transition, even on reheating the sample (green curve), since the bulky carboxylic acid group hinders molecular rotation. Not surprisingly, this behaviour is also seen for cetyl palmitate (figure 6.18).

§ 6.4.2 Mixtures

Towards the end of the project, an attempt was made to construct the phase diagram of an alkane doped with a long chain ester. Figure 6.19 shows the relationship between thermal profiles and the phase diagram for the hypothetical system **A-B**[27].

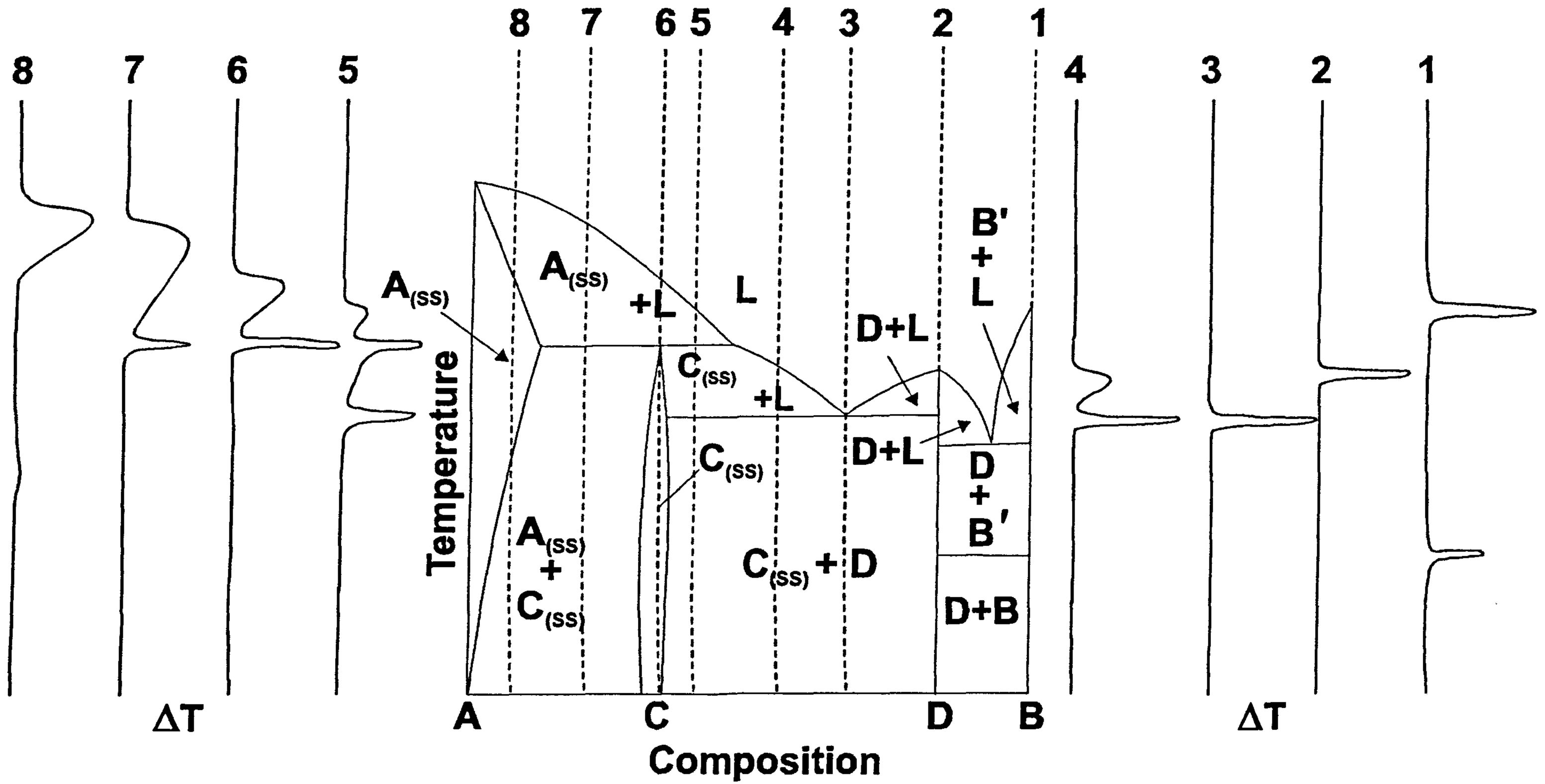

Figure 6.19 *Hypothetical phase diagram for **A**-**B** from thermal analysis.*

However, since the cetyl palmitate had been synthesised for use as a dopant in the measurement of vapour pressures, the lack of available sample meant that only a few data points were obtained. Figure 6.20 shows the partial phase diagram for the dotriacontane/cetyl palmitate system. The solid lines are predicted from depression of freezing point using literature values for the melting points and heats of fusion of the pure components. Simple eutectic behaviour is predicted by analogy to the system $C_{36}H_{74}$ / $C_{17}H_{35}COOC_{18}H_{37}$ [17] and the few data points obtained for the liquidus fit very well.

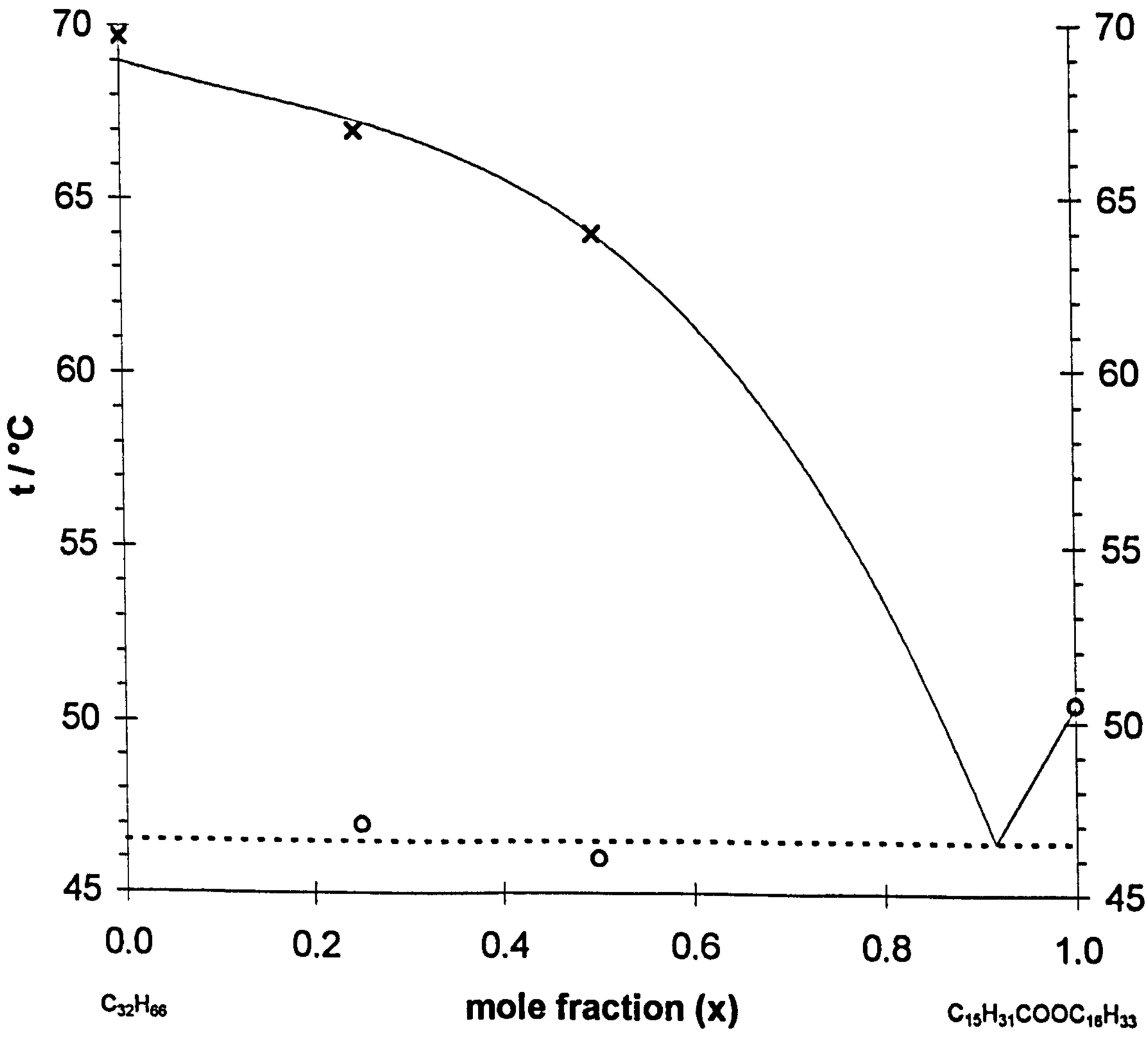

Figure 6.20 *Partial phase diagram for $C_{32}H_{66}$ / $C_{15}H_{31}COOC_{16}H_{33}$ from D.S.C.*

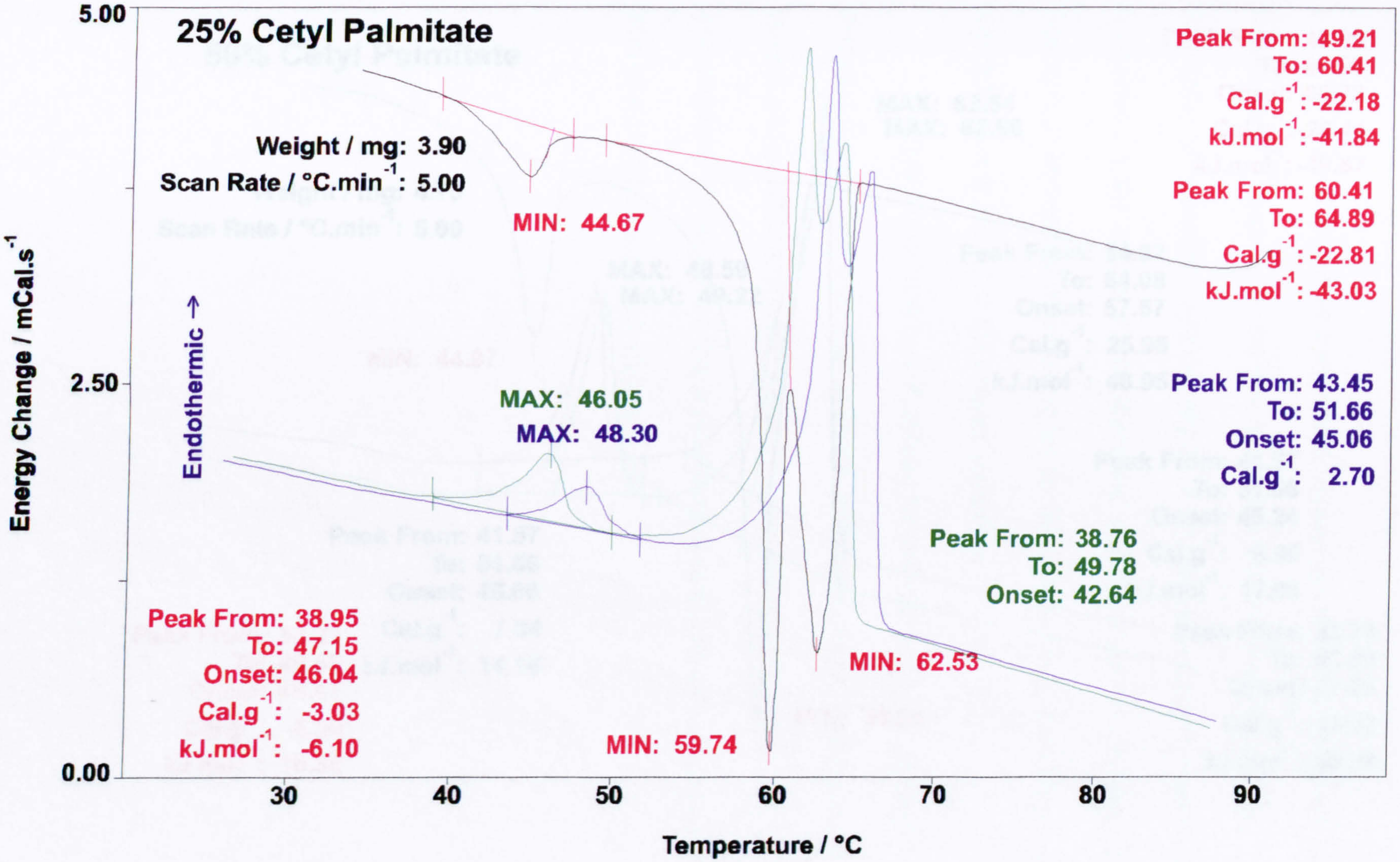

Figure 6.21 *D.S.C. for 25% cetyl palmitate in dotriacontane.*

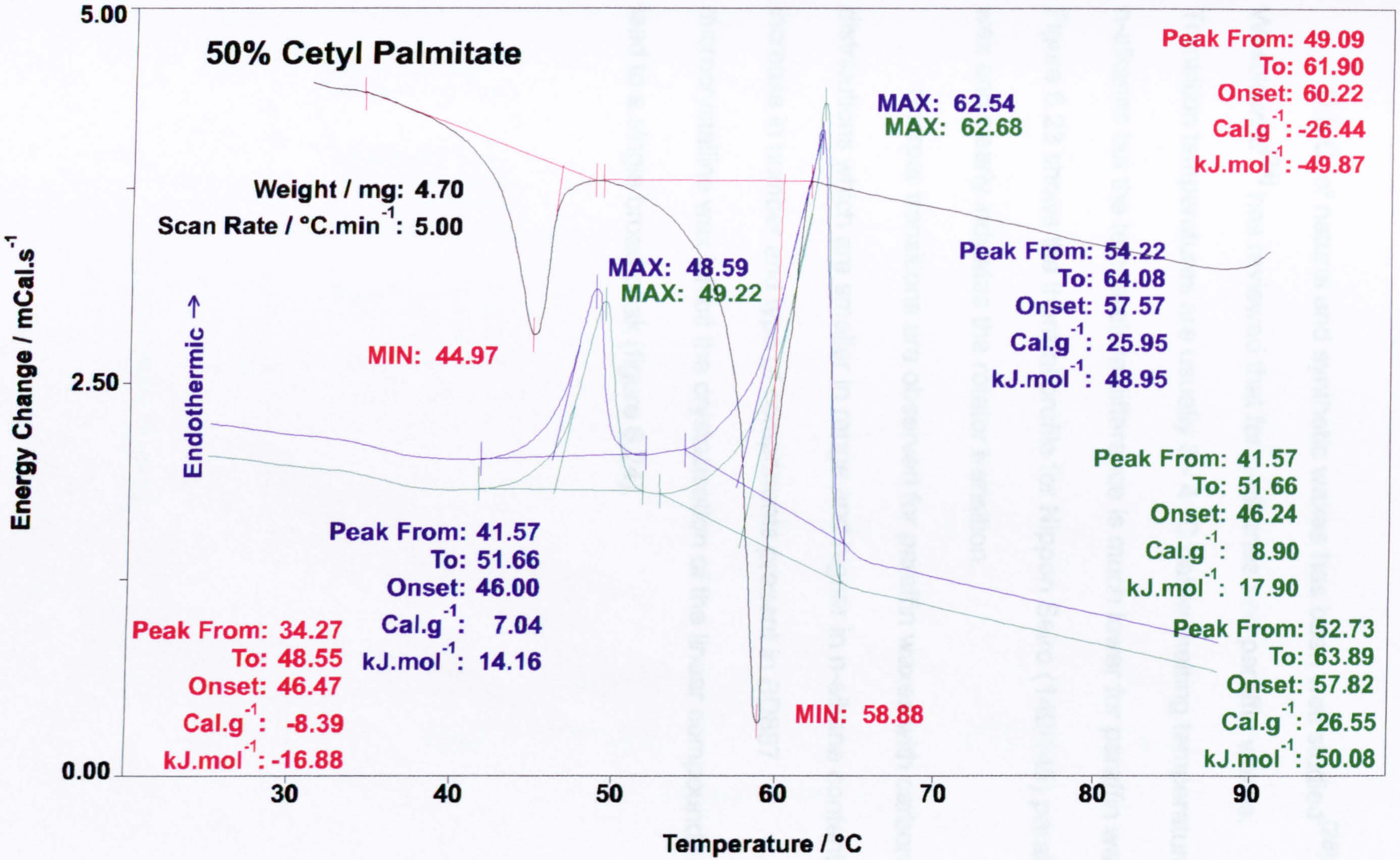

Figure 6.22 *D.S.C. for 50% cetyl palmitate in dotriacontane.*

§ 6.4.3 Waxes

D.S.C. of natural and synthetic waxes has been well studied[28] and Wesolowski[29] has reviewed that for n-alkanes and paraffin waxes.

Transition temperatures are usually 3 - 4 °C below melting temperatures for n-alkanes but the temperature difference is much lower for paraffin waxes. Figure 6.23 shows the thermal profile for Nippon Seiro (140/145) paraffin wax and clearly indicates the rotator transition.

Sharper transitions are observed for paraffin waxes with carbon distributions which are smaller in range and higher in n-alkane content. The increase in number and type of components present in BD887 microcrystalline wax inhibit the crystallisation of the linear compounds and lead to a single broad peak (figure 6.24).

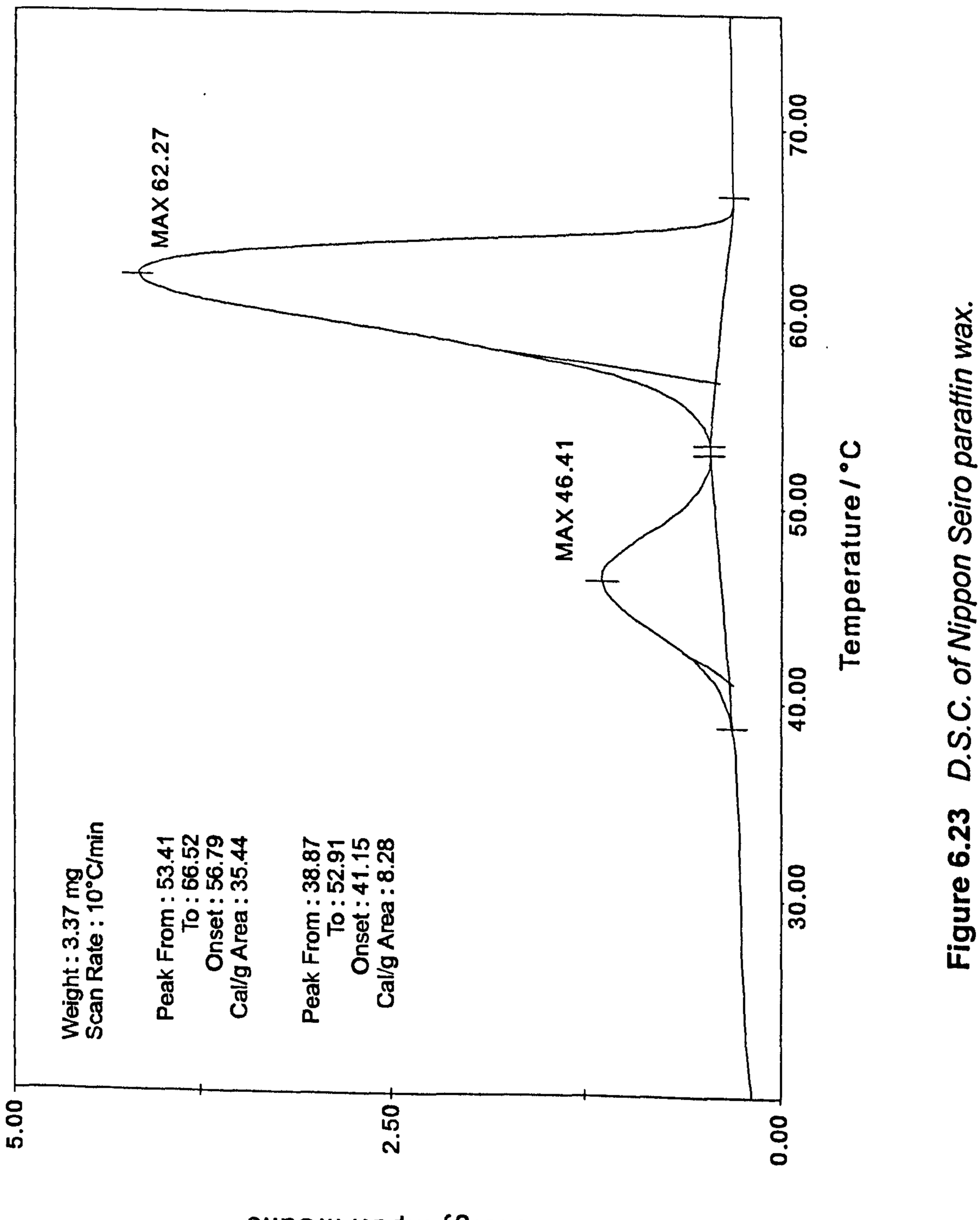

Figure 6.23 *D.S.C. of Nippon Seiro paraffin wax.*

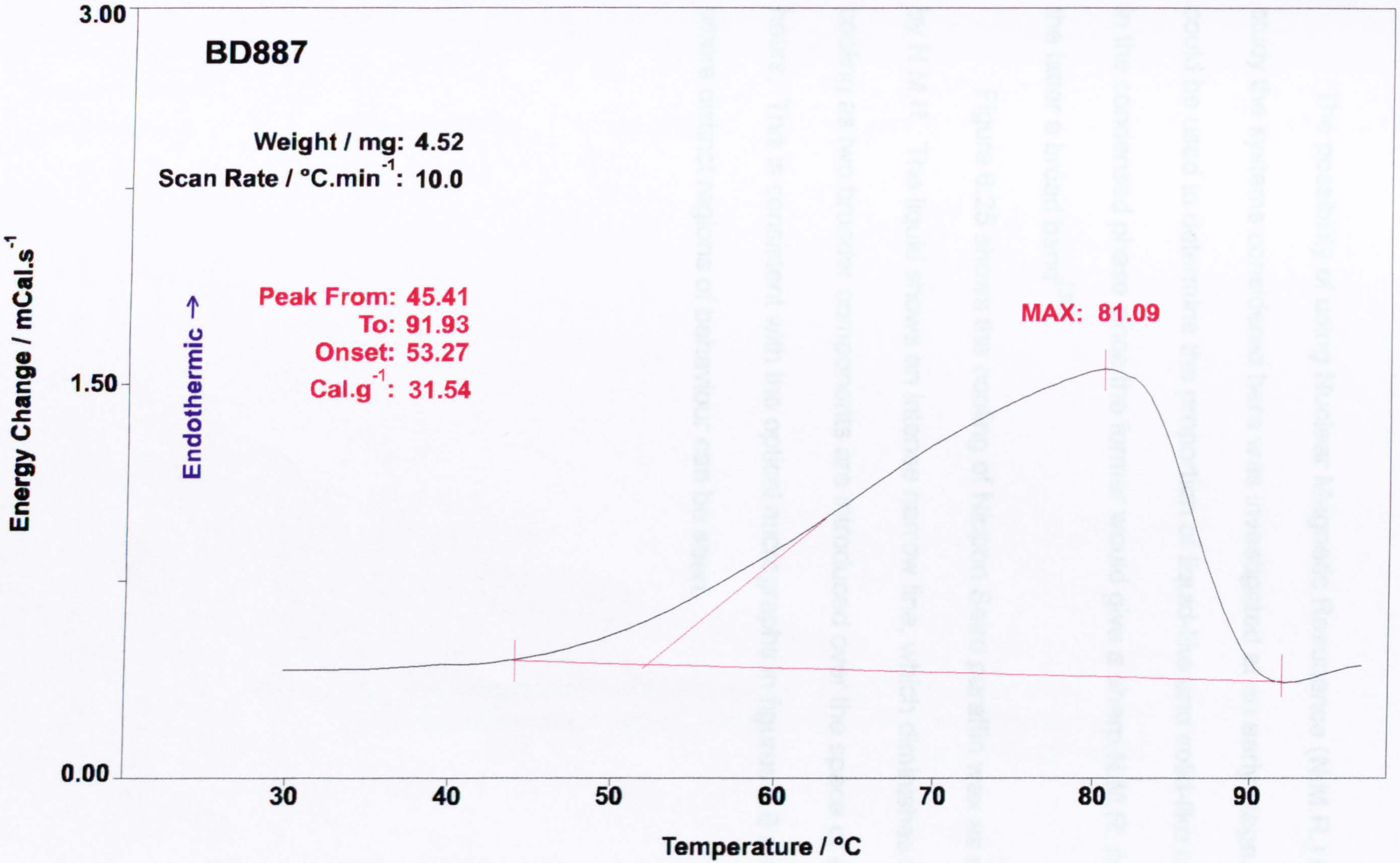

Figure 6.24 *D.S.C. of BD887 microcrystalline wax.*

§ 6.5 Nuclear Magnetic Resonance

The possibility of using Nuclear Magnetic Resonance (N.M.R.) to study the systems considered here was investigated at an early stage. This could be used to determine the proportion of liquid-like and solid-like regions in the condensed phase since the former would give a sharp N.M.R. line and the latter a broad band[30].

Figure 6.25 shows the cooling of Nippon Seiro paraffin wax as studied by N.M.R. The liquid shows an intense narrow line, which diminishes on cooling as two broader components are introduced over the space of several hours. This is consistent with the optical micrographs in figures 6.6 and 6.7 where distinct regions of behaviour can be seen.

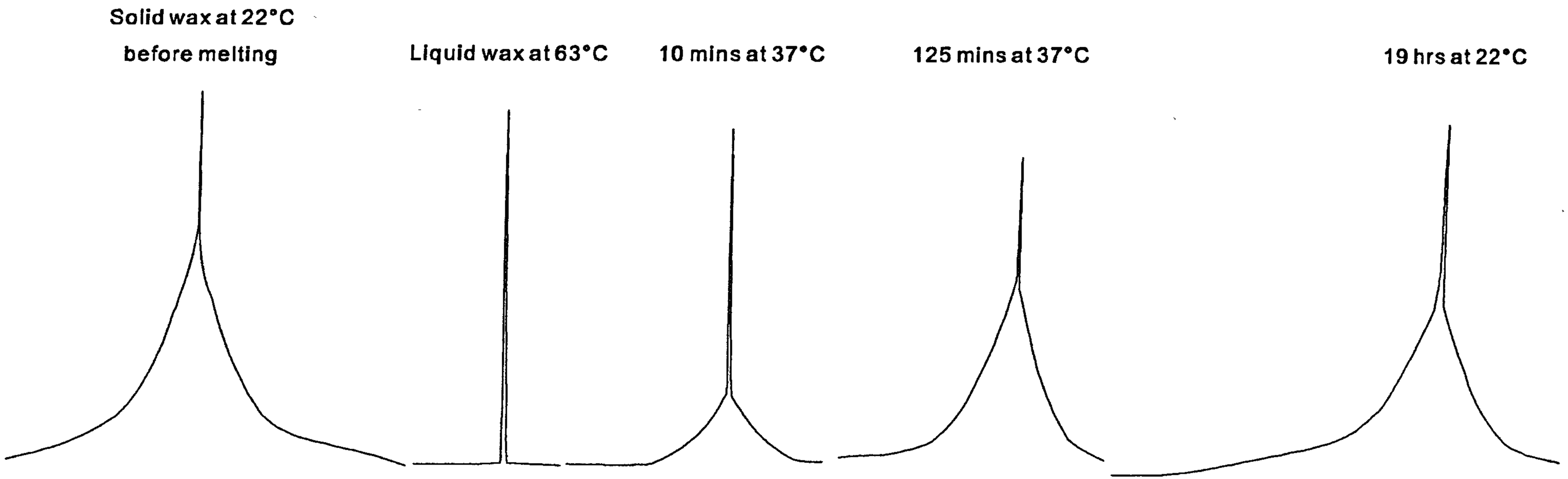

Notes (i) The frequency scale is constant. The Y gain is variable
(ii) Approximate transition temperatures are: solid-solid = 40°C
solid-liquid = 60°C

Figure 6.25 *N.M.R. study of Nippon Seiro paraffin wax.*

Figure 6.26 shows the percentage of solids present in various paraffin waxes as a function of temperature[31]. Of the waxes studied, it is known from experience of formulation work, that Nippon Seiro is the one most suitable for paste polishes, whereas Parawax and M.K.R. wax are totally unsuitable.

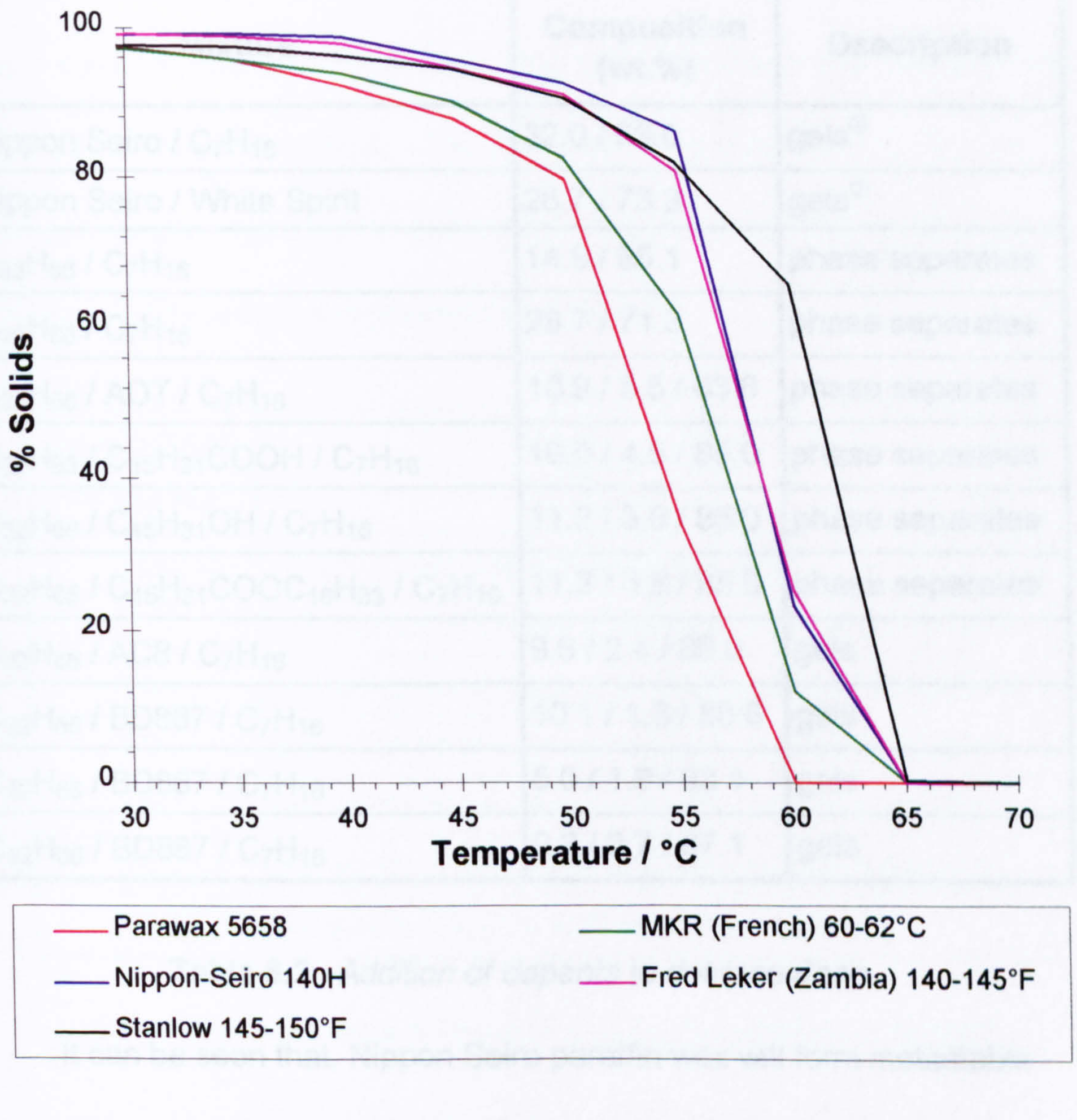

Figure 6.26 *N.M.R. study of various paraffin waxes.*

This ability to produce a satisfactory product can be correlated with the percentage of solids present at a temperature below the melting point when crystallisation has started to occur (~55°C).

§ 6.6 Test-tube miscibility studies

In parallel with the vapour pressure studies, test-tube observations of the ability of various paste formulations to gel were made. The results are summarised in table 6.2.

Mixture	Composition (wt.%)	Description
Nippon Seiro / C_7H_{16}	32.0 / 68.0	gels①
Nippon Seiro / White Spirit	26.7 / 73.3	gels①
$C_{32}H_{66}$ / C_7H_{16}	14.9 / 85.1	phase separates
$C_{32}H_{66}$ / C_7H_{16}	28.7 / 71.3	phase separates
$C_{32}H_{66}$ / AOT / C_7H_{16}	10.9 / 5.5 / 83.6	phase separates
$C_{32}H_{66}$ / $C_{15}H_{31}COOH$ / C_7H_{16}	10.5 / 4.5 / 85.0	phase separates
$C_{32}H_{66}$ / $C_{15}H_{31}OH$ / C_7H_{16}	11.2 / 3.8 / 85.0	phase separates
$C_{32}H_{66}$ / $C_{15}H_{31}COOC_{16}H_{33}$ / C_7H_{16}	11.2 / 3.8 / 85.0	phase separates
$C_{32}H_{66}$ / AC8 / C_7H_{16}	9.6 / 2.4 / 88.0	gels
$C_{32}H_{66}$ / BD887 / C_7H_{16}	10.1 / 1.3 / 88.6	gels
$C_{32}H_{66}$ / BD887 / C_7H_{16}	5.0 / 1.9 / 93.1	gels
$C_{32}H_{66}$ / BD887 / C_7H_{16}	9.2 / 3.7 / 87.1	gels

Table 6.2 *Addition of dopants to dotriacontane.*

It can be seen that, Nippon Seiro paraffin wax will form metastable gels with both heptane and white spirits as solvent which last, undisturbed, for about a week. When modelled by pure dotriacontane and heptane, gelation does not occur and the mixture always phase separates on cooling.

① Phase separates after one week.

If single component dopants are used, we are still unable to induce the formation of a gel. It is only when more complex dopants, having a range of components, are used that more stable networks are produced.

A series of sealed tubes of heptane and dotriacontane doped with BD887 microcrystalline wax was prepared in order to try and determine some sort of critical gel concentration. The ratio of BD887 to dotriacontane was varied and added to 30 cm^3 heptane such that the overall concentration of solids remained at 10 wt.%. The tubes were thermostatted to 70°C to form a homogeneous solution and then slowly cooled to 30°C over a period of 6 hours. The results are presented in table 6.3.

Wt.% BD887 in $C_{32}H_{66}$	Description
0.00	cloudy phase separated suspension
0.11	soft gel which phase separates with gentle agitation
0.45	soft gel which phase separates with gentle agitation
1.04	gel which phase separates with vigorous agitation
3.40	gel which phase separates with vigorous agitation
5.03	gel which phase separates with vigorous agitation
10.00	gel which remains with extreme agitation

Table 6.3 *Slow cool gelation of $C_{32}H_{66}$ by addition of BD887.*

The results suggest that the addition of as little as 0.5 wt.% of microcrystalline dopant can induce the formation of a gel, albeit a weak one which breaks down on gentle agitation. When increased to above 1 wt.% however the strength of the network formed increases dramatically such that

vigorous agitation is required to induce phase separation. At 10 wt.% the resulting paste is extremely stable and no degree of mechanical disturbance causes the system to break down.

If the same sealed tubes are reheated and then quenched to form a gel, similar observations are seen (table 6.4).

Wt.% BD887 in $C_{32}H_{66}$	Description
0.00	cloudy phase separated suspension
0.11	soft gel which phase separates with gentle agitation
0.45	soft gel which phase separates with gentle agitation
1.04	gel which flows with vigorous agitation but no separation of solvent
3.40	gel which flows with vigorous agitation but no separation of solvent
5.03	gel which remains with extreme agitation
10.00	gel which remains with extreme agitation

Table 6.4 *Fast cool gelation of $C_{32}H_{66}$ by addition of BD887.*

As pointed out in chapter 3, complex solutes such as BD887 microcrystalline wax will fractionate in a solvent such as heptane. A 20 wt.% solution in heptane was made and on cooling the insoluble fraction removed by filtration. On evaporation of the solvent, a solid remained which consists essentially of n-alkanes and will be called "microcrystalline extracts (MCX)". More sealed tubes were prepared in the same manner as described above and the results are presented in tables 6.5 and 6.6.

Wt.% MCX in $C_{32}H_{66}$	Description
0.10	soft gel which phase separates with gentle agitation
0.50	soft gel which phase separates with gentle agitation
1.01	soft gel which phase separates with agitation
4.99	gel which phase separates with vigorous agitation
10.06	gel which flows with vigorous agitation but no separation of solvent

Table 6.5 *Slow cool gelation of $C_{32}H_{66}$ by addition of BD887.*

Wt.% MCX in $C_{32}H_{66}$	Description
0.10	soft gel which phase separates with gentle agitation
0.50	soft gel which phase separates with gentle agitation
1.01	soft gel which phase separates with agitation
4.99	gel which flows with vigorous agitation but no separation of solvent
10.06	gel which flows with vigorous agitation but no separation of solvent

Table 6.6 *Fast cool gelation of $C_{32}H_{66}$ by addition of MCX.*

Here we can see that on increasing the concentration of dopant, the tendency to produce a rigid network increases but, in comparison to BD887, the gels formed with MCX are less stable.

§ 6.7 References

1 M.G. Broadhurst, **J.Res.Nat.Bur.Stand.**, 66A,241,(1962).

2 A.I. Kitaigorodskii, Yu V. Mnyukh and Yu G. Asadov, **J.Phys.Chem.Solids**, 26,463,(1965).

3 W.R. Turner, **Ind.Eng.Chem.Prod.Res.Dev.**, 10,238,(1971).

4 D.W. M^{c}Clure, **J.Chem.Phys.**, 49,1830,(1968).

5 W.M. Mazee, **Analytica Chimica Acta**, 17,97,(1957).

6 D.L. Dorset, **Macromolecules**, 18,2158,(1985).

7 R. Salzgeber, **Comptes Rendus - Acad. des Sci.**, 240,1642,(1955).

8 A.I. Kitaigorodskii, Iu V. Mniukh and N.A. Nechitailo, **Sov.Phys.-Crystallography**, 3,303,(1958).

9 Y. Kim, H.L. Strauss and R.G. Snyder, **J.Phys.Chem.**,93,485,(1989).

10 G.A. Holder and J. Winkler, **J.Inst.Petroleum**, 51,499,(1965).

11 D.L. Dorset, **Macromolecules**, 19,2965,(1986).

12 R.B. Prime and B. Wunderlich, **J.Pol.Sci.A2**, 7,2073,(1969).

13 S.P. Srivastava, J. Hendoo, K.M. Agrawal and G.C. Joshi, **J.Phys.Chem Solids**, 54(6),639,(1993).

14 (i) G. Friedel, **Ann.Physique,** 18,273,(1922).

(ii) N.H. Hartshorne and A. Stuart (1970), "Crystals and the Polarising Microscope", 4th edition, E. Arnold, London.

15 G.A. Holder, **A.C.S.,Div.Polym.Chem.,Preprints**, 7(1),306,(1966).

16 G.A. Holder, **J.Macromol.Sci.-Chem.**, A4(5),1049,(1970).

17 D.L. Dorset, **J.Pol.Sci.B,Pol.Phys.**, 27,1161,(1989).

18 F.W. Padgett, D.G. Hefley and A. Hendriksen, **Ind. and Eng.Chem.**, 18(8),832,(1926).

19 S.W. Ferris, H.C. Cowles and L.M. Henderson, **Ind. and Eng.Chem.**, 23(6),681,(1931).

20 S.W. Ferris and H.C. Cowles, **Ind. and Eng.Chem.**, 37,1054,(1945).

21 R.T. Edwards, **Ind. and Eng.Chem.**, 49,750,(1957).

22 H. Zocher and R.D. Machado, **Acta Cryst.**, 12,122,(1959).

23 G.A. Holder and J. Winkler, **A.C.S.,Div.Petrol.Chem.,Preprints**, 10(2),D49,(1965).

24 G.A. Holder and J. Winkler, **Nature**, 207,719,(1965).

25 G.A. Holder and J. Winkler, **A.C.S.,Div.Polym.Chem.,Preprints**, 6(2),850,(1965).

26 (i) E.M. Barrall II, R.S. Porter and J.F. Johnson, **J.Phys.Chem.**, 71,1224,(1967).

(ii) D.A. Skoog and J.J. Leary (1992), "Principles of Instrumental Analysis", 4th edition, Saunders College Printing, Philadelphia.

27 "Differential Thermal Analysis", Volume 2, Chapter 9, p97 R.C. Mackenzie (Ed.), Congress Library Classification QD515 M1v2.

28 B. Flaherty, **J.Appl.Chem.Biotechnol.**, 21,144,(1971).

29 M. Wesolowski, **Thermochimica Acta**, 46,21,(1981).

30 E.R. Andrew, **J.Chem.Phys.**, 18,607,(1950).

31 Internal report, Reckitt and Colman, Household and Toiletries Division, Hull.

Chapter Seven

Conclusions

§ 7.1 Conclusions

This research has succeeded in its aim of providing the first quantitative interpretation of the systems of industrial and commercial interest. The purpose and effect of adding components such as high melting microcrystalline wax and lime / stearin has been shown. This is the stabilisation by steric hindrance of thermodynamically non-equilibrium states such as gels.

The principal advance has been the design and development of a successful technique for the measurement of vapour pressure in such systems. The value of such measurements in interpreting complex behaviour has been demonstrated.

Other techniques have been applied and their advantages and limitations in studies of this kind have been assessed.

In particular, this work has led to the modification of shoe polish formulations as used by Reckitt and Colman. The instability of pastes which include aqueous components has resulted in the use of purely non-aqueous systems. Also, the more expensive waxes which impart important polish characteristics such as depth of gloss and solvent retention properties, have been partially replaced by cheaper, synthetic ingredients.

Appendices

Selected physical properties of common wax components[1]

Fatty acids of the stearic acid series - $C_nH_{2n+1}COOH$

n	Systematic Name	Trivial Name	Mol. Wt. $gmol^{-1}$	M.P. °C	Density[2] gcm^{-3}	$.H_{fus}$[3] / $kJmol^{-1}$
11	dodecanoic	lauric	200.32	44.5	0.8557^{70}	36.7
13	tetradecanoic	myristic	228.38	54.4	0.8448^{80}	45.0
15	hexadecanoic	palmitic	256.43	62.8	0.8420^{80}	54.9
17	octadecanoic	stearic	284.48	69.6	$0.847^{69.5}$	61.3
19	eicosanoic	arachidic (arachic)	312.54	75.3	0.838^{80}	71.0
21	docosanoic	behenic	340.59	80.0	0.837^{80}	78.6
23	tetracosanoic	lignoceric	368.65	84.2	0.8207^{100}	88.4
25	hexacosanoic	cerotic	396.70	87.7	0.8198^{100}	(96)
27	octacosanoic	montanic	424.75	90.99	0.8191^{100}	(105)
29	triacontanoic	melissic (myricic)	452.81	93.6	(0.819^{100})	(113)

---

[1] (a) Crossfire plus service at MIDAS using database BS9702AB provided by Beilstein Informationssysteme GmbH. (b) Kirk-Othmer, "Encyclopedia of Chemical Technology", 3rd Edition (1984), John Wiley & Sons. (c) R.C. Weast, "CRC Handbook of Chemistry and Physics", 56th Edition (1975-6), CRC Press, Ohio.

[2] Superscripted values indicate temperature (in °C) of density measurement.

[3] Parentheses indicate extrapolated values.

Fatty acids of the oleic acid series - $C_nH_{2n-1}COOH$

n	Systematic Name	Trivial Name	Mol. Wt. $gmol^{-1}$	M.P. °C	Density gcm^{-3}
13	*cis*-tetradec-9-enoic	myristoleic	226.36	- 4	0.9018^{20}
15	*cis*-hexadec-9-enoic	palmitoleic	254.41	0.5	0.8637^{70}
15	*trans*-hexadec-9-enoic	palmitelaidic	254.41	—	—
17	*cis*-octadec-6-enoic	petroselinic	282.47	29.4	0.8681^{40}
17	*trans*-octadec-6-enoic	petroselaidic	282.47	54	—
17	*cis*-octadec-9-enoic	oleic	282.47	13.3	0.8907^{20}
17	*trans*-octadec-9-enoic	elaidic	282.47	44	0.8701^{50}
17	*cis*-octadec-11-enoic	*cis*-vaccenic	282.47	14.5	—
17	*trans*-octadec-11-enoic	*trans*-vaccenic	282.47	44	0.856^{70}
19	*cis*-eicos-9-enoic	gadoleic	310.52	~ 24.5	—
21	*cis*-docos-11-enoic	cetoleic	338.58	—	—
21	*cis*-docos-13-enoic	erucic	338.58	34.7	0.8532^{70}
21	*trans*-docos-13-enoic	brassidic	338.58	61.9	0.8500^{70}

Some polyfunctional C_{18} fatty acids

Formula	Systematic Name	Trivial Name	Mol. Wt. $gmol^{-1}$	M.P. °C	Density gcm^{-3}
$C_{17}H_{31}COOH$	*cis*,*cis*-octadeca-9,12-dienoic	linoleic	280.45	-5.3	0.9059^{20}
$C_{17}H_{31}COOH$	*trans*,*trans*-octadeca-9,12-dienoic	linolelaidic	280.45	28	—
$C_{17}H_{29}COOH$	*cis*,*cis*,*cis*-octadeca-9,12,15-trienoic	linolenic	278.44	-12	0.9107^{20}
$C_{17}H_{29}COOH$	*cis*,*trans*,*trans*-octadeca-9,11,13-trienoic	α-eleostearic	278.44	48.5	0.9028^{50}
$C_{17}H_{29}COOH$	*trans*,*trans*,*trans*-octadeca-9,11,13-trienoic	β-eleostearic	278.44	71.5	0.8909^{75}
$C_{17}H_{29}COOH$	*cis*,*cis*,*trans*-octadeca-9,11,13-trienoic	punicic trichosanic	278.44	43	0.9025^{50}
$C_{17}H_{29}COOH$	*trans*,*trans*,*trans*-octadeca-9,12,15-trienoic	linolenelaidic	278.44	29.5	—
$C_{17}H_{32}(OH)COOH$	12-hydroxy-*cis*-octadec-9-enoic	ricinoleic	298.47	~ 8	$0.940^{15.5}$
$C_{17}H_{32}(OH)COOH$	12-hydroxy-*trans*-octadec-9-enoic	ricinelaidic	298.47	52.5	—

Physical properties of common waxes[4]

Wax	M.P. °C	Specific Gravity[5]	Acid Value[6]	Saponification Value[7]
Beeswax, crude	62 - 66	0.927 - 0.970	17 - 36	89 - 149
Beeswax, yellow	62 - 65	0.960 - 0.964	18 - 24	90 - 97
Candelilla, refined	67 - 69	0.982 - 0.986	13 - 18	35 - 86
Carnauba	83 - 86	0.990 - 1.001	3 - 10	78 - 95
Chinese insect	81.5 - 84	0.950 - 0.970	0.2 - 1.5	73 - 93
Esparto	68 - 78	0.988 - 0.990	23 - 24	70 - 79
Microcrystalline	71 - 89	0.928 - 0.941	0	0
Montan, refined	77 - 84	$1.010 - 1.030^{25°}$	24 - 43	72 - 103
Ouricuri, refined	79 - 84	1.053 - 1.060	3 - 21	62 - 86
Ozokerite, refined	74.4 - 75	0.907 - 0.920	0	0
Paraffin, American	49 - 63	0.896 - 0.925	0	0
Shellac wax	79 - 82	0.971 - 0.980	12 - 24	64 - 83
Spermacetti	42 - 50	0.905 - 0.945	2.0 - 5.2	108 - 134

---

[4] (a) R.C. Weast, "CRC Handbook of Chemistry and Physics", 56th Edition (1975-6), CRC Press, Ohio. (b) Kirk-Othmer, "Encyclopedia of Chemical Technology", 2nd Edition (1970), John Wiley & Sons.

[5] density of wax / density of water (at 15°C unless specified).

[6] DGF-M-IV 2(57) = number of mg of KOH needed to neutralise the free acids contained in 1g of wax

where DGF = Deutsche Gesellschaft für Fettwissenschaft, obtainable from Wissenschaftliche Verlagsgesellschaft mbH, Stuttgart-N, Birkenwaldstraße 44, Germany.

[7] Number of mg of KOH needed to neutralise the free acids and split the esters contained in 1g of wax.